University of Calgary

PRISM Repository **https://prism.ucalgary.ca**

The Vault Open Theses and Dissertations

2016

Phase Interference in Multiphase Flow in Thin Gaps

Raza, Salim

Raza, S. (2016). Phase Interference in Multiphase Flow in Thin Gaps (Doctoral thesis, University of Calgary, Calgary, Canada). Retrieved from https://prism.ucalgary.ca. doi:10.11575/PRISM/27327 http://hdl.handle.net/11023/3180

Downloaded from PRISM Repository, University of Calgary

UNIVERSITY OF CALGARY

Phase Interference in Multiphase Flow in Thin Gaps

by

Salim Raza

A THESIS

SUBMITTED TO THE FACULTY OF GRADUATE STUDIES

IN PARTIAL FULFILMENT OF THE REQUIREMENTS FOR THE

DEGREE OF DOCTOR OF PHILOSOPHY

GRADUATE PROGRAM IN CHEMICAL AND PETROLEUM ENGINEERING

CALGARY, ALBERTA

JULY, 2016

© Salim Raza 2016

Abstract

An immense quantity of hydrocarbon fuel is trapped in the fractured reservoirs, which is challenging to recover due to a number of issues such as heterogeneity of the reservoir's properties, higher permeability of fractures than that of the matrix, and multiphase flow through the fractures. On average, the recovery of oil from these reservoirs is relatively low and there is a requirement to improve the performance of recovery processes in these systems. The research documented in this thesis deals with multiphase flow, in particular parallel flow of oil and water, in fractures, modelled as a single narrow gap Hele-Shaw cell. The effects of additives such as polymer, surfactant, and rod-like nanoparticles have been examined to determine how they impact the nature of the interfaces between the oil and water and the amount of oil displaced from the gap. Differential pressure, flow rates and images of the flow structures were acquired to provide a basis for both quantitative and qualitative analyses of the flows. In the case of co-injection of water and oil, different flow structures observed changed with phase flow rates – oil entrapment occurred in several forms including trapped connected oil as well as irregular and immobile droplets. The relative permeability and hysteresis observed in the experiments demonstrated the dependence of the flow on the direction of wetting phase saturation change. Surfactant (sodium dodecyl sulfate) addition to the water revealed that with the associated interfacial tension reduction, oil displacement improved and oil droplets formed at the oil-water interface. The addition of polymer (polyethylene oxide) to the water raised the viscosity of the aqueous phase which in turn improved the displacement of oil. Another key observation was the adsorption of polymer on the plates of the Hele-Shaw cell which changed the wettability of the plates leading to enhanced oil displacement. The addition of cellulose nanocrystals (CNC) to the water significantly improved oil displacement due to viscosity enhancement of the aqueous phase as well as reduction of the interfacial tension. Microscope observation also revealed the formation of a microemulsion adjacent to the oil-water interface.

Acknowledgements

I would like to express my regards, deep sense of gratitude and sincere appreciation to my supervisor Dr. Ian D. Gates for his exceptional moral and academic support, encouragement and guidance during this study and my co-supervisor Dr. Hossein Hijazi for his brilliant ideas, constant assistance and continuous advice. Without their support, it would be impossible to complete this study.

I would like to extend my sincere thanks to members of my supervisory and examination committee Dr. Hector De La Hoz Siegler, Dr. Shengnan (Nancy) Chen, Professor Mingzhe Dong, Dr. Michael S Kallos, Dr. Amir Sanati Nezhad for their constructive guidance and contribution to this work. I am really grateful to Dr. George M. Homsy, for accepting our request as external examiner in the final defense examination. His outstanding research is not only a great help for my work but an honor for the world's researchers in the field.

I am thankful and acknowledge the funding support from NSERC, Department of Chemical and Petroleum Engineering, University of Calgary and University of Engineering and Technology (UET) Peshawar, Pakistan. I also appreciate Dr. Ranjani Kannaiyan for her support in conducting the microscopic examination of the phases. My regards and thanks from the core of heart is for Dr. Noor Mohammad, Dean, UET Peshawar, for his guidance and constant moral support during my stay and study at the University of Calgary.

I would also like to acknowledge all help and support, I received during my studies from my friends and colleagues. My love and special thanks go to my family especially my mother, wife, kids and my siblings for their patience and continuous and endless support during all these years. Their unconditional love and support were always a great strength for me throughout this research work.

Finally, my prayers, regards and endlessly gratitude for my father Nawab Khan, who passed away during this study. He has been a constant inspiration for me and his advice,

guidance, desire for completing my PhD and providing every kind of support in his life that I needed, enabled me to complete this research. May Allah rest him in peace. Aameen

Dedication

I would like to dedicate this thesis to my father ‘NAWAB KHAN’, mother, wife and kids.

Table of Contents

Abstract ii

Acknowledgements iii

Dedication v

Table of Contents vi

List of Tables xi

List of Figures and Illustrations xii

Chapter One: Introduction 1

1.1. Introduction 1

1.2. Liquid-Liquid Flow In Narrow Gaps 2

1.3. Basic Fluid Mechanics Of Liquid-Liquid Flow In Narrow Gaps 3

1.4. Research Questions 6

1.5. Organization Of The Thesis 7

Chapter Two: Literature Review 9

2.1. Introduction 9

2.2. Multiphase Flow 10

2.3. Multiphase Flow in Pipes 11

2.4. Multiphase Flow in Narrow Gaps 16

2.4.1. Gas-Liquid Flow in Narrow Gaps 17

2.4.2. Liquid-Liquid Flow in Narrow Gaps 22

2.4.2.1. Oil - Water Flow Through a Thin Gap or Fractured Media 22

2.4.2.2. Oil - Surfactant Solution Flow Through a Thin Gap or Fractured Media 28

2.4.2.3. Oil and Polymer Flow in Fractures/Fractured Media 35

2.4.2.4. Nanocrystals and its Application in the Oil Industry 41

2.5. What is Missing in the Literature? 46

Chapter Three: Two Phase Flow of Liquids in a Narrow Gap: Phase Interference and Hysteresis 47

3.1. Abstract 47

3.2. Introduction 48

3.3. Methods and Materials 51

3.4. Theory 54

3.4.1. Single Phase Flow: Evaluation of Hydraulic Gap and Absolute Permeability 54

3.4.2. Two Phase Flow 55

3.5. Results and Discussion 56

3.6 Conclusions 69

References 72

Chapter Four: Impact of Interfacial Tension on Two Phase Flow in a Narrow Gap 77

4.1. Abstract 77

4.2. Introduction 78

4.3. Experimental Apparatus, Materials, and Procedure 80

4.3.1. Fluid Properties 82

4.4. Results and Discussion 84

4.4.1. Flow Pattern Analysis 86

4.4.2. Effect of Surfactants on the Capillary Number 94

4.5. Conclusion 95

References 97

Chapter Five: Impact of Polymer on Flow Behaviour, Phase Interference, and Displacement in a Hele-Shaw Cell 100

5.1. Abstract 100

5.2. Introduction 101

5.3. Experimental Apparatus and Methodology 104

5.4. Results and Discussion 105

5.4.1. Impact of Polymer on Viscosities and Interfacial Tensions of the Fluids . 105

5.4.2. Phase Flow Patterns Analysis 107

5.4.3. Impact of Polymer on Relative Permeabilities, Saturations of the Phases, Reynolds Numbers and Mobility Ratios 121

5.4.4. Microscopic Analysis of the Interfaces Between PEO Polymer and Oil ... 125

5.5. Conclusions 127

References 130

Chapter 6: Impact of Cellulose Nanocrystals on the Water-Oil Interfaces and Displacement 132

6.1. Abstract 132

6.2. Introduction 133

6.3. Background 134

6.3.1. Capillary Number and Relative Permeability 136

6.4. Methodology 138

6.5. Results and Discussion 139

6.5.1. Variation of Viscosity and Interfacial Tension with Nanocrystals 139

6.5.2. Mobility Ratios 141

6.5.3. Effects of Nanocrystals on the Capillary Number 142

6.5.4. Macroscopic and Microscopic Flow Patterns and Relative Permeability Analysis 143

6.5.4.1. 1 wt. % CNC Suspension 144

6.5.4.1.1. Flow Patterns Observations 144

6.5.4.1.2. Microscopic Analysis of the Interfaces 145

6.5.4.1.3. Relative Permeabilities 148

6.5.4.2 2 wt. % CNC Suspension 149

6.5.4.2.1. Flow Patterns Analysis 149

6.5.4.2.2 Relative Permeability in the Case of 2 wt.% CNC Suspension 152

6.5. Conclusions 153

References 155

Chapter 7: Conclusions and Future Work 159

7.1. Co-current Flow of Oil and Water 159

7.2. Co-current Flow of Oil and Surfactant Solution 159

7.3. Co-current Flow of Oil and Polymer Solution 160

7.4. Co-current Flow of Oil and Cellulose Nanocrystals Suspension 160

7.5. Recommendations for Future Work 160

References 162

Appendix-A 182

List of Tables

Table 2.1. Summary of air/gas and water flow through fracture or fractured porous media 19

Table 2.2. Summary of oil-water flow through fracture or fractured porous media 24

Table 2.3. Summary of oil-surfactants flow through fracture or fractured porous media 30

Table 2.4. Summary of oil-polymer flow through fracture or fractured porous media 38

Table 2.5. Summary of the nanocrystals use in the oil industry 43

Table 3.1: Properties of oil and water used in the experiments 54

Table 4.1: Properties of the oil, de-ionized water and 2 wt.% aqueous phase of SDS 82

Table 4.2: Comparison of water-oil and SDS (2wt.%) + water-oil flow patterns acquired at the same time and flow rates. The mineral oil is shown transparent whereas the aqueous phase is red in colour. Inlet is on the right side of the cell 88

Table 5.1: Comparison of water-oil and polymer (1.5 wt. %) solution-oil data and images 109

Table 5.2: Comparison of the data and calculated values obtained during water with 0.5%, 1% and 1.5% PEO experiments. Shaded rows show maximum and unshaded the averaged values for the entire experiment 125

Table 6.1: Viscosity and interfacial tension variation with different concentrations of CNC suspension 141

Table 6.2: Mobility ratios of the oil-aqueous system examined 142

Table 6.3: Capillary number calculated for each set phases system. 143

List of Figures and Illustrations

Figure 2.1: Flow patterns observed by Charles et al. (1961) in the oil-water through a pipe. (a): Flow patterns created in the flow of water flowing at constant velocity (0.3m/s) with 16.8 cP oil flowing at different velocities, (b): water flowing at 0.21 m/s with 16.8 cP oil flowing at different velocities, (c): water velocity 0.62 m/s and 16.8 cP oil flowing at different velocities 13

Figure 2.2: Flow patterns classified by Charles et al., (1961) in the flow of water with 6.26 cP and 16.8 cP oils at different superficial velocities in a pipe 14

Figure 2.3: Flow patterns observed by McQuillan et al., (1985) in gas/liquid upward flow through a vertical pipe. 1. Bubble, 2. Slug, 3. Churn and 4. Annular.....15

Figure 2.4: Flow patterns observed by Angeli et al., (1999) in an oil-water flow mixture at different velocities through pipe. (a) stratified wavy with drops flow pattern, (b) three layers flow patterns, (c) stratified mixed with water layer flow pattern, and (d) mixed flow pattern (Angeli et al., 1999) 16

Figure 2.5. Experimental set up and fingering observed by Benham and Olson, (1963)..36

Figure 2.6: Interfaces and fingerings at two viscosity ratios observed by Mungan (1977): injection of polymer solution into the glycerin-wetted Hele-Shaw cell stabilizes the front.....37

Figure 3.1. (a) Experimental set up (adapted from Al-Turki, 2013, with the permission of the author), (b) side view of the cell showing the shim stock and its thickness, and (c) top view of the cell showing area of interest and inlet/outlet ports....53

Figure 3.2: Relationship of q_w and ΔP to find hydraulic gap and absolute permeability of the fracture in single-phase flow.....55

Figure 3.3: Averaged relative permeability results from three replicate experiments. The error bars show the standard deviation of the experiments.....57

Figure 3.4: Relative permeability curves for water and oil in drainage and imbibition processes. Oil is the wetting phase. Water saturation drops initially in the both processes. Values of q_o and q_w respectively are given for each image in ml/min: Image 1: 0.5, 0.2; Image 2: 0.5, 0.3; Image 3: 0.5, 2; Image 4: 0.5, 9; Image 5: 0.1, 9; Image 6: 0.025, 9; Image 7: 0.2, 9; Image 8: 0.4, 9; Image 9: 0.5, 8; Image 10: 0.5, 2; Image 11: 0.5, 0.25; Image 12: 0.5, 0.15 59

Figure 3.5: Evolution of flow state as water injection rate is increased to 3 ml/min at constant oil injection rate equal to 0.5 ml/min. The flow direction is from the right to the left side of the images 61

Figure 3.6: Schematic of various flow regimes development in the immiscible displacement of oil by variable water injection rate (A) linear displacement flow regime (B) frontal instabilities in the form of fingering advancement before breakthrough (C) frontal instabilities in the form of fingering normal to the flow and droplet formation after breakthrough 63

Figure 3.7. Evolution of water saturations versus time 64

Figure 3.8: Evolution of flow state as water (red) injection rate is increased from 4.5 to 9 ml/min with oil injection rate varying from 0.5 to 0.025 ml/min. The flow direction is from the right to the left side of the images 66

Figure 3.9. Saturations and flow rates of oil and water versus time during drainage process (wetting phase is oil) 67

Figure 3.10: Change of two-phase capillary number versus water saturation 68

Figure 4.1: Schematic of experimental apparatus 82

Figure 4.2: Viscosity of SDS+water solutions versus SDS concentration at 22.46°C (instrumental error = ±0.1%). Data shown is average of five measurements (maximum standard deviation is 0.000255 cP) 83

Figure 4.3: Relationship among interfacial tension between oil and aqueous phases and SDS concentration. Instrumental error could be ±0.01 mN/m 84

Figure 4.4: Relative permeability curves for water-oil and 2 wt.% SDS+water-oil flow in the drainage process.....90

Figure 4.5: Comparison of flow patterns of de-ionized water and surfactant (2 wt.%SDS) flooding with oil at the same saturations. The red colour shows the aqueous phase of the surfactant whereas the transparent phase is the mineral oil.....91

Figure 4.6 Microscopic images of the interfaces developed in water-oil system. The light green color shows water while dark green is oil.....92

Figure 4.7: Lenses of Surfactant solution and interfaces created in water + SDS - oil systems. Light green shows surfactant while the dark green is the oil solution.....93

Figure 4.8: Comparison of capillary numbers (Ca) vs saturation obtained from de-ionized water and SDS 2 wt.% solution flooding with the oil through the fracture....94

Figure 5.1: Schematic of the experimental set up (adapted from Raza et al., 2016).....105

Figure 5.2: Relationship of viscosity of the polymer (PEO) aqueous phase to its concentration.....106

Figure: 5.3. Interfacial tension between oil and polymer aqueous phase versus concentration of PEO.....107

Figure 5.4. Relationship of capillary numbers of water and different concentrations of PEO 117

Figure 5.5: Comparison of the factor *F*, introduced by Abrams (1975) for different concentrations of PEO 118

Figure 5.6: Mobility of the water changes with different concentrations of the polymer (PEO) 120

Figure 5.7: Changes of mobility of oil with different concentrations of polymer.....120

Figure 5.8: Examples of 0.1 ml water droplets placed on the Hele-Shaw plates before PEO flood and after PEO flood.....121

Figure 5.9: (a) Relative permeabilities of oil with water and 1 and 1.5 wt.% polymer solution and (b) comparison of relative permeability curves for water (before PEO flood) and water (after PEO flood with thin layer of PEO on Hele-Shaw plates) 123

Figure 5.10: Microscopic images of the interfaces between the polymers aqueous phase (light green) and oil (dark green) phase: (a) interface at start of the observation, (b) image after 8 seconds (aqueous phase moves from right to left), (c) image after 16 seconds, (d) zoom in of a trapped oil droplet, (e) zoomed in (closer) view of interface, and (f) zoomed in view of interface 126

Figure 6.1: Experimental set shows the injection pumps, Hele-Shaw cell, data acquisition system, camera, and pressure transducers etc 139

Figure 6.2. Images retrieved during 1wt.% CNC suspension (red color) and oil (white color) phases flow through the cell. 145

Figure 6.3: Microscopic images of 1 wt.% CNC (light green) in oil (dark green). (a). CNC solution droplets in the oil phase, size 200 µm, (b). A portion of the (a), size 100 µm, (c, d, e, f) larger scale images (20 µm) of different portions of the image in part(b) 147

Figure 6.4: Microscopic schematic of interface among the mineral oil and 1% CNC suspension and various layers inside the oil phase. Dark green in the microscopic image shows the oil while light green is the CNC phase 148

Figure 6.5: Relative permeability curves for 1 wt.% CNC aqueous and oil phases flowing through the Hele-Shaw cell in the case of drainage 149

Figure 6.6. Images acquired during 2wt.% CNC suspension (red color) co-current flow with oil (white color) through the Hele-Shaw cell 151

Figure 6.7: Relative permeability curves (k_r) for oil and 2 wt.% CNC suspension vs saturation of the aqueous phase (S_w) 153

Chapter One: Introduction

1.1. Introduction

Multiphase flow in thin gaps is abundant in many natural and industrial systems such as oil-water flows in fractures/fractured reservoir rock, flow of pollutants underground e.g. radioactive waste, drainage water, dense non-aqueous phases of liquids, geothermal energy development, geological storage of carbon dioxide, supply of nutrient and oxygen for in situ treatment of polluted domains, immiscible non-aqueous phase liquids (seepage into underground water sources), food industry, cooling industry, refining industry, mineral transport and thin film coating (Kazemi, et al., 1993; Romm, 1996; Pan, 1999; Hughes et al., 2001; Konzak, 2001; Rutqvist, et al., 2002; Brennen, 2005; Doughty, 2007; Kolev, 2013). Multiphase flow occurs at almost every stage of the petroleum industry from reservoir conditions to refining. Since fractures in fractured rocks are highly permeable as compared to the matrix rock, higher flow rates occur within fractures. Consequently, multiphase flow and its structures in fractures become important since they are the major conduits of petroleum within these reservoirs.

It is estimated that hydrocarbon in fractured reservoirs provide more than 20% of the oil reserves and production of the world (Firoozabadi, 2000; Izadi et al, 2012). Majority of these reservoirs are hosted in carbonate rocks and provide challenges for oil recovery. After primary production, in typical practice, 40 to 60% of the original oil in place remains within fractured reservoirs which provides potentially significant opportunities for additional oil by using secondary and tertiary recovery processes (Boggs, Jr. 2000; SyedAkram and Mamora, 2011; Izadi et al. 2012; Schlumberger, 2016; Agada, 2016). Thus, a firm understanding of multiphase flows in fractured reservoirs is critical for maximizing production of oil from these systems.

1.2. Liquid-Liquid Flow in Narrow Gaps

At length scales similar to that of the aperture of fractures (typically of order of millimeters or a fraction of a millimeter), the behaviour of oil-water flow and interaction in fractures due to their irregular surfaces is complex, e.g. instabilities associated with multiphase flow. To understand these flows, the role of capillary forces relative to viscous and pressure forces, needs to be investigated. Due to small dimensions of the apertures of fractures in reservoir rock, capillary forces are often dominant (Romm, 1966; Fourar et al., 1993; 1995; Agada, 2016).

In the case of large fractures (greater than a few millimeters in aperture) with high flow rates, viscous forces dominate (Fourar et al., 1993; Forar and Bories, 1993; 1995; Merrill, 1975), whereas in narrow fractures with low flow rates, capillary forces dominate which leads to phase interference and fingering as observed by Horle et al., (1990); Rossen et al., (1992); Chown, (1994); Persoff et al., (1995); Longino et al., (1999); Agada, (2016). Phase interference is mixing of one phase with other in the form of droplets or it is interrupting paths of one phase by the other. Phase interference increases with tortuosity of the flow paths and the mobility ratio of the phases. Konzak, (2001) described that flow through rough and wetted fractures creates finger-like channels where the wetting phase flows more readily through larger channels.

Two phase liquid-liquid flow was first investigated by Romm, (1966) for relative permeabilities in a co-current flow configuration using kerosene oil and water through a Hele-Shaw cell. Romm concluded that the relative permeability of a phase is equal to its saturation and sum of relative permeabilities of the phases is equal to unity. A number of researchers conducted experiments to validate Romm's observation. In general, they concluded that although Romm's relative permeability relationship provides a good starting point for estimating the relative permeability but actually the relative permeability of a phase is not equal to its saturation in a fracture. Apart from the analysis of relative permeabilities, two phase liquid-liquid flow through fractures is analytically studied by Pruess et al., (1990); Pyrak-Nolte et al., (1990); Mendoza et al., (1991); Fourar. (1993);

Glass, (1993); Fourar and Bories, (1995); Pan et al., (1999); Keller et al., (2000); Chen et al., (2004); Liu et al., 2013 and many more. Ye, (2014) numerically simulated effects of the aperture distribution in the two phase flow through rough and smooth walled fractures by using a two-dimensional (2D) porous media approach with capillary forces dominating the flow. They concluded that the sum of the relative permeabilities is less than unity due to phase interference especially at moderate saturations.

Hill (1952), Saffman-Taylor (1958) and Chouke et al., (1959) developed criteria for onset of instability during two phase flow in a thin gap. Kopf-Sill and Homsy, (1987) studied flow of a single bubble under pressure gradient in a horizontal thin gap. They classified bubbles into near circles, flattened, elongated, long tail, short tail and the Tavneer-bubble shapes. They concluded that the shape and size of a bubble depend up on the velocity and capillary numbers. Fernandez and Homsy (2005) also studied two phase flow in thin gaps for viscous fingering or instabilities created in the interfaces, detail of their research is given in the following chapters.

1.3. Basic Fluid Mechanics of Liquid-Liquid Flow in Narrow Gaps

Laminar, viscous, and incompressible flow between two parallel glass plates is studied by a number of authors such as Huitt, (1955); Polubarinova-Kochina, (1962); Snow, (1965); Romm, (1966); Louis, (1969); Bear, (1972); Gale, (1975); Shad, (2010), and Al-Turki, (2013) etc. In general, these authors examined fluid-fluid flow in thin gaps analytically, numerically or conceptually by investigating flow structures created in the flows. Most approaches started from the Navier Stokes (N.S.) equations or Darcy's law together with the mass continuity equation. Hubbert (1956); Neuman (1975) and many others reported that in case of low Reynolds number, the inertial terms in the N.S. equation could be ignored. Reynolds number named after Osborne Reynolds (1842 – 1912) (Rott, 1990), - the ratio of inertial forces to the viscous forces (Falkovich, 2011), is used to differentiate laminar and turbulent flows. Mathematically, Reynolds number can be defined as:

$$Re = \frac{Inertial\ Forces}{Viscous\ Forces} = \frac{\rho VL}{\mu} = \frac{VL}{v} \quad (1)$$

V is the maximum velocity of the phase, *L* is the characteristic length and is equal to hydraulic gap in case of rectangular Hele-Shaw cell, μ is the dynamic viscosity and *v* is kinematic viscosity of the phase.

A simple model for steady, incompressible flow in a narrow gap is given by the planar Poiseuille's equation which can be derived from N.S. equation by assuming steady state, Newtonian, and one directional flow. In the derivation of Poiseuille's equation, it is also assumed that the fracture gap is very small as compared to the width of the fracture which implies that the variation of the velocity in the cross-direction is negligible. In the case of horizontal flow in a horizontal gap, the action of gravity is negligible. Considering no gravity effects and no slip boundary conditions in the N.S. equation for a single phase flow through a rectangular gap, Planar Poiseuille's equation is simplified to find hydraulic gap:

$$q = \frac{Wb^3\Delta P}{12\mu L} \quad (2)$$

where 'q' is the flow rate, 'W' is the width (the cross-direction, into the page), 'ΔP' is the pressure difference, 'L' is the length over which the pressure difference is applied, 'b' is the hydraulic gap (distance between the two planes), and 'μ' is viscosity of the fluid. On combining the Planar Poiseuille's equation (equation 1) with the Darcy's law (equation 3) for flow through porous media, the equation for absolute permeability of the gap is obtained by Equation 4:

$$\frac{q}{A} = \frac{k_{abs}\Delta P}{\mu L} \quad (3)$$

where '$A = b\ W$', the absolute permeability of the gap is:

$$k_{abs} = \frac{b^2}{12} \quad (4)$$

In the context of flow through fractures, Equation (2) has sometimes been referred to as the cubic law because the volumetric flow rate per unit area of a single fracture is a function of the aperture cubed (Iwai, 1976). In the two phase flow, using the cubic law and Darcy's law for multiphase flow, an equation for the relative permeability of each phase flowing in the gap (Equation 4) is obtained by:

$$k_{ri} = \frac{q_i \mu_i}{A k_{abs} \left(\frac{\Delta p}{L}\right)} \tag{5}$$

where the subscript "i" represents oil and water/displacing phase accordingly.

In porous media, the flow rate of a phase depends on the saturation of that phase (which in turn sets the capillary pressure) and this dependence is expressed through the relative permeability (Collins, 1962). In fractures, previous results show that the densities, viscosities, and interfacial tension (capillary pressure) are responsible for determining the nature of the flow and the effective relative permeabilities of each phase.

To understand the physics of multiphase flow in narrow gaps, the interaction of viscous and capillary forces is needed. The capillary number, defined by the ratio of viscous to capillary forces, determines the efficiency of displacement of one phase by another in the system. Capillary number is calculated on the basis of individual velocities and viscosities of the phases and interfacial tension between them (Moore et al., 1955). The equation for the capillary number becomes:

$$C_a = \frac{\mu_i U_j}{\sigma_{ij}} \tag{6}$$

where μ_i is viscosity of the displaced phase, U_j is velocity of the displacing phase finger and $\sigma_{ij}$is the interfacial tension between the displacing phases *'i'* and displaced phase *'j'*.

1.4. Research Questions

The efficiency of an oil recovery method employed in fractured reservoirs depends on the thorough understanding of flow behaviour in fractures. Despite extensive research in this area, there are still gaps in understanding of the flow structures within a single fracture. This includes hysteresis – does the relative permeability depends on the direction of the change of the wetting phase saturation in the gap? This also includes the effect of additives on the flow ehaviour in the gap – this comprised of surfactant, polymer, and nanoparticles and their impact on the flow within the gap.

Here, hysteresis and the addition of a surfactant, polymer, and cellulose nanocrystal is experimentally examined using Hele-Shaw cell as a prototype for a fracture. The effect of surfactant addition is the reduction of the interfacial tension between the phases. The addition of polymer raises viscosity of the aqueous phase and the addition of the nanocrystals both reduce the interfacial tension and raise the aqueous phase viscosity simultaneously. The impact on flow structures and relative permeability is explored to understand the dynamics of the systems.

The specific research questions that are investigated in the research documented in this thesis are as follows:

- How does direction of the change of the wetting phase saturation affect the flow behaviour of two immiscible liquid phases in a narrow gap? Is there evidence for hysteresis when the wetting phase saturation changes through time? For the research conducted here the liquids consist of water and mineral oil.

- What are the flow structures for water-oil flow in a narrow gap? What is the relative permeability behaviour for water-oil flow within a narrow gap?

- What is the impact of surfactant on water-oil flow within a narrow gap? How does the addition of surfactant change the configuration of interfaces and structures?

- What is the impact of viscosified water (via addition of polymer to water) on water-oil flow within a narrow gap? How does the addition of polymer change the configuration of interfaces and structure?

- What is the impact of cellulose nanocrystals added to the water in the water-oil flow through a narrow gap? How does the addition of nanocrystal change the configuration of interfaces and structure?

The key difference between the experiments conducted here and the majority of the literature is that both the phases, oil and aqueous, are co-injected into the narrow gap. In nearly all of the literature, a single phase is displaced from the Hele-Shaw cell by using another single phase. Here, to model displacement of oil from a section of a fracture with entering water and oil, co-currently injected into the Hele-Shaw cell. The research conducted and reported in this thesis is the first to examine hysteresis and the impact of the additives on such a flow system.

1.5. Organization of the Thesis

The research conducted is documented in seven chapters. A summary of each chapter is as follows:

- Chapter 2 consists of a literature review on the multiphase flow in general and multiphase flow through fractures or fractured media, in particular. The studies carried out for analyzing multiphase flows in narrow gaps is divided into two main groups i.e., gas-liquid flow and liquid-liquid flow through narrow gaps. The liquid-liquid studies are further grouped into water-oil, surfactant-oil, polymer-oil, and nanofluids-oil.

- In Chapter 3, research on hysteresis of multiphase flow in the Hele-Shaw cell is explored.

- Chapter 4 reports on the impact of the addition of surfactant on flow behaviour in the Hele-Shaw cell.

- In Chapter 5, the impact of polymer additive to the water phase on multiphase flow in the Hele-Shaw cell is explored.
- Chapter 6 describes the impact of cellulose nanocrystal on multiphase flow in the Hele-Shaw cell.
- Conclusions and recommendations for future work are discussed in Chapter 7.

Chapter Two: Literature Review

2.1. Introduction

Petroleum is a naturally occurring hydrocarbon that accumulates in reservoirs with sufficient porosity and permeability (Craft et al., 2014; Boggs, Jr., 2006; Terry et al., 2014). Reservoirs chiefly contain one or more of oil, gas, and water typically in sandstone or limestone rocks (Terry and Rogers, 2014). Petroleum was first explored about four thousand years ago in Babylon and Greece (Chisholm, Hugh, ed., 1911; Totten, 2007) whereas the first oil well was drilled in China in 347AD (Totten, 2007). It was recognized earlier that on average, roughly two-third or more of the original oil in place remains in the reservoir after primary production (Boggs, Jr., 2000; SyedAkram and Mamora, 2011; Shlumberger, 2016). The key challenge always faced by reservoir and production engineers is on how to raise the recovery factor (the fraction of the original oil in place that is produced); this is accomplished by enhanced oil recovery processes such as water flooding, chemical (e.g. surfactant, polymer etc) flooding or thermal recovery processes. The focus of the research documented here is on water flooding based methods.

Globally, fractured carbonate reservoirs are major sources of the oil. On a planetary basis, more than 60% of the remaining petroleum reserves are hosted in carbonate reservoirs which are mostly oil wet (Boggs, Jr., 2006; Agada, 2016). Depending on reservoir properties, secondary recovery processes such as water flooding have typically yielded an incremental 10 to 40% recovery factor but even after secondary recovery, a significant fraction of the oil remains in the reservoir. The main reasons for less than ideal recovery factor from these reservoirs is associated with multiphase flow within fractures, heterogeneity of the reservoir, the amount of storage of oil in the matrix, and ability of the oil to move from matrix to the fractures. To increase recovery from the reservoirs, a thorough investigation of the physics of the fluids is needed to analyse multiphase flow through fractures and interfaces developed during the flows.

2.2. Multiphase Flow

Single-phase flow is the flow of a fluid or combination of completely miscible solutions, which are chemically homogenous, isolated and distinct from the other parts of the system. Multiphase flow is a simultaneous flow of two or more immiscible fluids separated by a boundary/interface (Bear and Bachmat, 1991). Multiphase flows in a system can also be defined as the flow of two or more materials with different states/phases and different chemical properties. Multiphase flows are important in many natural and engineering systems including the atmosphere, food industry, process industry, pipelines, cooling industry, petrochemical, and petroleum industry, to name a few.

In the petroleum industry, multiphase flow occurs more or less at every stage of the recovery and production process. In reservoirs, oil exists mostly with gas, water, or both together within the formation rock that hosts the phases. The importance of multiphase flow increases in the oil recovery processes especially in secondary and tertiary recoveries. In secondary recovery processes, oil is produced by injecting water or gas to the reservoir. Waterflooding is considered the most effective and cheaper secondary recovery method, if feasible. Craft and Hawkins, (2014) described that waterflooding started more than 100 years ago. They suggested that reservoir characteristics (depth, heterogeneity, porosity, saturation, permeability etc.) and fluid characteristics (viscosity, density) affect the efficiency of water flooding. Fractures/faults in rocks, adverse reaction of water with the reservoir fluid, processing of the produced water to remove the hazardous material from the water, and viscous fingering are the major sources of problems associated with the waterflooding processes. Gas (nitrogen and carbon dioxide) flooding is often carried out in reservoirs with gas cap and in gravity drainage recovery process, where it is needed to maintain the pressure of the reservoir for efficient oil recovery. Inclination, permeability and depth of the reservoir mainly affect efficiency of the gas flooding (Craft and Hawkins, 2014).

In the tertiary/enhanced oil recovery methods, miscible, thermal and chemical flooding is carried out to recover the remaining oil from a reservoir. The oil, mostly trapped in small

pores or regions of the fractures due to capillary forces, which is challenging to move from the system to the production well. In the tertiary recovery processes, the oil is displaced from the surfaces/pores, which flow out to the production well by developing a displacing flow with the help of increasing the viscous forces and decreasing the capillary forces between the displacing and displaced phases. The residual oil can be mobilized by controlling the capillary number or mobility ratios (Craft and Hawkins, 2014), which are controlled in the chemical injection processes by using chemical additives such as surfactant or polymer that change the in-situ properties of the phases and pores/fractures surfaces (Ahmed, 2010, Craft and Hawkins, 2014). Miscible flooding processes are carried out by injecting a fluid phase (typically carbon dioxide or nitrogen) to the reservoir, which on mixing with the residual oil, lowers capillary forces (via interfacial tension) between the phases and improves oil recovery. In thermal recovery processes, migration of the heavy oil is carried out by injecting hot water or steam to the reservoir, which reduces viscosity of the oil consequently raising its mobility.

2.3. Multiphase Flow in Pipes

To understand multiphase flow in narrow gaps (fractures), it is instructive to examine multiphase flow in pipes.

Although there are many studies of two-phase flow in pipes in the literature, most of them focus on air-water flow, especially on flow patterns or instabilities created in multiphase flow through vertical, inclined and horizontal circular pipes. The earliest published work on classifying flow patterns in pipes was done by Baker,(1957) who observed eight flow regimes in the air water flow; many published studies have classified flow patterns created by the flow of air or gas and water through circular pipes (Gibson, 1913; Govier, 1958; Hewitt et al., 1970; Govier et al., 1972; Mandhane, 1974; Weisman, 1983; Troniewski et al., 1984; McQuillan et al., 1985; Brill et al., 1991; Ansari et al., 1994; Hasan et al., 1998; Furakawa et al., 2001; and Rozenblit et al., 2006). There are fewer studies on liquid-liquid flows in pipes. Russel et al., (1959) observed *bubble, stratified* and *mixed flow* patterns in

multiphase flow of oil (18 cP) and water in horizontal circular pipes. Charles et al. (1961) studied flow regimes created in the flow of water with three different viscosities (6.29 cP, 16.8 cP, and 65 cP) and same density 998 kg/m^3 oil at different flow rates of the phases in a pipe of 26.4 mm diameter and 7.3 m long test section (Figure-2.1). They noticed that the flow patterns of the phases depend on their superficial velocities. They observed same flow patterns for all the oils except at low water flow rates. They classified the flow patterns into water drops in oil, oil in water concentric, oil slugs in water, oil bubbles in water and oil drops in the water (Figure 2.2)

(a):

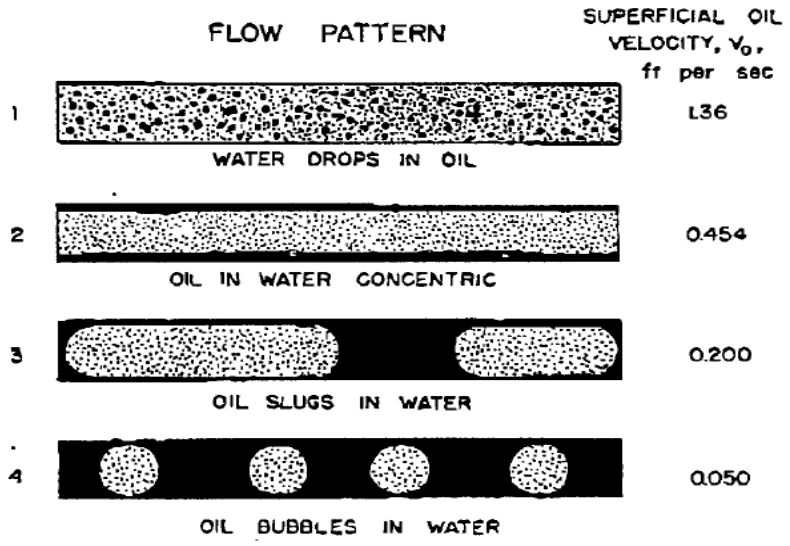

(b):

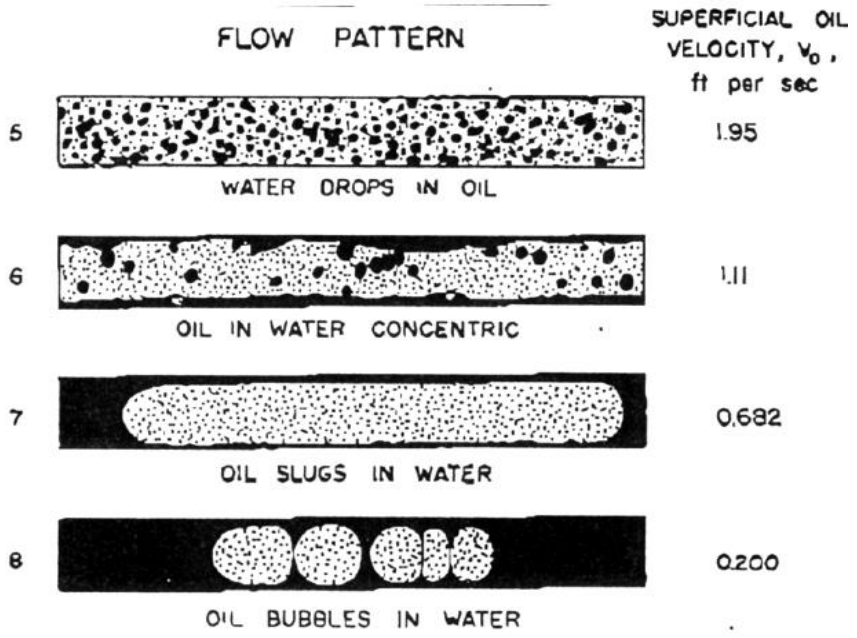

(c):

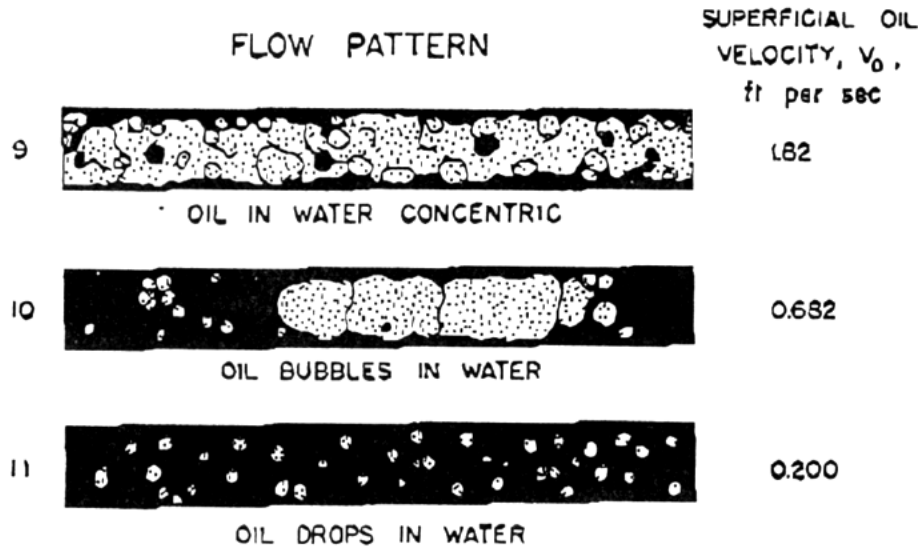

Figure 2.1: Flow patterns observed by Charles et al. (1961) in the oil-water through a pipe. (a): Flow patterns created in the flow of water flowing at constant velocity (0.3m/s) with 16.8 cP oil flowing at different velocities, (b): water flowing at 0.21 m/s with 16.8 cP oil flowing at different velocities, (c): water velocity 0.62 m/s and 16.8 cP oil flowing at different velocities

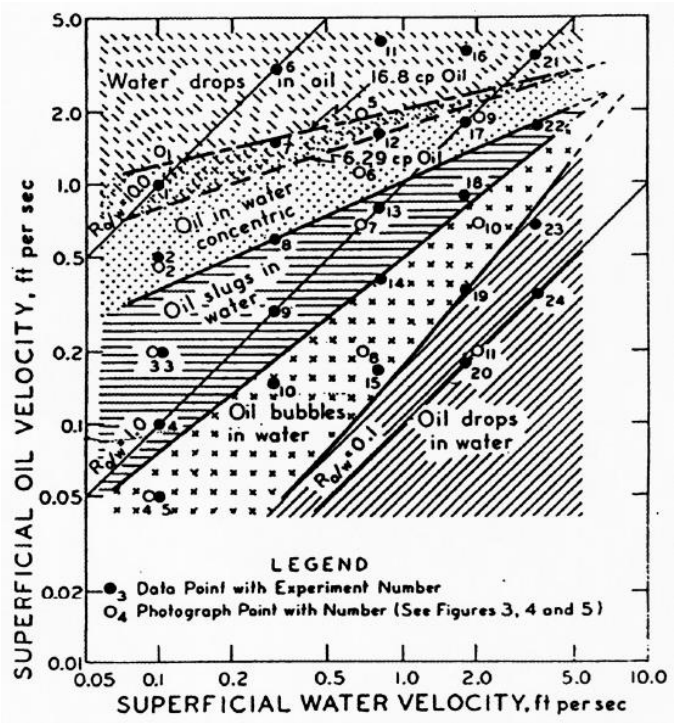

Figure 2.2: Flow patterns classified by Charles et al., (1961) in the flow of water with 6.26 cP and 16.8 cP oils at different superficial velocities in a pipe

Hewitt et al., (1970) and McQuillan et al., (1985) classified flow patterns created in a gas-liquid vertical upward flow as *bubble, slug, churn* and *annular* flows, displayed in Figure 2.3, which depend on the flow rates of the phases, pipe geometry, and flow conditions. In the figure, the gas flow rate is increased from left to right. Each flow pattern has different differential pressures, which depicts the importance of the flow patterns with increasing flow rates.

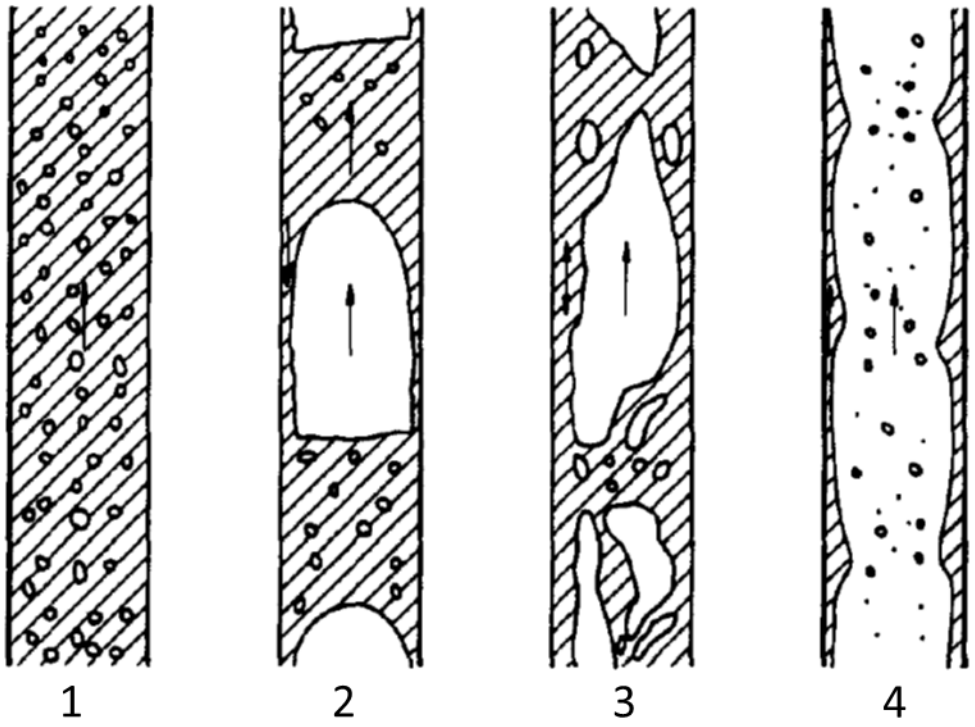

Figure 2.3: Flow patterns observed by McQuillan et al., (1985) in gas/liquid upward flow through a vertical pipe. 1. Bubble, 2. Slug, 3. Churn and 4. Annular

Brauner et al., (1992) concluded that the pipe diameter and fluid properties affect the nature of the flow regimes. Johnson, (1998) witnessed air-water flow patterns in a 1-inch diameter horizontal pipe and classified them into stratified, slug, annular mist and elongated bubble which were obtained at increasing velocities of air. Angeli et al., (1999) investigated flow patterns in oil (viscosity 1.6 cP and density 801 kg/m^3) and water flowing through horizontal 1-inch pipes made of different materials. They injected mixture of the phases with velocities ranging from 0.2 to 3.9 m/s. They observed that the flow patterns change with increase in velocity of the phases and were classified into four groups as illustrated in Figure 2.4. The first one is stratified wavy, where the phases are segregated due to the density difference between the phases with a disturbed interface between the two phases. The second one is stratified wavy with drops appeared near the interface. The third type is

the three layers' flow pattern' where the water and oil flow at the top and bottom of the pipe while the droplets are at the interface. The fourth one is referred to as stratified mixed where the faster phase is continuous and the other phase flows as drops with both phases dispersed in each other.

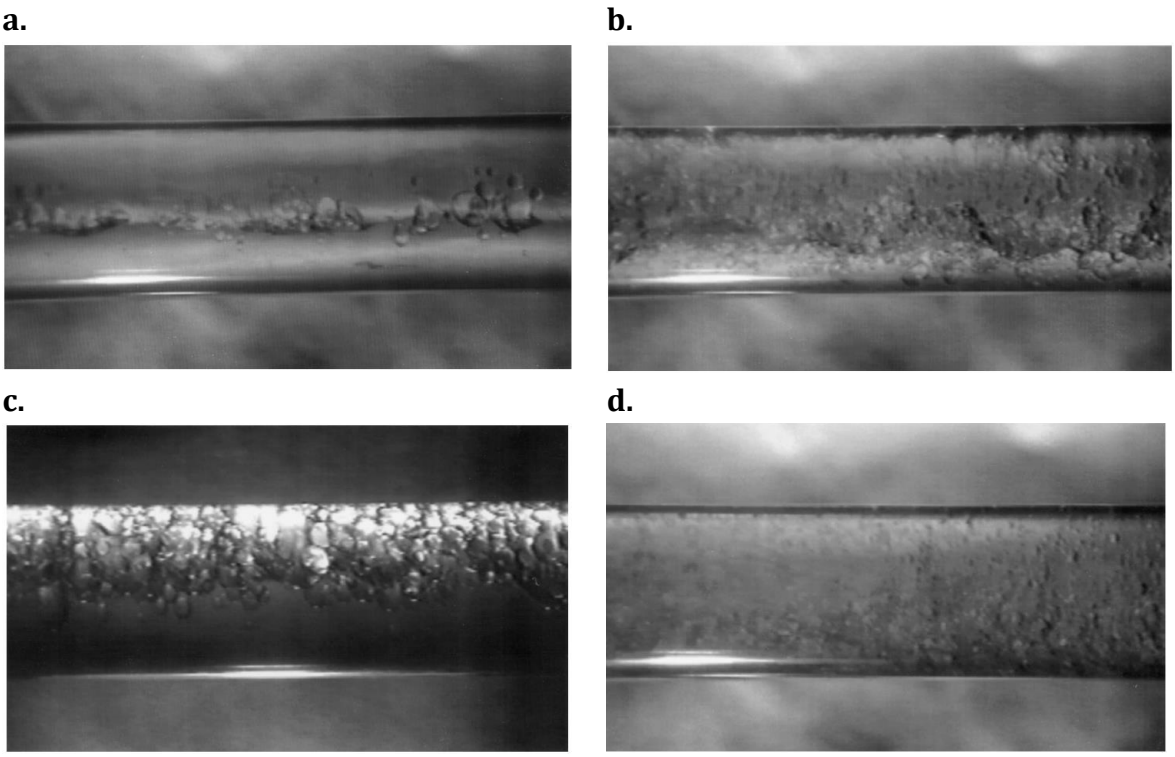

Figure 2.4: Flow patterns observed by Angeli et al., (1999) in an oil-water flow mixture at different velocities through pipe. (a) stratified wavy with drops flow pattern, (b) three layers flow patterns, (c) stratified mixed with water layer flow pattern, and (d) mixed flow pattern (Angeli et al., 1999)

2.4. Multiphase Flow in Narrow Gaps

Similar to multiphase flows in pipe, multiphase flow in planar gaps exhibits multiple flow regimes each of which occur at different flow rates of the phases and at different pressure gradients. A number of literature focussed on multiphase flow in fractures, most being on air/gas and water systems (Fourar et al., 1993a; 1995b; Persoff et al., 1995; Kneafsy et al.,

1998) and many more, while Katsuhiko, (1976); Reis, (1990); Jensen, (1992); Rossen et al., (1994); Dindoruk, (1995); Babdagli, (1995); Sumnu et al., (1996); Nicholl et al., (2001); Penny et al., (2005); Ayatollahi, (2005); Shad et al., (2008a), (2010b), and Al-Turki et al., (2012a), (2013b) studied liquid-liquid flow through fractures. Most of them focussed on the study of flow regimes created in the two-phase flow, which play a vital role for an efficient oil recovery.

Apart from flow structures, multiphase flow through narrow gaps were quantified through relative permeability curves and interference analysis of the phases (Scheidegger, 1974; Shad et al., 2010; Al-Turki et al., 2012). Relative permeability of a phase can be calculated by using Darcy's law. There are also some other models developed for calculating relative permeabilities for example X-Curve Model (Romm, 1966); Corey Model (Corey, 1954); Brokes-Corey Model (Brooks and Corey, 1964); Viscous Coupling Model (Fourar and Lenormand, 1998); Aguilera Model, (Aguilera, 1995); Homogeneous Single Phase Model (Delhaye, 1981); Lockhart and Martinelli's Model (Lockhart and Martinelli, 1949), and Shad and Gates Model, (Shad et al., 2010). Most of them depend on the saturation of the phases (volumetric fraction of phase in the total fluid volume) and pressure gradient.

2.4.1. Gas-Liquid Flow in Narrow Gaps

In case of two-phase air/gas-water flow in narrow gaps, a number of studies in the published literature evaluated flow regimes including Troniewski et al., (1984); Ali et al., (1991); Mishima et al., (1992); Wilmarth et al., (1993); Fourar and Bories, (1993, 1995); Polonsky et al., (1998); Indraratna et al., (2003); Sotiradies et.al., (2003) and many more. Majority of them focussed on the study of flow structures created in the flow of the phases and the overall behaviour of the multiphase flow. For example, Fourar and Bories, (1993) experimentally investigated air-water flow through horizontal smooth and roughened walled fractures and concluded that the flow structures change from bubble to chaotic with an increase in the flow rates. They explored the homogeneous single phase model (HSPM) where the two phases are represented as a single homogeneous equivalent phase and found

that this model yields a good fit to relative permeabilities as derived from the experimental data. In 1995, Fourar and Bories repeated their experiments for different gaps and concluded that the flow structures are consistent to those observed in their 1993 study.

Indraratna et al., (2003) conducted experiments on the air-water flow through rough walled fractures to analyse the flow using relative permeability analysis. They concluded that the sum of the relative permeabilities is less than unity, which implies phase interference. They developed a model, which was valid for two phase laminar and steady state flow.

Diomampo, (2001); Chen et.al., (2005); Chen et al., (2007); and Chima et al., (2012) also investigated air/gas-water flow through narrow gaps or fractures. Their work along the research carried out by Fourar et al., (1993, 1995) and Indraratna et al., (2003) is summarized in Table 2.1.

Table 2.1. Summary of air/gas and water flow through fracture or fractured porous media

Reference	Objectives	Fluids Used	Experimental Set up and Method	Findings
Fourar and Bories, (1993)	To study 2 Phase flow through a fracture	Air-water	• Horizontal gaps of contacted surfaces, 1mm and 1.1mm, (1fracture of smooth & 3 of rough surfaces each has 0.5 x 1 m area	• At low q_{gs}, bubbles flow patterns and high P_c while at higher q_{gs}, chaotic flow pattern, with no change in dp observed.
Fourar and Bories, (1995)	To analyse flow structures in different gaps	Air-water	• Gaps used: 1mm made of glass plates & fractures of different gaps from 2 bricks.	• Six types of flow patterns at different air flow rate. • Analytical equation developed for pressure gradient had a good agreement with Lochart-Martinelli model.
Indraratna et al., (2003)	To study 2 phase flow in rough fractures	Air - water	• Experimental and numerical modeling • Use of extended Darcy's law and k_{rs} concept	• Cubic law is not valid at high ∇P_s in tight and rough fractures and $\sum K_{rs} < 1$ at same pressures of water & oil • Hydraulic diameter and tortuosity decrease with roughness.

Reference	Objectives	Fluids Used	Experimental Set up and Method	Findings
Diomompo (2001)	To verify that k_r curves follow X-curve or Corey model.	Nitrogen/ gas-water	• Smooth and rough fractures of area 12" × 14" • The gas water ratios ranged from 10^{-1} to 10^{4}. • Added a fraction factor to Darcy's equation.	• Instability of pressure, no specific flow patterns. • At $P_s < 0.5$ psi, k_{abs} changed due to pushing the plates away by the fluids but at $P_s > 0.5$ psi k_{abs} const. • No match of results of smooth and rough fracture
Chen, (2005)	To model effects of phase changes and roughness on k_{rs}	Air-water, &steam-water	• Single fracture in Hele-Shaw Cell	• Strong interactions b/w fluids and fracture roughness • Steam-water's k_r, flow structures, and residual phase saturations is different than air water flow

Reference	Objectives	Fluids Used	Experimental Set up and Method	Findings
Chen and Horne, (2005)	To study effects of roughness on k_{rs} and to develop a tortuous model	Nitrogen - deionized water	• Water wet fracture - smooth, homogenously rough (HR) and randomly rough (RR). • Increasing flow of gas and decreasing of water • Used ime averaged data of pressure, flow rates and saturations for calculating kr_{avg}	• At high gas flow rates, more regular tortuous paths formed in HR fractures as compared to RR fractures. • The k_{rws} are irregular at high water saturations • Tortuous Channel Model (TCM) yielded good results • The flow structures depend upon saturations
Chen et al., (2007)	To analyse flow structures effects on k_{rs} & develop a model	Air water	• Air wetted single fracture • Validation of X-curve model, use of Stokes equation, Darcy's & locally applied Cubic laws.	• In no Δp, k_{rs}=saturations, 5 structures observed depended on the viscous forces and flow rate of the gas, and new model considers deviation from X-curves
Chima and Geiger, (2012)	To develop a model and validate Romm's equation	Gas-water	• Numerical model for k_{rs} developed for flow in parallel smooth walled fracture (1×0.5×0.001m) fracture in glass plates.	• Non-linear k_r curves obtained by the model, function of saturation and viscosities, yielded good match with experimental results than Romms's model

2.4.2. Liquid-Liquid Flow in Narrow Gaps

Flow in thin fractures is different from the flow in the big sized rectangular ducts, because in thin gaps, capillary forces often dominate over viscous forces, gravity, and pressure (Sadatomi, 1982). Liquid-liquid flow in gaps depend on the viscosities, densities, interfacial tensions between the phases, flow rates of the phases, and geometry of the fracture. To understand the behaviour of two-phase flow, it is important to analyse the structures created in the flow, which are mostly effected by viscosity, density (in vertical flow), flow rates, and other properties of the phases. In reference to the difference of the viscosities Hill, (1952); Chouke et al., (1959); Saffman-Taylor, (1958); Pan et al., (1996); Fernandez et al., (2005); Al-Turki, (2012), and many others studied liquid-liquid flow in thin gaps.

2.4.2.1. Oil - Water Flow Through a Thin Gap or Fractured Media

Majority of the studies on multiphase flow in narrow gaps have focused on gas-liquid flow. There are limited number of studies on liquid-liquid, and in particular, oil-water flow in narrow gaps (Romm, 1966; Pieters et al., 1994; Pan et al., 1996; Shad et al., 2008; Shad, 2009, and Al-Turki, 2013) are a few of them. A summary of key studies is provided in Table 2.2

In addition to flow regimes, many studies have examined relative permeabilities as a mean to understand the nature of multiphase flow in narrow gaps. This follows the application of relative permeabilities to study multiphase flow in porous media. For example, Meloney et al., (1997) analysed oil-water flow through vertical smooth walled fractures with 787 and 51 micron gaps. They determined that density and flow direction of the fluids are key parameters that affect relative permeability behaviour. They concluded that in large gaps, the relative permeabilities of the phases are not depended on their saturations but in narrow gaps, saturation plays a vital role in setting of the relative permeability of a phase.

Kulatilake et al., (2001) applied different normal stresses on a single fracture in core and investigated flow of fluids, effective area distribution, and fracture closure at each stress condition. They passed water through fracture at different flow rates and measured the fracture closure by using a profilometer. They observed that orientation of a fracture and nature of the fractures network affects the flow of fluids moving through it. They claimed that in rough walled fractures, the cubic law (based on planar Poiseuille's equation) is invalid since the phase channels are tortuous and the effective stresses are not uniformly distributed within. In addition, Putra et al., (2004) numerically simulated and experimentally observed oil-water flow through a single fracture within rock cores at different confining pressures. They applied 500, 1000 and 1500 psig confining pressures on fracture apertures with gaps of 56.4, 40, and 20 μm, respectively. In the case of simulation, they changed the pressures with flow rate of water equal to 5 cc/hr. They found that the relative permeability, calculated by Darcy's equation with the assumption of smooth fracture surfaces, are not correct because of tortuous flow induced from the surface roughness. Due to the surface roughness, simulations of the flow rates and differential pressures at same conditions are not identical. On the basis of this analysis, they added a friction factor to the calculation, which is a ratio of the absolute roughness to the hydraulic diameter. The equation developed considered roughness of the surface and the deviation of permeability from the cubic law. They concluded that there is a linear relationship between the fluid flow rates and fracture apertures. After including the friction factor for relative permeabilities in the simulation, their experimental results were consistent to the simulation. Therefore, they recommended that for rough surfaces, accurate modeling is possible provided the roughness is included in the model.

Table 2.2. Summary of oil-water flow through fracture or fractured porous media

Reference	Objectives	Fluids Used	Experimental Set up and Method	Findings
Romm, (1966)	To analyse fluids flow by k_{rw} and k_{ro}	Kerosene oil-water	• Smooth walled fracture	• K_r of a liquid is equal to its saturation • Sum of k_{rs} is equal to unity
Pieters & Graves, (1994)	To validate E. S. Romm's claim	Kerosene and water	• Kerosene oil saturated fracture (0.00254cm), Hele-Shaw Cell is used. • k_{rs} were calculated by Weldge's equation.	• k_{rs} of fluids are not linear with saturations. • K_{rs} are effected by different factors as the fracture behaves like a porous media.
Pan et al., (1996)	To find phase interference and their k_{rs} of phases	Oil and water	• Smooth walled horizontal fractures were used • Model-I: Injected fluids separately • Model-II: Injected mixture of fluids	• Phase interference is a function of capillary forces (F_c) • K_{rs} in Model-II < Model-I and their sum in both is < 1 • Water fingering and chaotic flow in Model-I at high q_o

Reference	Objectives	Fluids Used	Experimental Set up and Method	Findings
Shad et al., (2008)	To develop analytical model for k_r and study flow structures	Heavy oil and water	• Drainage and imbibition processes through vertical and horizontal, oil wetted smooth walled fracture	• Droplets creation & k_r variability is high at low q_s & Δp_s • Water fingering increased with increase in q_w • Their model fits well with experimental data but overestimated k_{ro} and underestimated k_{rw}
Shad et al., (2008)	To study motion and structures of liquid flowing in a vertical thin gap	Heavy Oil and Water	• Vertical Hele-Shaw Cell & horizontal flow • Gap = 0.0226cm. • Numerical model developed for k_{rs} considered Nc, μ_s ratio, gap & droplet sizes	• Small droplets, elongated droplets, churn and channel flow patterns observed. • Experimental results fitted well with the numerical models results.
Shad et al., (2010)	To analyse the fluid patterns changes and its effects on the transition limits	Heavy oil and water	• Horizontal and vertical Hele Shaw cells • Drainage	• Flow patterns change with flow direction, rates, k_r and geometry of the fracture and affected mass, momentum and energy exchange rates and pressure drop. • Velocity, shape and stability of discontinuous phase depend upon the μ_s, $\Delta\rho_s$, P_c and gap

Reference	Objectives	Fluids Used	Experimental Set up and Method	Findings
Al-Turki, (2012)	To studies frontal displacement in a single fracture at different inclinations and opposite directions flows	Light oil and Water	• Drainage and Imbibition in Hele-Shaw Cell (single smooth/rough oil wetted fracture) at 0, 30, 60 90 degrees inclination). • Model-I: gap = 0.0127 cm • Model-II: gap = 0.0254 cm • Model-III: gap = 0.0381 cm • Used Darcy's for K_{rs} at N_{crs} <10	**Smooth Walled Fracture:** • Viscous forces dominate P_c in high water flow Rates/larger gaps/low saturations. • Aperture size affected K_{rw} slightly but not k_{ro} • Observed droplet and channels in all models • k_r increased with gap, inclination and down dip flow. In imbibition k_{rs} in horizontal > up-dip and down-dip flows **Rough Walled Fracture:** • Roughness increased viscous forces, phase interference & k_{rs} • K_r increased with inclination and down-dip flow • $\sum k_{rs} > 1$ in down-dip vertical fracture due to gravity • In imbibition, k_r curves moved to higher S_w in up-dip inclined flow than horizontal flow

Reference	Objectives	Fluids Used	Experimental Set up and Method	Findings
Khosravi, (2012)	To find k_{rs} in a fracture with different flow rates and displacement mechanisms	Oil-water	• Discussed Darcy's law, modified Darcy's equation, Corey Model for steam-water, Brooks-Corey Model for steam-water in porous media at capillary pressure and X-curves for K_r in fractures.	• Gravitational forces are not important on lab scale but it does on field scale. • Recommended steady state method for finding K_{rs}. • Suggested methods for transferring lab data to the reservoir and different flow directions give different S_{wis} and different production curves

2.4.2.2. Oil - Surfactant Solution Flow Through a Thin Gap or Fractured Media

The volumetric sweep efficiency and recovery of oil from a fractured medium is low in water flooding especially from an oil-wet fractured reservoir due to the absence of capillary imbibition and viscous displacement of the trapped oil in the matrix (Babadagli, 2002).

New methods are needed to recover trapped oil from the fractured reservoirs. One of them is the use of surfactants in the displacing fluid (water). Surfactants act at the interfaces of oil and water by diverting its non-polar part to the oil phase and polar end towards the water phase. As a result, the interfacial tension between oil and water phases drops meaning that the energy required to deform the interface, falls. This aids in displacing oil from tight pores or converting a continuous oil phase to droplets hosted in the water phase thus raising the effective mobility and overall recovery of the oil. Porter, (1991) discussed the dispersion of oil into droplets in the presence of a surfactant and explained that surfactants occupy the interface of oil and water and facilitates dispersion of oil into water phase in the form of droplets.

The first field test of micellar solutions for improving oil recovery was carried out in Easter Illinois oilfields, USA in 1962 (Geogarty et al., 1972). There was no pre-water flooding and therefore, surfactant flooding was not effective. However, in another attempts with a pre-water flooded reservoir, they achieved reasonably good results. Surfactant flooding for oil recovery was analysed by a number of researchers and majority of them concluded that the surfactant solution reduces interfacial tension between the displacing and displaced fluids and converts the rock surface from being less hydrophilic to more hydrophilic (Rosen et al., 2012; Ferno 2012).

Park et al., (1994) experimentally examined the effect of a surfactant on air bubble and water droplets of 1.3 to 2.1 cm plan-form diameter with and without surfactant driven in silicon oil (viscosity 97 cP) through a gap of 17.8 × 86.4 × 0.9 × 1.8 cm dimensions (Hele-Shaw cell). They concluded that the surfactant effect on the air bubble's shape and movement is not significant but the effects of organic surfactant (sodium dodecyl sulfate,

SDS) on the water droplet's shape are substantial which in turn reduce the translational velocity of water droplets. Wilkens et al., (2006) proposed that interfacial tension should be considered for predicting flow patterns in multiphase flow through porous media and concluded that interfacial tension is reduced after adding surfactant (SDS) to air-water flow through a horizontal system. Lioumbas et al., (2006) studied the interfaces in two-phase flow through inclined pipe and concluded that surfactant delays the formation of wavy flow regime and reduces the pressure drop. Kianinejad et al., (2013) experimentally showed that SDS yielded 79%, LABS 66% and water 32% oil recovery from a horizontally laying model etched with inclined fractures. The oil recovery is increased by SDS from a matrix by increasing the breakthrough time of the solution. They observed that the fractures oriented perpendicular to the pressure drop yields greater recovery than the fractures oriented in the direction of the pressure drop. In other studies, Chen et al., (2001), and Hirasaki and Zhang, (2004) used surfactants for oil recovery from fractured media and concluded that the surfactants enhance oil recovery from the rock. Simulations carried out by Abadli, (2012) also showed that the oil recovery improves with the addition of surfactant in the water flooding.

Oil-surfactant solution systems have been extensively studied by Standnes et al., (2000); Chen et al., (2001); Babadagli, (2001); Seethepalli et al., (2004); Adibhatla et al., (2008); SyedAkram et al., (2011); Samanta et al., (2011); Hirasaki et al., (2011); Abdali, (2012); EIMofty, (2012); Leonce, (2012); Ferno et al., (2012); Kianinejad et al., (2013); Park et al., (1994); Hashimoto et al., (2008); Razmi et al., (2012), and so on. A summary of some research carried out in surfactant-oil flow examination, is listed in Table 2.3. In general, most studies are consistent and show that the addition of surfactants raise oil recovery from the host medium.

Table 2.3. Summary of oil-surfactants flow through fracture or fractured porous media

Reference	Objectives	Fluids Used	Experimental Set up and Method	Findings
Park et al., (1994)	To evaluate effects of surfactant on air bubble & water droplets	Air, water, oil and surfactant	• Hele Shaw cell (17.8 cm x 86.4 cm) of 0.9 mm and 1.8 mm gaps	• Surfactants do not affect the shape & movement of the air bubble but it reduces translational movement and changes shapes of the water droplet.
Babadagli, (2001)	To study of recovery from cores by water, surfactant & polymer	Light/heavy oil, surfactant & polymer	• Flooded water, surfactant & polymer through cores saturated with light and heavy oil • Analysed recovery of the oil for all fluids	• Got a greater and faster oil recovery with surfactant than water and polymer.
Feranndez et al., (2005)	To examine instability in Hele-Shaw cell dipped in/out of surfactant solutions	Different Concentrations of SDS Surfactant	• (64×15×0.031cm) fracture in Hele Shaw cell • The cell is dipped in and withdrawal of a surfactant solution. • Instabilities developed at pulling/dipping	• Fingering depends upon the cell velocity and concentration of the SDS surfactant • Observed drifting fingers, merging of fingers, air bubbles ejection and steady patterns

Reference	Objectives	Fluids Used	Experimental Set up and Method	Findings
Seethepalli et al., (2005)	To experimentally study the interaction of surfactants with a core of carbonate reservoir	Oil and surfactant solutions	• Flooded oil saturated core with different surfactants • Examined the effects of wettability, recovery and fluid properties	• Anionic surfactants (SDS etc) • changed wettability to intermediate water wet, • reduced interfacial tension • enhanced oil recovery by > 50% of the OOIP.
Adibhatla et al., (2008)	To find effects of surfactant on IFT, contact angle, k_{rs} & oil recovery	Oil and surfactant solution	• Wetted fractured carbonate reservoir rock core with oil • Flooded it with 0.05 wt% anionic surfactant.	• IFT & contact angle reduced, gravity drainage, K_r & oil recovery (50% of OOIP) increased • Change in the surfactant concentration effected IFT and wettability but not oil recovery

Reference	Objectives	Fluids Used	Experimental Set up and Method	Findings
Hashimoto et al., (2008)	To observe dynamic instabilities and flow patterns of a water droplet in hexadecane.	Oil, Tween20 and Span 80 surfactants	• Hexadecane saturated fracture in Hele Shaw cell (2-5 mm wide) are flooded by the surfactants in different experiments	• The droplet expanded side wise & broke into small droplets due to shear driven instability at low IFT • At low surfactant concentrations, the water droplets unite, 3% surfactant is needed to keep it intact • Instabilities depended on the fluids flow.
Samanta et al., (2011)	To examine oil recovery by flooding SDS and polymer.	99% SDS, PHPA Polymer	• Flood SDS (99%) surfactant and PHPA polymer through an oil saturated sand pack.	• 0.5PV-SDS increased oil recovery by 20% OOIP • PHPA after SDS flooding increased oil recovery by 2.78% OOIP more than surfactant.

Reference	Objectives	Fluids Used	Experimental Set up and Method	Findings
SyedAkram & Mamora, (2011)	To simulate effects of natural fracture on polymer-surfactant efficiency in a carbonate light oil reservoir.	Oil, polymer and surfactant	• Used DPDP model and CMG Stars for simulating chemical EOR processes from a 1/8 of a 20-acre 5-spot pattern • Water is injected before and after chemicals. Fracture is represented by zero P_c and straight line k_r and considered adsorption in the rock	• The chemicals increased viscosity and mobility of oil. • DPDO has drawbacks in fracture spacing, length, orientation and matrix flow in heterogeneous system. • Water-Surfactant polymer (WSP) flooding has 15 % more recovery than a base case model. • Polymer oil recovery is faster and more than surfactant • Surfactants in water lowered oil recovery at high S_{ws}
Razmi et al., (2012)	To investigate oil recovery from fractures	Heavy Oil, SDS, LABS and water	• Flooded different angled micromodels fractures in glass plates by SDS & LABS	• SDS yielded more recovery than LABS and water • Oil recovery increased with number of fractures and in orthogonal fractures than parallel

Reference	Objectives	Fluids Used	Experimental Set up and Method	Findings
Ferno et al., (2012)	To observe surfactant flooding through oil wet fractured carbonate core after two water floods.	Surfactant solution and oil	• 1mm gap in core is placed between two cores and is flooded for 24 hours with surfactant at 2cc/hour. • Average saturations is found from material balance by MRI signals.	• Surfactant increased water wettability, gravity effect and oil recovery, and reduced IFT. • S_w increases with increase in water injection. • Surfactant effected outlet & fractured core more than inlet and reduced ΔP requirement for water flooding.
Kianinejad et al., (2013)	Examine surfactant efficiency in fractures	Surfactant & oil	• 5 spot system in an oil wet fracture of different sizes and is flooded with SDS surfactant	• Surfactant increased breakthrough time & oil recovery. • Longer perpendicular to the ΔP fractures yield more oil

2.4.2.3. Oil and Polymer Flow in Fractures/Fractured Media

The use of aqueous polymer solutions for improving oil recovery due to mobility control and viscous fingering reduction has been widely reported. White et al., (1973) explained that different polymers behave differently but typically it is expected that polymer enhances viscosity of the injected fluids consequently lowers its mobility and its flow rate through the media. As a result, the effective permeabilities of both the aqueous (mainly) and oil (to a lesser extent) phases declines due to adsorption of polymer on the pore throats. They reported that polymer reduces brine permeability by 77%, whereas the oil permeability is reduced only by 6%. The results suggested that polymers reduce the water-oil ratio (WOR) and increase oil recovery.

Benham and Olson, (1963) conducted polymer-flooding experiments in two Hele-Shaw cells, one unpacked and other packed with glass beds. Their experimental set up and fingering observations obtained are shown in Figure 2.5. They measured saturation and velocity of fingers from images taken during their experiments by tracing them on large sheets. They noticed that the fingers do not originate from one point but evolve from different points in different directions. Frontal distortion rate increases linearly with position (up to 22.5 inches) and beyond this length, it starts to decrease due to diffusion that becomes prominent after about 24 inches of front movement. In the case of mobility ratio effects on fingering, they reported that finger growth increases with enlargement of the mobility ratio but their growth in the packed model is less than that of the unpacked Hele-Shaw model. The finger's growth rate has linear relation with the finger velocity but in the packed model, the finger velocity has less effect on its growth. In addition, the growth rate of the finger is not affected by the initial shape and frequency of the fingers. From decay of the fingers with distance, Benham and Olson expected that fingers would diminish in long cells. This has not been proven in the field scale reservoir operations where water breakthrough occurs.

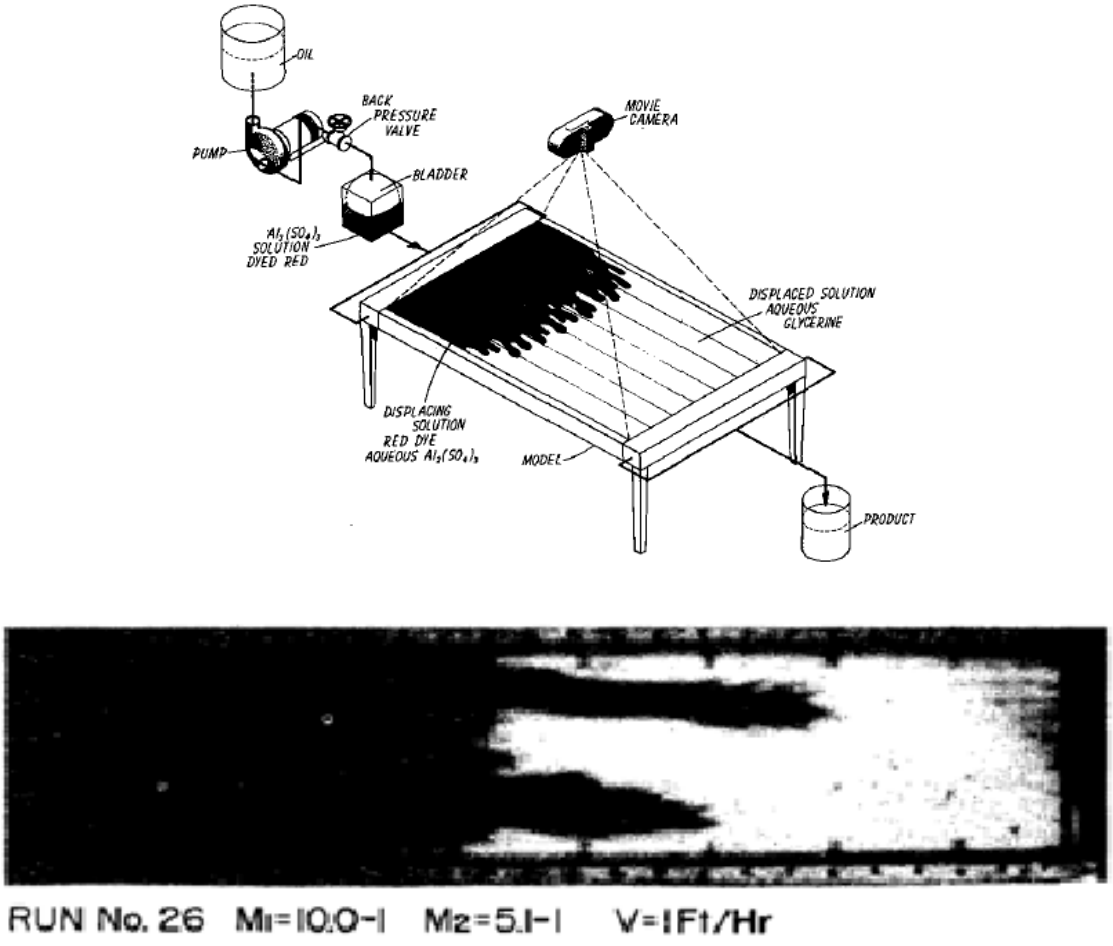

Figure 2.5. Experimental set up and fingering observed by Benham and Olson, (1963)

Mungan, (1977) studied the role of rheological properties, polymer concentration, and surface action of polymer on oil recovery in polymer solution flooding. As depicted in Figure 2.6, addition of polymer to the injected solution reduces the mobility contrast and consequently a stable displacement is resulted.

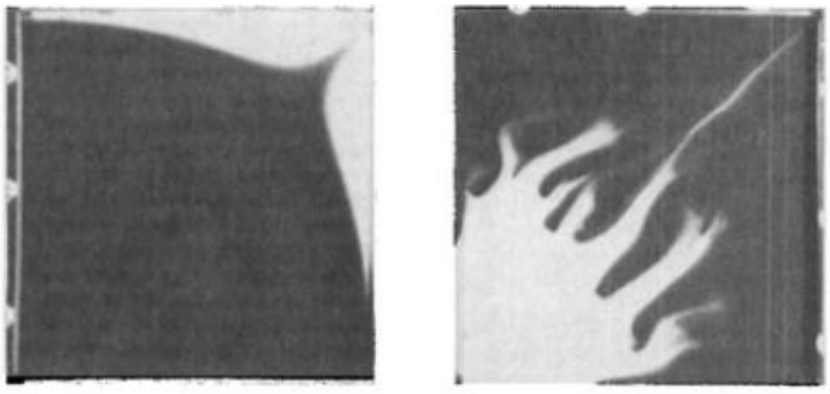

Favorable viscosity ratio, 3 (stable)

Un-favorable viscosity ratio, 30 (uns]table)

Figure 2.6: Interfaces and fingerings at two viscosity ratios observed by Mungan (1977): injection of polymer solution into the glycerin-wetted Hele-Shaw cell stabilizes the front

Lakatos et al., (1981), and Broseta et al., (1995) investigated polymer retention on the rock surface and its effects on the fluid flow. Daripa and Pasa, (2005) analytically and Donaldson, (1985); Wassmuth et al., (2009); SyedAkram and Mamora, (2011); Clemens et al., (2012), and Ying-jie et al. (2013) experimentally observed that polymer solution increases oil recovery from reservoirs. A summary of their work along other research is listed in Table 2.4.

Table 2.4. Summary of oil-polymer flow through fracture or fractured porous media

Reference	Objectives	Fluids Used	Experimental Set up and Method	Findings
Benham et al., (1963)	To study fingering and effects of various parameters and properties on the fingers	Less viscous mineral oil, polymer & glycerin	• A gap (1×4×0.0052ft)- Hele-Shaw cell. • Two models are prepared, one with smooth walled & other roughened walled. • Different mobility ratios	• Observed long fingers and less oil recovery in the first model, while short fingers and more recovery in 2nd. • Fingers growth rate and velocity is greater in open Hele-Shaw cell than packed cell. • No effect of finger's shape on its growth
Mungan, (1971)	To examine rheological properties of polymers	Polymer solution, light oil and glycerin	• Different concentrations of polymer adsorbed on silica sand pack samples of 20×2 in (dia) • Finger analysis in (26.8×26.8×0.006cm) gap in Hele-Shaw cell and a porous media of 12 x 12 x1 inch sandstone blocks were used	• Polyelectrolytes increased viscosity more than others • Viscous fingering behaviour has linear relation with its concentration due to x-linking of molecules. • Oil recovery increased by 84% & 28%for viscosity ratios of 0.03 & 30 respectively.

Reference	Objectives	Fluids Used	Experimental Set up and Method	Findings
Abrams, (1975)	To study changes in IFT, viscosity, flow rates after mixing chemicals with the water	Chemical dissolved water, oil	• A short core is wetted with water and then oil. • The oil is displaced with a chemical added water.	• Oil recovery increased with decrease in IFT, increase in viscosity by adding some chemicals. • Equation developed for efficient recovery considers viscous & capillary forces, viscosities ratios & required concentration and amount of polymer.
Daripa & Pasa, (2005)	To find an optimal /intermediate μ fluid b/w oil and water in the 2 and 3 layers systems	Polymer solution, oil and water	• In 2 layers fluids, injection of water and oil (middle layer has variable viscosity) • In three layers system, water is injected after polymers (polysolution) which has low viscosity at water side but high at oil side.	• Intermediate layer controlled the viscosity jump which controlled oil recovery • Viscous fingering reduced oil recovery considerably. • Polymer reduced IFT between water and oil and increases oil recovery
Wassmuth et al., (2009)	To observe polymer recovery from a rock sample	Polymer solution and oil	• A core sample taken from East Bodo reservoir is flooded with water cut upto 95% before polymer injection.	• The polymer enhanced incremental oil recovery by 20%OOIP after water flooding.

Reference	Objectives	Fluids Used	Experimental Set up and Method	Findings
Hematpour et al., (2011)	To study the effects of polymer types on the displacement of low viscous oil	Different polymers and less viscous oil	• 2 simplified glass micromodels were used. • The oil saturated cells were flooded with three different polymers with a constant flow rate of 0.0008 cc/min.	• Polymer reduced mobility of water • Hydrolyzed polyacrylamide (25%) yields more recovery than other polymers. • Low flow rates, yield less fingering and high recovery.
Ying-jie et al., (2013)	To analyse effects of pore structures on polymer and reservoir brine flooding in glass micromodel	Polymer solution with synthetic reservoir brine and oil	• They etched glass model (3×2×0.04cm) which represented a sample of an oil field. • The heterogeneous reservoir and 95% water cut was flooded initially by water at constant flow rate and then by polymer solutions. Polymer ($Mv=400x10^4$)	• Water bypassed the narrow channels and flew through the large pores/channels. • Pore throat ratio effected recovery more than the coordination number because higher PTR, means more heterogeneity, less CN and low recovery. • Polymer increased oil recovery in all models.

2.4.2.4. Nanocrystals and its Application in the Oil Industry

Nanocellulose is a nanocrystal that has explored for use in oil recovery processes. Azizi Samir et al., (2005) reported on the potentials of nanocellulose in plastic, automotive, railway, aircraft, furniture, and sports industries due to its renewable nature, availability, low cost, reduced energy consumption, strength and easy processability.

When nanocellulose is added to water, the aqueous phase viscosity rises and the interfacial tension between the aqueous and oil phases drops (Zhang 2010; Salas et al., 2014). It is observed that nanocrystals help in forming a stable emulsion (Zhang et al., 2010). The emulsion can control mobility of the phases and enhances oil recovery from the reservoirs (Zhang et al., 2010). Nanoparticles, due to their smaller sizes can easily flow through pore spaces in the reservoirs without much retention on the rock surface. Fleming et al., (2001); Habibi et al., (2010), and Xhanari et al., (2011) reported on stability of oil-water emulsions after adding cellulose nanocrystals to the system. Xhanari et al., (2011) concluded that the emulsion of water and oil in the presence of microfibrillated cellulose remained stable for more than one year and this stability is achieved by the network of microfibrillated cellulose that forms on the interface of oil and water. Zhang et al. further explained that wettability and adsorption of surfaces could be controlled by adding Silanol groups to either the nanoparticles or the surface, which alters the nanoparticle's surface to be more hydrophilic and increases stability of oil in the water emulsion. Due to higher stability of the emulsion, nanoparticles are mainly used in drilling industry. Zhang et al., (2010) prepared different emulsions with nanoparticles coated by different surface coatings and analysed their stability. They concluded that the emulsions with 0.5 weight percent or higher are stable remaining intact for time scales of order of months. They concluded that the average droplet size in the emulsion decreases with rise of the concentration of the nanoparticles. Some of the research conducted in the field of nanofluids/nanocrystals and its application in oil industry is discussed in Chapter 6 in detail, which is listed in Table 2.5. For the oil industry, the use of nanocrystals is reported by Lenk et al., (1992); Westland

et al., (1994); Wasan and Nikoloy, (2003); Rodriguez et al., (2013), Wu et a., (2012); Cheraghian et al., (2013); Rincon et al., (2013), and Lafitte et al., (2013). Majority of the published studies explored applications of nanocrystals for increasing stability of drilling fluids, reducing friction losses in casings and drilling tools, reinforcing geological formations, and increasing oil recovery.

Table 2.5. Summary of the nanocrystals use in the oil industry

Reference	Objectives	Fluids Used	Experimental Set up and Method	Findings
Lenk et al., (1992)	To study rheological properties of the drilling fluids	Nanocrystals in drilling mud	• Nano crystals are added to the drilling fluid	• The nanocrystals enhanced rheological properties of the drilling mud/fluids
Westland et al. (1994)	To study nanofluids for use in oil industry	Drilling mud	• The nanoparticles in mud are investigated for stability of the solution and formations	• Friction losses in casings reduced, geological formations became stronger with the nanocrystals.
Wasan and Nikoloy, (2003)	To study oil recovery from nanochannels	Oil-nanoparticles	• Nanochannels created and recovered oil from them	• The oil water flow increased through the nanochannels • The oil recovery increased
Rodriguez et al., (2013)	To study two types of nanocrystals in oil recovery	Drilling fluids, nanofluids	• Nanoparticles coated with polymer • Cores of limestone and sandstones are flooded with the nanofluids	• Polymer reduced its adsorption on surfaces • No slip condition is no more valid, due to movement of particles along the surface • Viscosity of the fluids and oil recovery increased

Reference	Objectives	Fluids Used	Experimental Set up and Method	Findings
Kalashnikova et al., (2011)	Microscopic study of oil water interface and nanoparticles emulsion	Oil, nanofluids	• Microscopic and SEM study of bacterial cellulose nanocrystals (70%) and oil (30%)	• Oil droplet remained in suspension for 7 months unless disturbed • Stability of interface increases and droplet sizes decreased with increase in concentration
Wu et al., (2012)	Microscopic study of nanoparticles movement in the oil-water on surface	Oil, water and nanoparticles	• Microscopically followed the nanoparticles • Study the oil/water interface	• Nanoparticles adsorbed on the clay surface. • Oil dispersed in the water • Oil recovery increased with increase in viscosity and reduction in interfacial tension.
Cheraghian et al., (2013)	To study nanofluids in drilling and recovery	Drilling fluids, nanofluids oil	• Two types of nanoparticles are used • They are added to the drilling fluids • Study its movement	• The nanoparticles increased oil recovery, altered the surface water wet, improved mobility, increased yield point of the drilling fluids and its velocity. • Suspension of drill cuttings in the mud increased.

Reference	Objectives	Fluids Used	Experimental Set up and Method	Findings
Lafitte et al., (2013)	To compare nanofluids and polymer	Nanofluids, oil	• Checked the use of nanofluids for oil recovery	• The nanofluids increased oil recovery same as polymer. • It could be a better replacement of polymers
Rincon et al., (2013)	To use nanocrystals for fracturing and cementations	Cement, water	• Addition of nanocrystals to the cement slurry • Addition of nanocrystals to the fracturing fluid	• The cement strength and packing increased • The fracturing efficiency increased • Viscosity increased with nanocrystals

2.5. What is Missing in the Literature?

Previous works on multiphase flows in Hele-Shaw cells are mainly focused on the displacement of one phase by another one. Most of these studies use Hele-Shaw cell as a visual porous medium prototype to understand enhanced oil recovery mechanisms using water and additives. On the other hand, for flow patterns studies, many experiments dealt with the gas-liquid, i.e. air-water, systems. Currently, there are a few studies reporting the flow structures in co-current flow of oil and other solutions, especially at various rates. This is of importance to oil recovery from fractured reservoirs, as there is a continuous feed of oil and formation water from matrix blocks and injected solutions into the fractures. Thus, simultaneous flows of oil-solutions encountered in fractures, narrow gaps between two matrix blocks. Furthermore, there are even less studies that examine the impact of new materials such as nanocrystal suspensions for oil recovery. Hence, we are motivated to perform through experiments to address such a gap in the literature.

In the research described in this thesis, the focus is on oil-water, oil-surfactant solution, oil-polymer solution, and oil-nanocrystals flow within a narrow gap. The research examines flow structures, phase interference, and microscale imaging to understand the dynamics of multiphase flow within a narrow gap, an idealized model of a fracture.

Chapter Three: Two Phase Flow of Liquids in a Narrow Gap: Phase Interference and Hysteresis

3.1. Abstract

Co-current flow of two immiscible liquids, such as oil and water in a planar fracture, exhibits nonlinear structures which become important in many natural and engineering systems such as subsurface flows, multiphase flows in lubrication joints, and coating flows. In this context, co-current flow of oil and water with variable rates is experimentally studied in a Hele-Shaw cell, various flow regimes are classified and relative permeabilities for the phases are analysed thoroughly. Similar to multiphase pipe flows, multiphase flow in planar gaps shows various flow regimes, each having different flow rate/pressure gradient behaviour. As well as recovering the known results in the immiscible displacements in Hele-Shaw cell where the fluid-fluid interface remains stable/unstable for favorable/adverse viscosity ratios, it is found that the co-current flow of two fluids with different viscosities results in three distinct flow regimes. Before breakthrough of non-wetting phase, i.e. water, a 'linear displacement' flow regime initially establishes at very low water injection rates. This stable movement turns into a 'fingering advancement' flow regime at high water flow rates and Saffman-Taylor instability develops in the direction of the flow. After the breakthrough, a 'droplet formation' flow regime is identified where the droplets of wetting phase, oil, are trapped in the water phase. For subsurface flow applications, we quantify these regimes through relative permeability curves. It is reported that as the water flow rate increases, the relative permeabilities and flow channels become smooth and regular. This behaviour of relative permeability and saturations shows dominance of capillary forces at low flow rates and viscous forces at higher flow rates. Variable injection rates provide the interface structures for both drainage and imbibition process where the wetting phase saturation decreases and increases respectively. It is shown that relative permeability curves exhibit hysteresis, thus the process is irreversible.

3.2. Introduction

Simultaneous flows of two immiscible fluids or miscible solutions in thin gaps find many applications in the natural sciences and engineering processes. For instance, one may refer to the subsurface flows of oil, water and gas in underground fractures (Wu, 2000; Craft et al., 2014; Kuchuk, 2015), multiphase flow of oil, water and gas in rock joints (Indrarantna et al., 2003) and multiphase flows in coating processes (Akita and Ito, 1980). There are several works addressing various aspects of multiphase flows in thin gaps. Fourar and Bories, (1993) examined the relationship between air and water flow rates, pressure drops, and phase saturations through horizontal smooth and rough walled gaps in glass plates. They observed that at low gas flow rates, flow structures such as bubbles develop and capillary pressure becomes prominent whereas at higher gas flow rates, the flow becomes chaotic. They also found that the flow structure changes with the flow rate of each phase but this does not affect the pressure change. They examined various available theoretical models which demonstrate the relative movement of each phase with respect to another through relative permeability, to find the best fit for their experimental results. They reported that the Homogenous Single Phase Model (HSPM), first described by Delhaye, (1981), matches the experimental results better than Lockhart and Martinelli's, (1949) model. Following that, Fourar and Bories, (1995) analyzed different flow structures formed during air-water flow through a single fracture with a gap of 1 mm. They repeated the experiments for different gaps and concluded that the flow structures change with the increase in gas flow rates as observed in pipes. They developed analytical-based criteria to calculate the pressure gradient given the flow rates of the liquid and gas phases, the result of which is in agreement with both Lochart and Martinelli's model and experimental results, especially for the laminar flow cases. Diomampo, (2001) experimentally and numerically investigated the relative permeabilities of nitrogen and water in a smooth and rough walled fracture. She added a friction factor to Darcy's equation to calculate the relative permeabilities. In the case of a smooth walled fracture, she observed a continuous pressure fluctuation due to unsteady/intermittent localized flow and that the relative permeabilities change significantly below 0.5 psi due to deformation of the bounding plates but remain constant at pressures more than 0.5 psi. Following that, Chen and Horne, (2005) studied the effect of roughness on relative permeabilities of

nitrogen and deionized water through a two-dimensional (2D) artificial fracture. They observed that at high gas flow rates, increasingly more regular tortuous paths form in a homogenously roughened fracture as compared to a randomly roughened fracture. They also concluded that the channel tortuosity of water and gas increases with decrease in their saturations. In another work, Chen et al., (2007) injected air and water through a single fracture to study the effects of flow structures on relative permeability. They reported that interference formation between the phases and the fracture can be considered as similar in behaviour, with respect to multiphase flow, to that of porous medium or pipe flow. The saturation and flow rate changes cause fluctuations of pressure, instability of the flow and creation of bubbles. At high gas and low water flow rates, tortuous gas channels form that have direct impact on the differential pressure. They developed an analytic model to consider tortuosity and deviation from the straight line relative permeability curves (X-Curves model, sometimes referred to the stick curve model) especially at tortuosity values less than unity.

Romm, (1966) was the first to perform kerosene and water flow through a smooth walled Hele-Shaw cell. His work was mainly focused on the understanding of underground oil and water flow through relative permeability analysis. He concluded that the relative permeability of a liquid in a fracture is equal to its saturation and that the summation of relative permeabilities is equal to unity. Chima et al., (2012) concluded that although Romm's model is a good guide but actually the relative permeability of a phase is not equal to its saturation. In another work, Pieters and Graves, (1994) assessed the validity of the Romm's, (1966) observation of near linear relative permeability curves for co-current kerosene and water flow through a Hele-Shaw Cell and concluded that the curves are not linear in case of kerosene and water flow through porous media. Moreover, Lee et al., (1996) analyzed the interference and relative permeabilities of oil and water in single, smooth walled, water-wet, horizontal fracture of 45 to 150 μm size, in a series of experiments. At low oil injection rates, they observed oil drops of varying sizes dispersed in water. A gradual increase of the oil injection rate increased the size of the oil drops. At high oil flow rates, water flow channels in the form of fingers in the continuous oil phase. In the second series of experiments oil and water were mixed before injection, no major flow pattern changes occurred except uniform distribution of the phases in the fracture with the formation of

multi-channels of oil and water. They concluded that due to phase interference, the sum of the relative permeabilities for two phase flow is less than unity for a smooth-walled fracture and that the capillary forces are not dominant. They found that in fracture of 45 to 150 μm size, the viscosities and the fracture gap do not affect the characteristics of the two phase flow. Lee and Kang, (1999) performed oil displacement experiments in fractures created using two Berea sandstone rock samples. They reported that at low water injection rate, oil recovery in both samples is similar but at higher injection rate, oil recovery decreases due to water fingering and bypassing of some pores by water.

Multiphase flows in narrow gaps were also analyzed by Shad et al., (2009) for the case of water and heavy oil with the viscosity of 30 cP. The authors developed an analytical model for relative permeabilities of heavy oil and water in a single fracture and studied the droplet formation and changes of relative permeability with pressure drop, water fingering and flow rates in a horizontal and vertical fracture. They also studied properties affecting flow patterns and flow regimes during heavy oil and water flow through the single fracture. In a continuing work, Shad, (2010) reported various flow structures such as small bubbles, elongated bubbles, churn flow and channel flow at different flow rate ratios in a vertical microchannel. Al-Turki, (2012) studied the effect of fracture roughness, fracture inclination and flow directions on relative permeabilities of water and oil in Hele-Shaw Cells with various gaps. They concluded that viscous forces are stronger than capillary pressures in higher water flow rates, larger gaps, or low water saturations. The results showed droplet, mixed flow patterns at low water flow rates and stable channels at higher water to oil flow rate ratio, while the engulfed oil droplet does not move.

In spite of the important application of co-current immiscible fluids in narrows gaps such as fractures, there are few related studies mostly focusing on the oil and gas engineering applications through relative permeability measurements. In this study, we perform drainage and imbibition experiments on the co-injection of oil and water through a Hele-Shaw cell and study the fluid interface structure. Flow rates are variable, so many scenarios in terms of fluid-fluid interactions can be formed. Interface development mechanisms at various relative injection rates of oil and water are distinguished. The data is analyzed for subsurface flows through relative permeability

curves. Moreover, we reverse the injection process to study the effect of saturation history on the flow structures.

The chapter is organized as follows. First, we introduce the experimental methodology and materials. Then we present a brief theory behind the multiphase flows in fractures and porous media. Experimental results are presented and discussed in Section 3.5 followed by the conclusion.

3.3. Methods and Materials

Fracture flow experiments are performed in a Hele-Shaw cell: two parallel plates with a narrow gap which represents a porous medium. Figure 3.1(a) depicts a schematic of the Hele-Shaw apparatus with the total flow area, i.e., length by width of 66.5 cm by 14 cm, respectively. The observation area, i.e., the domain in which we captured the flow structures, is 35 cm long and 14 cm wide. A nominal fracture gap of 0.397 mm is used in all the experiments because fractures in natural rocks bearing petroleum are typically from 0.015 to 1.8 mm in range (Romm, 1966; Raven et al., 1988; Park et al., 1994; Fourar and Bories, 1995; Hashimoto et al., 2008). The thin gap in the Hele-Shaw cell, as shown in Figure 3.1(b), is created by placing a 0.397 mm thick shim stock between the two bolted 4.5 cm thick each Plexiglas plates. To distribute the phases across the width of the cell, they are injected into a distribution chamber at the upstream end of the cell through three injection ports. Similarly, fluids are removed from the cell through a distribution chamber containing three outlet ports which discharges the fluids to atmospheric pressure. The injection and production distribution chambers each consist of a 1 mm deep, 3.8 mm wide, and 12.7 mm long rectangular opening into which the oil and water are injected through three ports. For the injection chamber, water is injected through the central port and oil through the outer ports.

To ensure that the interfaces are clearly visible, lights are placed under the cell and a colorless mineral oil is passed through the fracture with de-ionized water dyed with red food color (Chefmaster, Product No. C5001-SR). A thermocouple is placed at the lower surface of the lower plate to monitor temperature of the cell. Images of the fluids patterns are taken by a charged coupled device camera (Model scA1000-30gc, Basler) which are then processed to calculate sequential phase saturations, i.e. the areal fraction

of the image occupied by each phase. The properties of the oil and water are listed in Table 3.1. Two solid state pressure transducers (Model PX 209-015G5V, Omega Environmental Inc.) are placed in the pressure ports within the lower plate. The area of interest over which phase saturations are calculated is situated between the two pressure taps, and is equal to 35 cm by 14 cm, as shown in Figure 3.1(c). Oil and water are injected into the cell by the two injection pumps (Models 305 and 307, Gilson Inc.). Pulsation from the Gilson 305 pump is dampened by passing the exit flow through a long flexible tube and a circular water tank 43 cm long and 11.5 cm in diameter. A built-in pulsation dampener reduces pulsation in the Gilson 307 pump. The pumps, thermocouple, camera and two pressure transducers are connected to the data acquisition system to record flow rates of each phase, inlet and outlet pressures, temperature and images at each time step which are further processed to calculate the saturation of each phase.

(a)

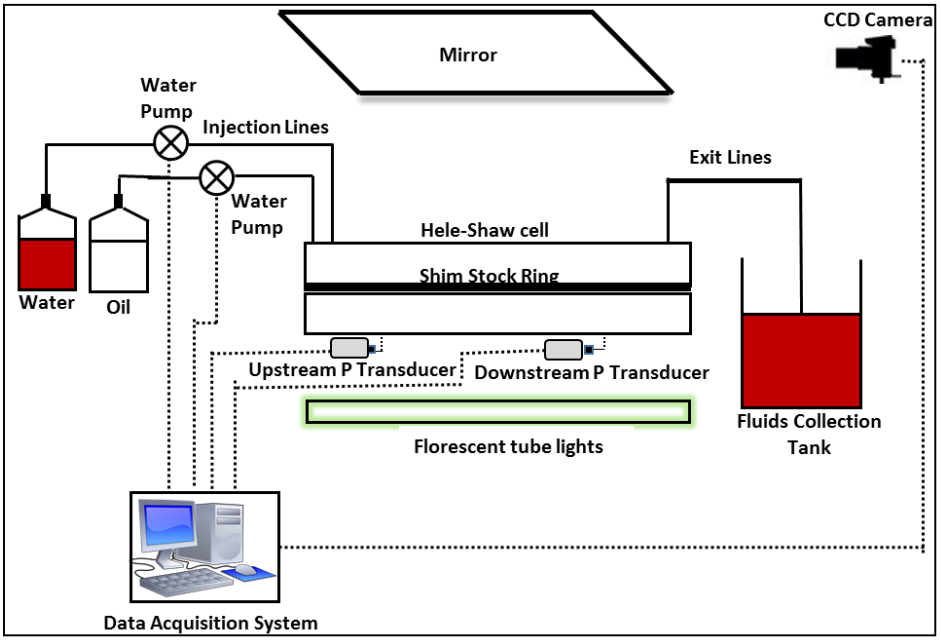

(b)

(c)

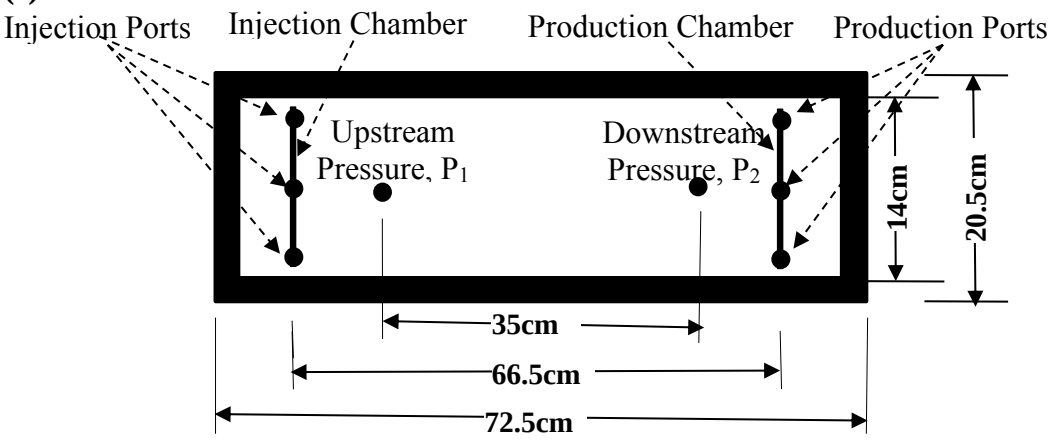

Figure 3.1. (a) Experimental set up (adapted from Al-Turki, 2013, with the permission of the author), (b) side view of the cell showing the shim stock and its thickness, and (c) top view of the cell showing area of interest and inlet/outlet ports

Table 3.1: Properties of oil and water used in the experiments

Property	Oil (Marcol 7)	De-ionized Dyed Water
Viscosity at 22.46°C (mPa.s)	20.236 ± 0.001	1.0997 ± 0.001
Density at 22.46°C (kg/m^3)	847.0 ± 0.0002	998.85 ± 0.0002

3.4. Theory

3.4.1. Single Phase Flow: Evaluation of Hydraulic Gap and Absolute Permeability

Under pressure-driven flow, steady rectilinear flow of a Newtonian fluid phase through a gap is given by planar Poiseuille's law (symbols defined in nomenclature):

$$q = \frac{Wb^3 \Delta P}{12 \mu L} \quad (1)$$

Equation 1 is used to determine the hydraulic gap, b, if all the other variables are known. Single-phase (water) experiments are conducted with results displayed in Figure 3.2. The linear relationship between differential pressure and flow rate indicates that the deformation of the gap versus pressure gradient is negligible over the pressures examined in this study. The slope can be used to find the hydraulic gap and absolute permeability of the fracture. From calculations of single phase (water) flow through the fracture at different flow rates, the hydraulic gap is found to be equal to 0.2973 mm. This is lower than the nominal gap (0.397 mm) established by the thickness of the shim stock. The reason for this is the compression exerted by the Hele-Shaw cell bolts located at the outer edges of the cell. From a comparison of Darcy's law with Poiseuille's equation, the absolute permeability of the gap is calculated by:

$$k = \frac{b^2}{12} \quad (2)$$

With hydraulic gap equal to 0.2973 mm, from Equation 1, the absolute permeability of the gap is equal to 7.365×10^{-9} m^2 calculated by using Equation 2.

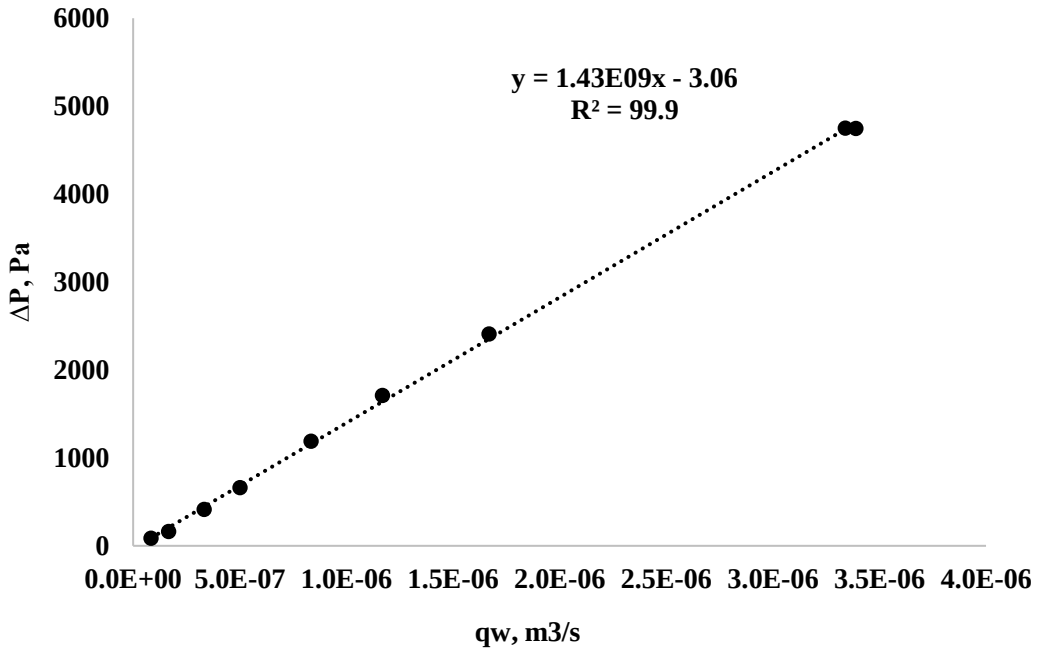

Figure 3.2: Relationship of q_w and ΔP to find hydraulic gap and absolute permeability of the fracture in single-phase flow

3.4.2. Two Phase Flow

In the two-phase flow experiments, oil is injected through the two outer injection ports whereas the dyed de-ionized water is injected through the central injection port. In the drainage process, the wetting phase saturation, i.e. oil, in the cell decreases with time, the water flow rate is step wise increased from 0.025 to 9 ml/minute while the oil flow rate is kept constant at 0.5 ml/minute. At 9 ml/minute water flow rate, the oil flow rate is reduced step by step from 0.5 to 0.025 ml/minute while the water flow rate is kept constant.

In the case of imbibition where the wetting phase saturation increases with time, the injection rates of the fluids are interchanged i.e., the oil flow rate is increased and the water flow rate is decreased. In both drainage and imbibition processes, inlet and outlet pressures, temperature, flow rates and saturations of each fluid are acquired by the data acquisition system at each time step (≈ 4 minutes).

If we assume that Darcy's law can be extended to multiphase flows in porous media, we can define the effective flow pathways available to each phase by the means of

relative permeability. One should note that the multiphase extension of Darcy's law has been widely used for the case of continuous flow of each phase. In the present work, as we describe below, we have situations where one phase is discontinuous and is carried through the other one. However, we assume extended Darcy's law holds and relative permeability curves for both oil and water are calculated by:

$$k_{ro} = \frac{q\,\mu_o}{Ak\left(\frac{\Delta P}{L}\right)} \tag{3}$$

$$k_{rw} = \frac{q_w\,\mu_w}{Ak\left(\frac{\Delta P}{L}\right)} \tag{4}$$

The relative permeabilities of the phases reveal how much each phase is interfering with the other phase – the lower the relative permeability of a given phase *i*, the greater the interference effects of the other phase on phase *i*. If the relative permeability is equal to unity, this means that the phase is flowing with effective permeability equal to the absolute permeability of the gap. We use the relative permeabilities as a tool to quantify the various flow scenarios in oil-water co-current flows in the Hele-Shaw cell.

3.5. Results and Discussion

Drainage is the process, where saturation of the wetting phase i.e., oil in the cell is decreased with time as the water is injected at increasing flow rate and the oil injection rate is reduced.

Figure 3.3 displays the averaged oil and water relative permeability curves for three replicate experiments operated in the drainage process. The error bars mark one standard deviation from the mean value. The average standard deviations of relative permeability for water and oil are ±0.018 and ±0.033, respectively. The figure reveals that the overall trend of the oil phase relative permeability curve is linear up to the cross-over point, defined as the point where the oil and water phase relative permeabilities are the same. After the cross over point, the water flow rate is kept constant at maximum rate (9 ml/minute) while the oil flow rate is reduced. The

reduction of the oil flow rate does not alter the linear behaviour of the water phase relative permeability curve and the linear behaviour persists until the water saturation reaches greater than 0.85. However, beyond the cross-over point, the oil relative permeability drops below the overall linear trend exhibited by the oil relative permeability above the cross-over point. The results show that the experiments are reproducible and that the water relative permeability is linear whereas the oil relative permeability curves exhibits two parts separated by the cross-over point.

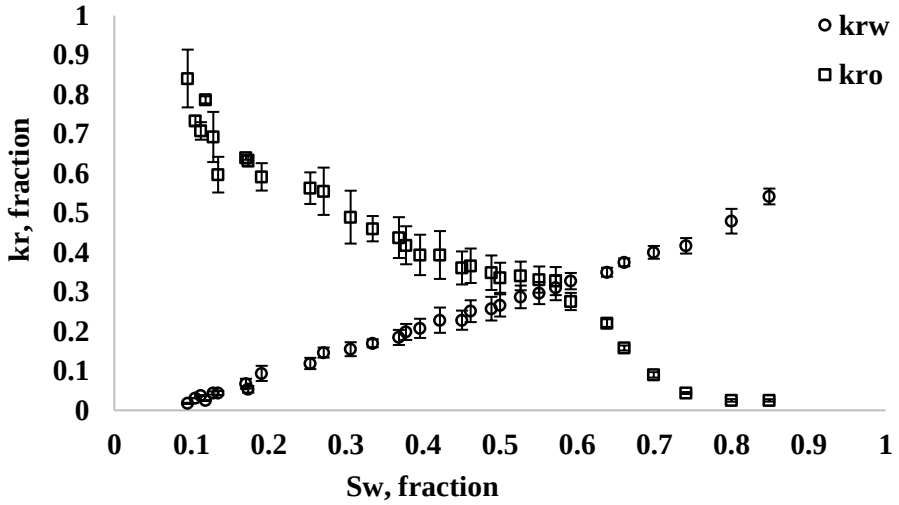

Figure 3.3: Averaged relative permeability results from three replicate experiments. The error bars show the standard deviation of the experiments

Figure 3.4 illustrates the co-current flow of oil and water in the Hele-Shaw cell through relative permeability curves plotted for each phase against water saturation in the drainage and imbibition processes in an experiment. For each step of flow rate, except Images 1 and 7, all images are recorded after the flow reached a quasi-steady behaviour – in other words, the pressure drop, oil and water flow rates, and saturations are stationary. The water phase relative permeability stays linear (Images 2 to 6, Figure 3.4), whereas the oil relative permeability is more scattered and appears to have a cyclic characteristic to its behaviour especially when the water saturation is below 0.55 (Images 1 to 4, Figure 3.4). This is due to the nature of the flow i.e., the oil phase is largely discontinuous within the water phase and thus it not only flows continuously at the edges of the water channel but also has droplets which produce a more scattered oil relative permeability. The overall trend of the oil phase relative permeability curve is

linear up to the cross-over point but it drops below the linear after the cross-over point (Images 5 and 6, Figure 3.4). This phenomenon is also observed in the situation when the oil flow rate is reduced and the water injection rate is constant at maximum rate (9 ml/minute). The reduction of the oil flow rate does not alter the linear behaviour of the water phase relative permeability curve however, the water relative permeability tends to become more scattered as water saturation increases (Images 5 and 6, Figure 3.4).

Imbibition process is started at the end of the drainage process when the wetting phase saturation reaches its minimum value. In imbibition, the injection rates of the phases are reversed i.e., the wetting phase saturation increases as we inject oil at increasing flow rate while the water injection rate is reduced. We investigate the reversibility of the process and hysteresis through qualitative analysis of images and also by evaluating the relative permeability curves as depicted in Figure 3.4. The water relative permeability curve obtained through imbibition has the same linear characteristics as its drainage counterpart. As there is already an established thick channel for water flow, the water relative permeability values resulted from the imbibition and drainage are very close. Only at low water saturations (Images 11 and 12, Figure 3.4), the imbibition process returns slightly lower values of water relative permeabilities than the drainage one. It means that there are fewer pathways available for the water to flow. We noted that since oil is more viscous than water, the oil-water interface on the water channel side is stable in the imbibition process; the water channel become stable, i.e. no more side fingering or oil droplet formation, and its width decreases. On the other hand, relative permeability of oil in the imbibition process especially before the breakthrough (Images 7 and 8, Figure 3.4) is higher and structurally different from the drainage. This is exactly the result of co-current injection of oil and water with a stable oil-water interface. Especially at high oil saturation, oil is forming its own flow pathways with less interference from the water phase (Images 11 and 12, Figure 3.4). Thus, the relative permeability curves exhibit hysteresis showing the importance of direction of increasing wetting phase saturation in setting the relative permeability curves.

Because the injection chamber has water injected through the central port and oil injected through the two outer ports, at low flow rates, the water tends to the central parts of the Hele-Shaw cell and the oil tends to the outer parts of the cell (Images 1, 2, 11, 12, Figure 3.4). However, at higher flow rates, a fraction of the oil is hosted in the

aqueous phase as droplets (Images 5,6,7,8, Figure 3.4). The overall observations of the results are independent of the injection pattern since the water and oil are well mixed within the distribution chamber.

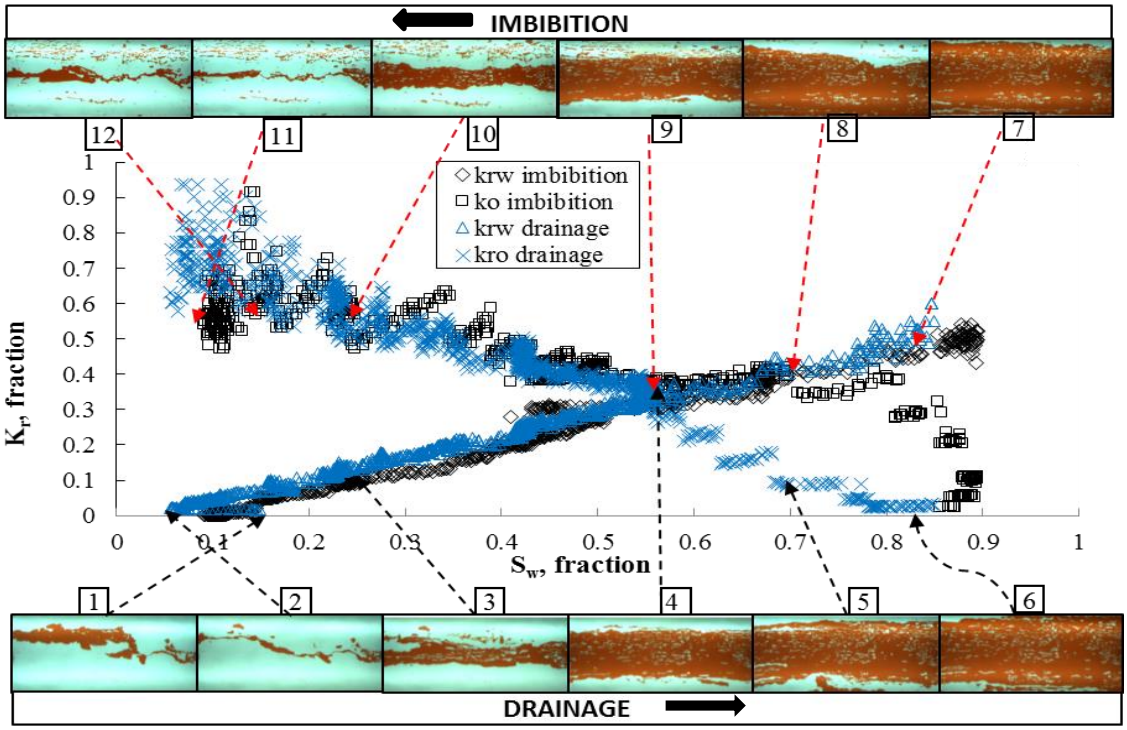

Figure 3.4: Relative permeability curves for water and oil in drainage and imbibition processes. Oil is the wetting phase. Water saturation drops initially in the both processes. Values of q_o and q_w respectively are given for each image in ml/min: Image 1: 0.5, 0.2; Image 2: 0.5, 0.3; Image 3: 0.5, 2; Image 4: 0.5, 9; Image 5: 0.1, 9; Image 6: 0.025, 9; Image 7: 0.2, 9; Image 8: 0.4, 9; Image 9: 0.5, 8; Image 10: 0.5, 2; Image 11: 0.5, 0.25; Image 12: 0.5, 0.15

Figure 3.5a-d display the time evolution of the water plume as it extends through the cell. Figure 3.5e-j display quasi-steady flows as the water injection rate is raised from 0.2 ml/minute to 3 ml/minute at constant oil injection rate equal to 0.5 ml/minute. Initially, the cell is completely filled with oil (the transparent phase in the images) as shown in Figure 3.5a. The initial injection rates of oil and water are equal to 0.5 and 0.1 ml/minute, respectively. At these injection rates, the volume of water accumulates in the cell as shown in Figure 3.5b-d and at the time of breakthrough, it reaches to a value of about 0.15 (Figure 3.5e). After breakthrough, the water channel thins as displayed in Figure 3.5f. The water saturation achieves a minimum value of 0.056 after

the water injection rate is raised to 0.3 ml/minute (Image 2 in Figures 3.4 and 3.5f). However, after this point, the channel grows as we increase the water flow rate with the continuous formation of isolated oil droplets. Figure 3.5g depicts that as the water flow rate is raised to 1 ml/minute and reaches a quasi-steady state, the water channel starts to thicken and consequently the water saturation rises. As the water channel thickens, it starts to engulf oil droplets and the complexity of the interfaces, both within the channel and the main channel periphery increases.

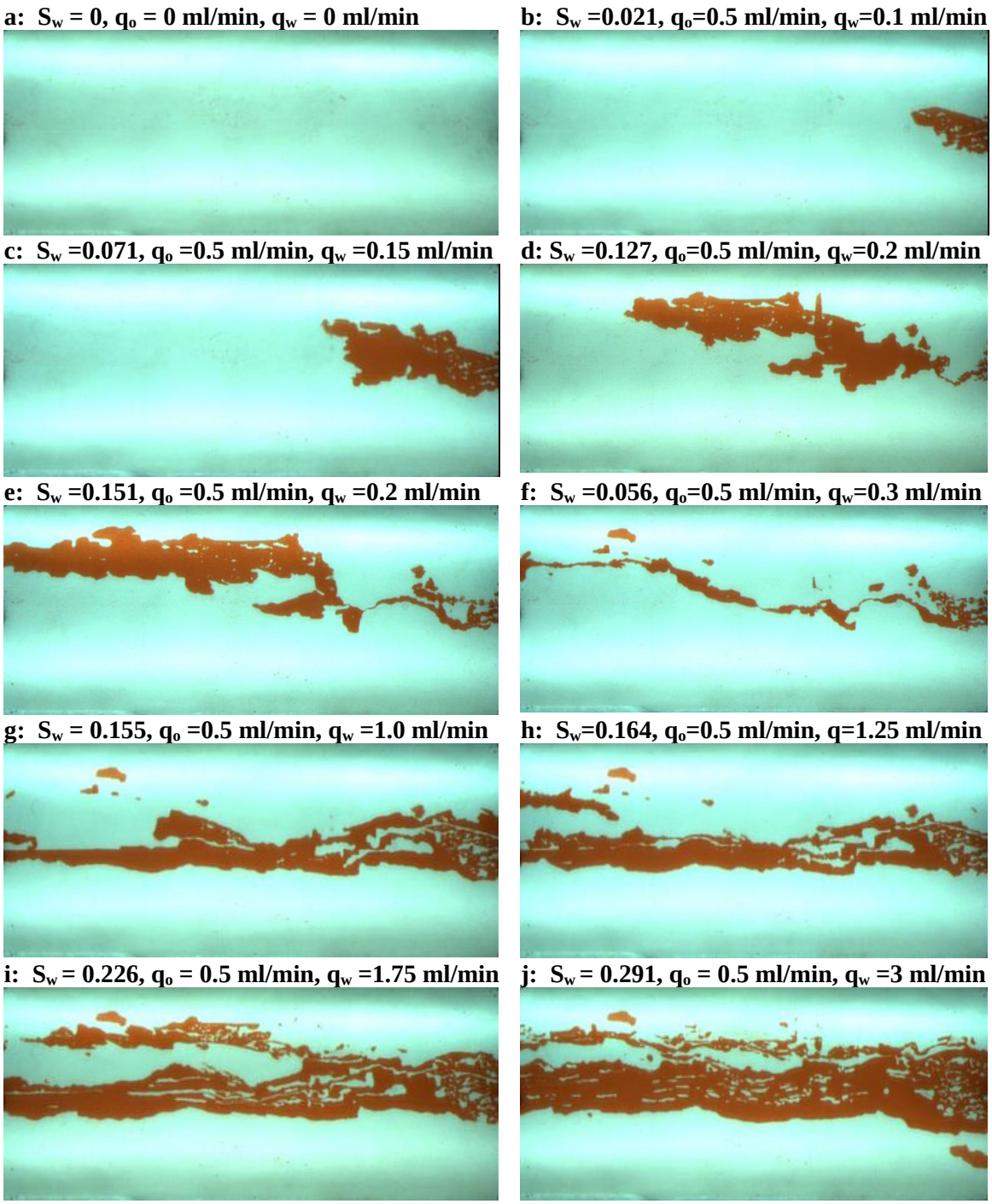

Figure 3.5: Evolution of flow state as water injection rate is increased to 3 ml/min at constant oil injection rate equal to 0.5 ml/min. The flow direction is from the right to the left side of the images

After the water injection rate is raised to 1.75 ml/minute, as shown in Figure 3.5i, the water channel is now wider and consists of several thinner channels with elongated oil droplets hosted within. The moving water is exerting shear on the oil and thus is extending the oil drops in the flow direction. At still higher water flow rate of 3 ml/minute, the lengths of the oil droplets are smaller – the elongated ones that existed at lower water injection rate are now being broken into smaller elongated droplets. Moreover, the high water flow rate and low oil rate results in an unstable water-oil interface on the sides of channel, hence, fingers with small wavelengths generate lots of tiny droplets. Figure 3.6 demonstrates the mechanism of droplet formation, and the development of flow regimes. Three flow regimes can be distinguished in the oil water immiscible displacement in the Hele-Shaw cell. Figure 3.6 schematically depicts these flow regimes. Initially, the oil is displaced with water at low injection rates $(q_w \leq 0.15\ ml/minute)$. At this stage, an almost planar interface is developed in the form of a wider finger in the middle of the cell; as demonstrated in Figure 3.6A, i.e. linear *displacement* flow regime. Note that we co-inject oil and water and water is only injected through the middle port. We expect to see a wider finger instead of a piston like displacement of oil along the cell cross-sectional area. As the water injection rate increases$(q_w = 0.2\ ml/minute)$, we pass the threshold velocity for the development of the frontal instability also referred to as the Saffman-Taylor instability, as depicted in Figure 3.6B, i.e. the fingering *advancement* flow regime. The previously thick and elongated finger starts to deform with one advancing finger at the tip and some secondary side-fingers. As most water is fed into the previously formed wide finger, which now acts like a large unstable and deformed interface, the base of the finger tends to contract. Once the advanced tip of the front reaches the production chamber, most of the water from the thick part of initial planar displacement regime is discharged. Therefore, after breakthrough, the wider finger (channel) of water disappears and is replaced by a narrow pathway for the water movement.

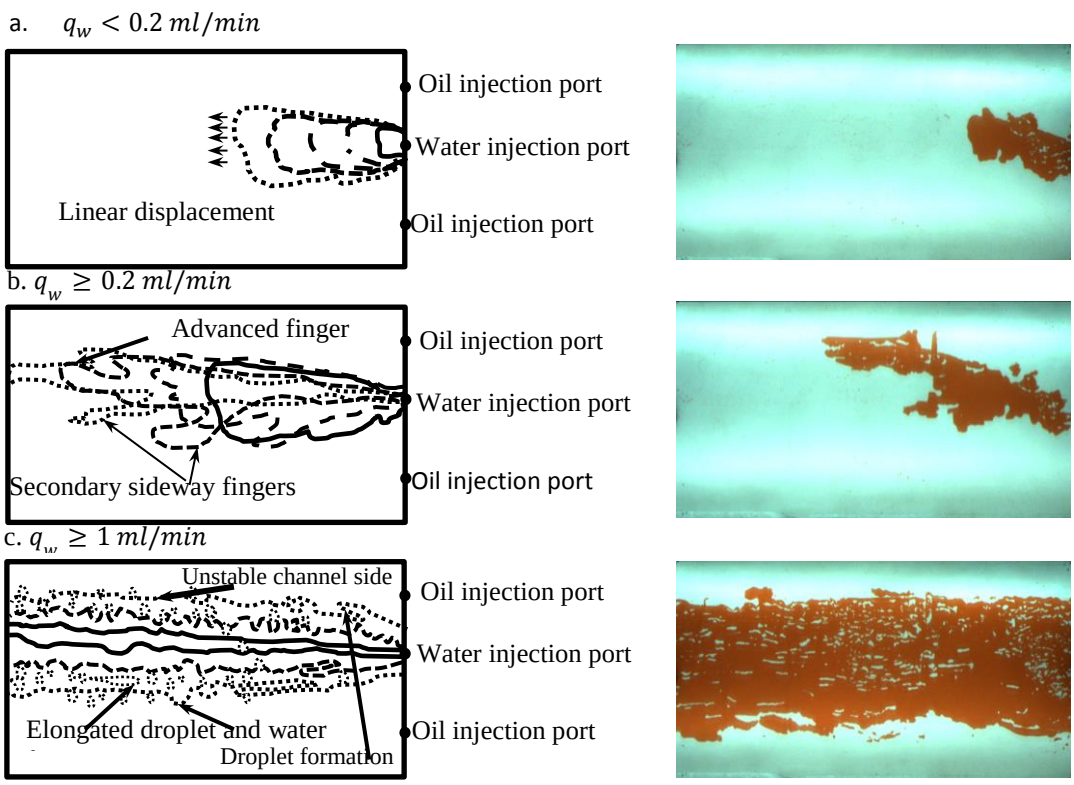

Figure 3.6: Schematic of various flow regimes development in the immiscible displacement of oil by variable water injection rate (A) linear displacement flow regime (B) frontal instabilities in the form of fingering advancement before breakthrough (C) frontal instabilities in the form of fingering normal to the flow and droplet formation after breakthrough

We speculate that the water phase contraction after breakthrough is due to capillary forces which tend to reduce the interfacial area. Thus, the complexity of the interface and its length decreases after breakthrough. This is evident by comparing Images 1 and 2 in Figure 3.4 and the observation of Figure 3.7 which shows the evolution of the water saturation with the passage of time. The water saturation rises from 0 (Figure 3.5a) to a peak value of 0.151 (Figure 3.5e) and then declines to a minimum value equal to 0.056 (Figure 3.5f) after which it rises regularly with increase in the water flow rates (Figure 3.5g and onward). The initial behaviour of the water channel to form a thin connected channel across the cell and consequently reduced water saturation has a severe implication for displacement of oil from fractures by water. If the water flow rates were kept constant, the volume of oil displaced from the gap would be small since the water channel once established only grows in thickness if the water flow rate rises or oil flow rate declines. The results suggest that effective displacement of oil from the fracture

will require a wide water flow channel before breakthrough and ever growing water flow rate after breakthrough of water. In fact, after the water breakthrough, most of the oil in the Hele-Shaw cell is bypassed. However, as we increase the water flow rates($q_w > 0.2\ ml/\text{min}$), more oil is displaced by the sidewise expansion of the water finger while some of the oil is entrapped in the form of (mostly immovable) isolated droplets, i.e. *droplet formation* flow regimes. This third flow regime, shown in Figure 3.6C, is identified from the time of the breakthrough and when we increase the water flow rate. After breakthrough, the frontal instability develops on the sides of the water channel normal to the mainstream. When the water and oil flow rates increases and decreases, respectively, the instability shows itself in the form of narrow fingers with small wavelengths towards the slow moving oil stream on both channel sides. The fingers initially extend normal to the flow, but then some are deviated and flow along the mainstream while others coalesce and form more oil droplets.

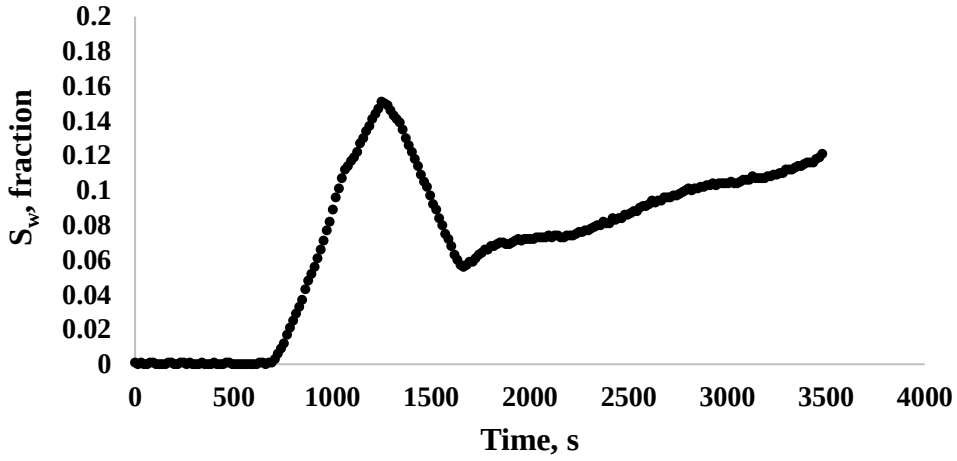

Figure 3.7. Evolution of water saturations versus time

Figures 3.8a-d display images of the evolution of the water and oil phases in the cell as the water flow rate is raised from 4.5 to 9 ml/minute at a constant oil flow rate (0.5 ml/minute). Figures 3.8e-h displays the oil and water flows when the water flow rate is kept constant at 9 ml/minute and the oil flow rate is reduced from 0.5 to 0.025 ml/minute. The results show that as the ratio of oil to water flow rates drops, the thickness of the water channels grows. A comparison of the images in Figure 3.8 reveals that many oil droplets within the water phase are not moving and are bypassed

by the water (encircled in Figures 3.8 (f,g,h). This explains why the oil relative permeability drops beyond the cross-over point. As the water flow rate grows relative to the oil flow rate, the water saturation within the cell rises. Thus, the water relative permeability increases linearly as the water saturation grows. On the other hand, a fraction of the oil droplets engulfed by the water as the water occupies more of the cell do not move and thus, they effectively become trapped. Hence, the oil relative permeability drops more than linearly as the relative amount of water flowing through the cell compared to oil increases.

This can also be confirmed from Figure 3.9, which shows the comparison of flow rates of each phase with its saturation. It can be observed from the results that the water saturation rises 63% in 255 minutes (over first 15,300 s, 87.3% of the total time) when the water flow rate is increased from 0 to 9 ml/minute at constant oil flow rate (0.5 ml/minute). The water saturation rises 36.95% in 38 minutes (starting at time equal to 16,300 s, 12.57% of the total time) after reducing the oil flow rate from 0.5 ml/minute to 0.025 ml/minute at constant water flow rate (9 ml/minute), which is a significant water saturation increase in a comparatively short interval of time. It can be concluded from this saturation and flow rate analysis that maximum oil could be recovered not only with high water flow rate but also by decreasing the oil flow rate.

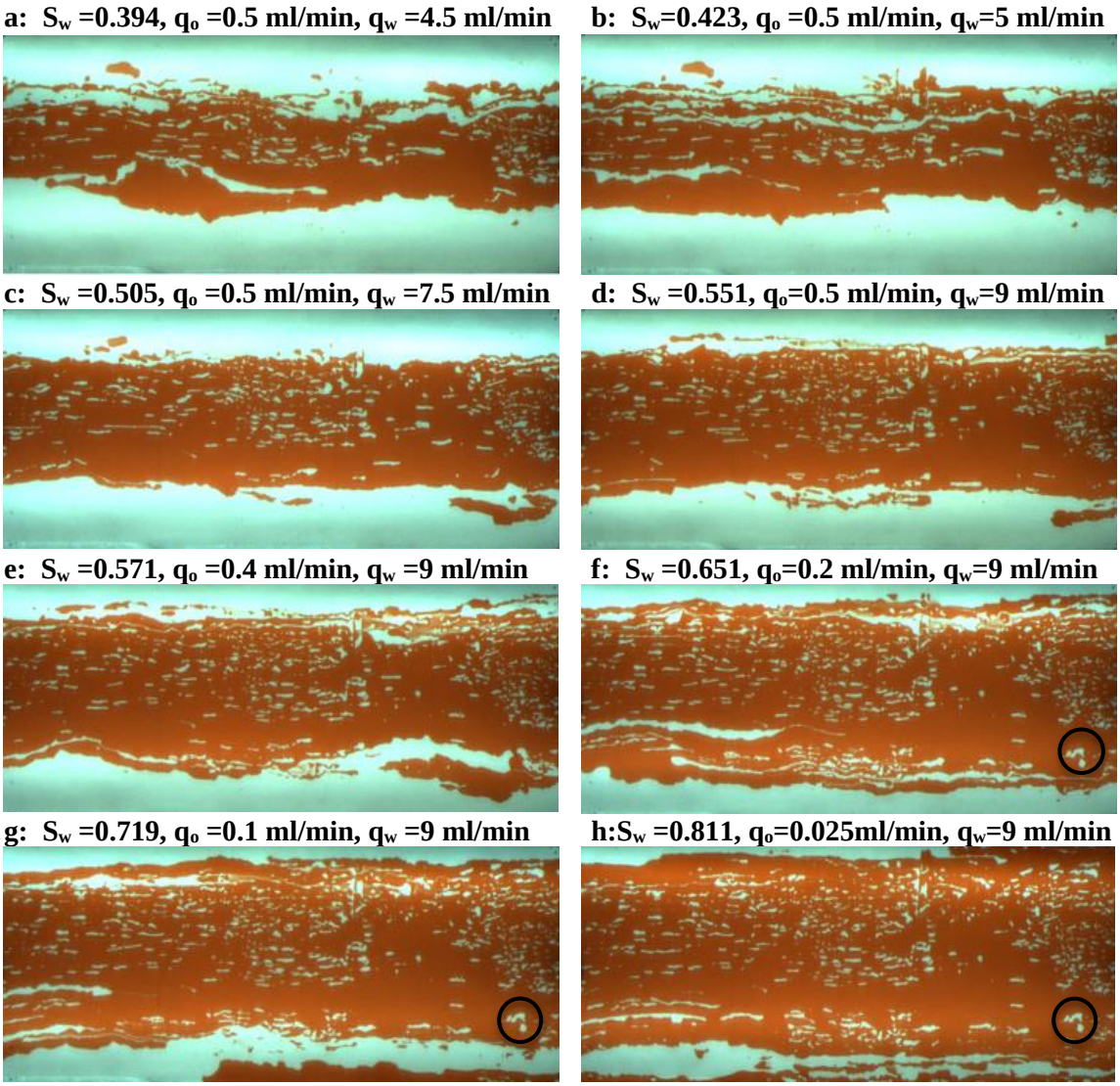

Figure 3.8: Evolution of flow state as water (red) injection rate is increased from 4.5 to 9 ml/min with oil injection rate varying from 0.5 to 0.025 ml/min. The flow direction is from the right to the left side of the images

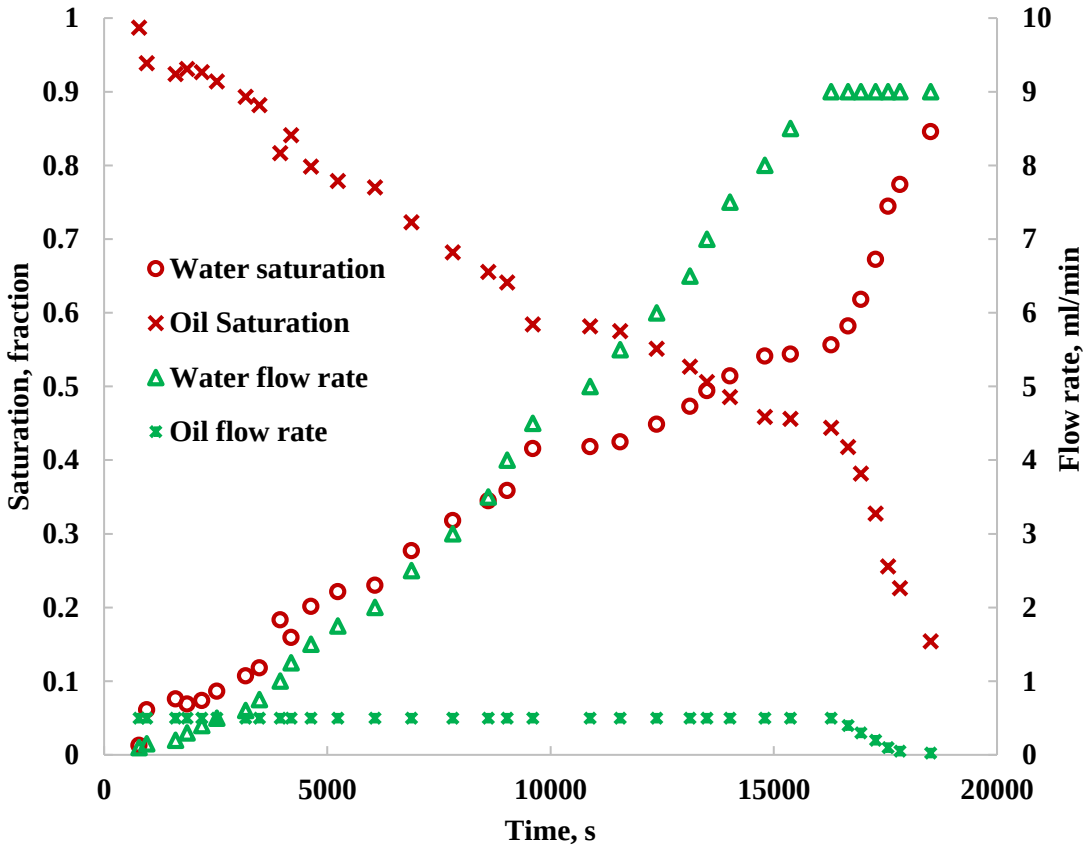

Figure 3.9. Saturations and flow rates of oil and water versus time during drainage process (wetting phase is oil)

As stated earlier, the cross-over point is the saturation where the oil and water relative permeabilities are equal. This implies that the effective permeabilities of the phases are equal and that both phases are equally interfering with each other. The relative role of interfacial and viscous forces can be described by the capillary number, N_c, defined as:

$$N_c = \frac{\mu U}{IFT} \tag{5}$$

where μ is the viscosity, U is a characteristic velocity of the flow, and IFT is the interfacial tension. For systems with two phases, the capillary number can be modified to include the effects of both phases by using an equivalent homogeneous fluid viscosity, μ_m, defined by (Dukler, et al., 1964):

$$\mu_m = \frac{\mu_o q_o + \mu_w q_w}{q_o + q_w} \quad (6)$$

and the homogeneous pseudo velocity of the two phases, given by (Dukler, et al., 1964):

$$U_m = \frac{q_o + q_w}{A} \quad (7)$$

where A is the cross-sectional area open to flow. For the oil-water system examined here, the interfacial tension is determined by Du Nouy ring method (Model TensioCAD-M, CAD Instruments) and is equal to 40.033 mN/m.

Figure 3.10 displays the two-phase capillary number versus the water saturation. The values are significantly less than unity which reveals that the interfacial forces are much larger than viscous forces. Before the cross-over point, the capillary number is rising which suggests that the relative role of interfacial forces is declining as the water flow rate is raised. Beyond the cross-over point, the capillary number drops which suggests that the relative role of interfacial tension is growing as the oil saturation drops. This suggests that the greatest phase interference would be seen towards the extreme ends of the saturations, that is, either at the low water saturation end or at the low oil saturation end.

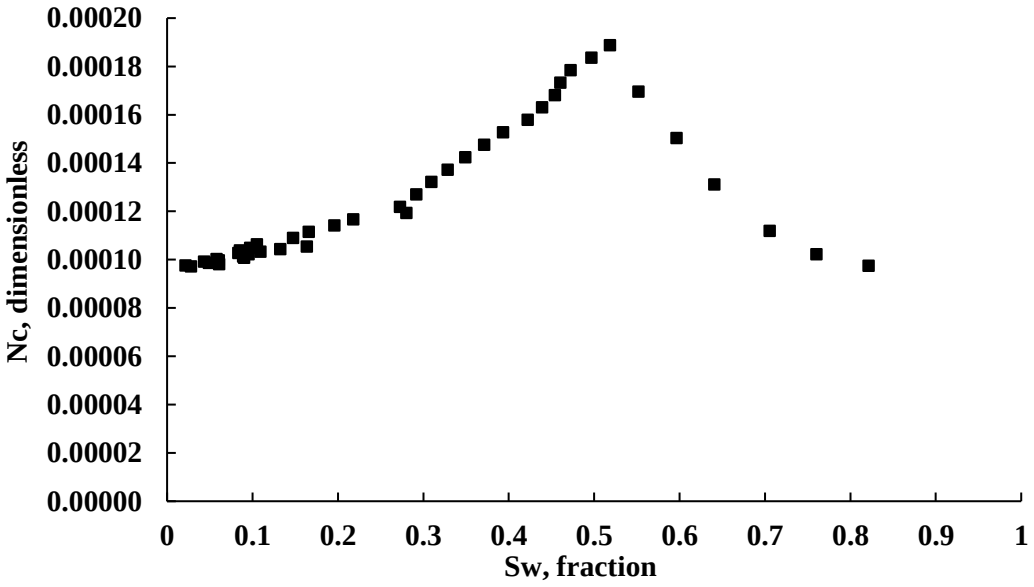

Figure 3.10: Change of two-phase capillary number versus water saturation

3.6 Conclusions

Experiments are conducted to understand hysteresis of co-current oil and water flow within a thin gap. It is found that in oil-water flow through the Hele-Shaw cell, different flow regimes are established depending on the relative oil and water flow rates and water breakthrough time. During the initial transient flow and before water breakthrough, the water saturation increases. This accumulation results in *linear displacement* of oil by the water when the water flow rate is low. At this stage, water accumulation forms a thick single finger. As, the water injection rate exceeds a threshold value, the planar interface becomes unstable (Saffman-Taylor instability) which exhibits itself physically in the form of low-viscosity water fingers penetrating into the viscous oil. Consequently, injected water feeds the new fingers at the tip and sides. Hence, the base of the water pathway close to the injection port shrinks. The moment that one advancing finger reaches the production port, the water channel spanning the cell thins and the water saturation drops due to increase in capillary pressure after breakthrough. Thereafter, a main water channel forms featuring unstable interfaces. By increasing the water injection rate, the water-oil interface develops fingers with small wavenumbers normal to the mainstream. These fingers merge and trap oil in the form of droplets. Some advanced fingers deviate to the direction of the flow and elongate.

The initially thick and then thin behaviour of the injected water channels reveal that for the subsurface oil recovery applications such as water flooding, if the water rate remains constant, little of the oil within the gap will be displaced. The results show that for efficient oil recovery from the gap, increasing water flow rates are required especially after breakthrough. This is very important as in such applications, we always have co-current flow of water and oil in fractures. Oil continuously drains into the fractures from the reservoir rock that, together with the injected water, form multiphase flow in fractures. We also quantify the experimental results through relative permeability curve evaluations. It is shown that after the cross-over point where oil and water have the same relative permeability, the oil relative permeability drops more than before the cross-over point due to the entrapment of the oil droplets within the water phase. Many

of these droplets, when trapped in the water phase, become relatively immobile. The capillary number for the phases is less than unity, which reveals that the interfacial forces are larger than viscous forces. The results show that the capillary number increases as the cross-over point is reached and then drops beyond this point. The capillary number rises as the water saturation/flow rate increases. This suggests that greatest phase interference occurs at low flow rates of each of the phases.

In drainage process, when the water saturation is rising, the relative permeability of the water phases increases linearly. During imbibition, when water saturation is falling, the water phase relative permeability falls roughly along the same relative permeability curve as that of drainage. For the oil phase, the relative permeability curves above the cross-over point are not the same during drainage and imbibition. This reveals that the oil phase behaviour exhibits hysteresis and that the relative permeability of the oil depends on the direction of saturation change.

At this stage, the present work should guide future experimental analysis and nonlinear simulations of co-current flows in Hele-Shaw cells. Future work on the effect of liquid-liquid interfacial properties on the flow regimes and nonlinear simulations of the process to confirm the hypothetical flow regime developments are underway.

List of Symbols

k_r = Relative permeability

k_{rw} = Relative Permeability of Water

k_{ro} = Relative permeability of Oil

k = Absolute Permeability (m^2)

b = Hydraulic gap (m)

P = Pressure (Pa)

q = Volumetric flow rate of the fluid (m^3/s)

q_w = Volumetric flow rate of water (m^3/s)

q_o = Volumetric flow rate of oil (m^3/s)

μ = Viscosity of the liquid (Pa.s)

L = Length of the cell (m)

W = Width of the cell (m)

ΔP = Differential pressure between the transducers (Pa)

A = Cross sectional area of the flow =b W (m^2)

V_m= Mean volumetric flux (m/s)

μ_m= Mean viscosity (Pa.s)

μ_o= Viscosity of the oil (Pa.s)

μ_w= Viscosity of the water (Pa.s)

U = Velocity of the fluid (m/s)

U_m = Mean volumetric flux (m/s)

N_c = Capillary number

S_w = Saturation of water, fraction

IFT = Interfacial tension (mN/m)

References

Akita, O., Ito, K. 1980. Analysis on the Stratified Multi-Phase Flow Polymer Melts in Wire Coating. Vol. 3. PP: 137 - 142

Al-Turki, A. A.B., Maini, B.B., Gates, I.D. (2013). The effect of fracture aperture and flow rate ratios on two phase flow in smooth-walled single fracture. J. Petroleum Explor. Prod. Tech. (2013), 3: 119-132.

Al-Turki, A.A.B., (2012). Two Phase Flow in Smooth and Rough Walled Single Fracture. PhD Thesis, University of Calgary.

Brooks, R.H., and Corey, A.T. Hydraulic Properties of Porous Media; Hydrol. Pap. 3, Civ. Eng. Dep., Colo. State Univ., Fort Collins, 1964

Chen, C.-Y. (2005). Liquid –Gas relative permeabilities in Fractures: Effects of flow structures, phase transformation and surface roughness. Stanford Geothermal Program Interdisciplinary Research in Engineering and Earth Sciences, Stanford University Stanford, California. SGP – TR-177

Chen, C., Li, K., and Horne, R.N. (2007). Experimental study of phase-transformation effects on relative permeabilities in fractures. 2004 SPE Annual Technical Conference and Exhibition, Houston, 26 – 29 September, 2004. Paper (SPE 90233) peer approved 10 April, 2007.

Chima, A; and Geiger, S. (2012). An analytical equation to predict gas-water relative permeability curves in fractures. SPE Latin American and Caribbean Petroleum Engineering Conference held in Mexico City, Mexico, 16-18 April, 2012. SPE 152252.

Claridge, E.L. (1972). A trapping Hele-Shaw Model for Miscible-Immiscible Flooding Studies. Society of Petroleum Engineers of AIME, (SPE)-4105; Pre-print presented at SPE-AIME 47 Annual Fall Meeting, San Antonio, TX, USA, 8-11, Oct. 1972

Corey, A. T. (1954). “The Interrelation Between Gas and Oil Relative Permeabilities,” Prod. Mon., 1954, pp. 19, 38.

Craft, B.C., Hawkins, M.F., Terry, R. E., (1991). Applied Petroleum Reservoir Engineering (Second Edition), Prentice Hall PTR PRENTICE-Hall, Inc. A Simon & Schuster Company Englewood Cliffs, New Jersey 07632

Dukler, A.E., Wicks, M., Cleveland, R.G. (1964). Frictional pressure drop in two phase flow: Comparison of existing correlation for pressure loss and hold-up. AIChE J., (10)1. pp: 38 – 43.

Diomampo, G. P. (2001). Relative Permeability through fractures. Stanford Geothermal Program Interdisciplinary Research in Engineering and Earth Sciences, Stanford University Stanford, California. SGP – TR-170

Felgueroso, L. C. and Juanes, R., (2014). A Phase-field Model of Two-Phase Hele-Shaw Flow, J. Fluid Mech. (2014), vol. 758, pp. 522 – 552. Cambridge University Press 2014.

Fourar, M., Bories, S. (1995). Experimental study of Air-Water two phase flow through a fracture (narrow channel). Int. J. Multiphase Flow, Vol. 21, No. 4, pp. 621 – 637.

Fourar, M; Lenormand R. (1998). A Viscous Coupling Model for Relative Permeabilities in a Fracture, SPE Annual Technical Conference and Exhibition, 27 – 30 September, New Orleans, L Sep/1998uisian. SPE – 49006-MS

Hashimoto, M., Garstecki, P., Stone, H.A., Whitesides, G.M. (2008). Interfacial instabilities in a microfluidic Hele-Shaw cell. RSC Publishing, Soft Matter, Vol. 4, Number 7, 7 July 2008. pp: 1329 - 1540

Horne, Roland N., Sotik, G., Mahiya, G.., Ambusso, W.., Tovar, R., Wange, C., Nassori, H. (2002). Steam-Water permeability. Stanford Geothermal Program, Stanford University, Stanford, CA 94305 – 2220, USA.

Indraratna, B., Ranjith, P.G., Price, J.R., Gale, W. (2003). Two Phase (Air and Water) Flow through Rock Joints: Analytical and Experimental Study, Journal of Geotechnical and Geoenvironmental Engineering, 2003, 129 (10), 918-928.

Khosravi, V. (2012). Various methods to determine relative permeability in fractured reservoirs. SPE Asia Pacific Oil and Gas Conference and Exhibition held in Perth, Australia, 22 – 24 October, 2012. SPE 158384.

Kuchuk, F., Biryukov, D. and Fitzpatric, T. (2015). Fractured reservoir modeling and interpretation. Society of Petroleum Engineers Journal 20(5), October 2015. pp:983 - 1004

Lee, J. and Kang, J.M. (1999). Oil recovery in a fracture of variable aperture with countercurrent imbibition: Experimental analysis. SPE 56416. Presented at the 1999 SPE Annual Technical Conference and Exhibition held in Houston, Texas, 3 – 6 October, 1999.

Leonce, D. (2012). Synthesis and Properties of soap. University of Dar Es Salaam.

Lockhart, R.W. and Martinelli, R.C. (1949). Proposed correction of data for isothermal two-phase two-component flow in pipes. Chemical Engineering Progress. Vol. 45. pp: 39 – 48.

Pan, X., Wong, R.C., Maini, B.B. (1996). Steady state two-phase in a smooth parallel fracture. 47th Annual Technical Meeting of the Petroleum Society in Calgary, Alberta, Canada, June 10 – 12, 1996. The Petroleum Society, Paper 96 -39.

Park, C. W.; Maruvada, S.R.K.; Yoon, Do-Young, (1994). The influence of surfactant on the bubble motion in Hele-Shaw cell, Phys. Fluids 6 (10), October, American Institute of Physics, 1994. pp: 3267 – 3275.

Pieters, D.A., and Graves, R.M. (1994). Fracture relative permeability: Linear or non-linear function of saturation. Presented at the 1994 SPE International Petroleum Conference and Exhibition, Soc. of . Eng. Veracruz, Mexico.

Putra, E., Alfred, D., Schechter, D. S. (2004). Modeling fluid flow through a single fracture using experimental, stochastic and simulation approaches. SPE/DOE Fourteenth Symposium on Improved Oil Recovery held in Tulsa, Oklahoma, USA., 17-21 April 2004.

Raven, K.G., Novakowski, K.S., Lapcevic, P.A. (1988). Interpretation of field tracer tests of a single fracture using transient solute storage model. J. o. Water Resource Reseach., Vol. 24 Issue 12, pp: 2019 – 2032.

Romm, E.S., Fluid Flow in Fractured Rocks; Publisher: Phillips Petroleum Company; 1st English edition (1972), 1966

Saffman, P.G., Taylor, S.G. (1958). The penetration of a fluid into a medium or Hele-Shaw cell containing a more viscous liquid. Proceedings of the Royal Society of London, Series A, Mathematical and Physical Sciences, Vol 245, No. 1242 (Jun. 24, 1958), pp. 312-329.

Sarkar, S., Toksöz, M. Nafi and Burns, D. R. 2002. Fluid Flow Simulation in Fractured Reservoirs. Earth Resources Laboratory, Department of Earth, Atmospheric and Planetary Sciences, Massachusetts Institute of Technology, Cambridge, MA 0213.

Shad, S. (2009) Two-Phase Flow in Single Fracture. PhD Dissertation, University of Calgary, Calgary.

Shad, S., Gates, I. D. (2010). Multiphase flow in fracture: Co-current and Counter-current flow in a fracture. Journal of Canadian Technology, Vol.49, No.2. February 2010, pp: 48 – 55.

Shad, S., Salarieh, M., Maini, B.B., Gates, I.D. (2009) The Velocity and Shape of Converted Elongated Liquid Drops in Vertical Narrow Gaps. Journal of Canadian Petroleum Technology, SPE-132163-PA, Vol. 48, No. 12. pp: 26 - 31

Shad, S., Maini, B. B., Gates, I. D. (2009). Investigation and visualization of liquid-liquid flow in a vertically mounted Hele-Shaw cell: flow regimes, velocity and

shape of droplets. J. Measurement Science and Technology, Volume 20, Issue 11, article ID. 114005, (2009).

Shad, S., Maini, B. B., Gates, I. D. (2010). Effect of Gap and Flow Orientation on Two-Phase Flow in an Oil-Wet Gap: Relative Permeability Curves and Flow Structures. International Journal of Multiphase Flow, Volume 57, December 2013, Pages 78–87.

Wu, Y.S., (2000). A virtual node method for handling well bore boundary in modeling multiphase flow in porous and fractured media. Water Resource Research, Vol. 36, No. 3. PP 807 – 814

Chapter Four: Impact of Interfacial Tension on Two Phase Flow in a Narrow Gap

4.1. Abstract

Co-current flow of oil with different concentrations of surfactants in thin gaps or Hele-Shaw cell has not been extensively studied experimentally for examining the interfacial behaviour, relative permeabilities and saturations. Here, in a series of experiments, we compare multiphase flow of oil and water through a thin gap (a Hele-Shaw cell) with and without sodium dodecyl sulfate (SDS) surfactant. The impact of SDS concentration on the oil-water interfacial tension (IFT), saturations, relative permeabilities and flow patterns within the Hele-Shaw cell are analyzed. The results reveal in both the two phase flow experiments and two phase microscopic analysis that the presence of SDS yields an emulsion near the interface by entrapping oil droplets in the SDS aqueous phase, which facilitates the oil flow with the SDS solution, in the flow experiments. On the other hand, this phenomenon is rarely witnessed in the water-oil system, where few oil droplets engulf by the water. Microscopic observations reveal that the SDS aqueous phase, on contact with the oil phase, channels into the oil phase up to certain distance where it accumulates, becomes a droplet, which further divides into several small round-shaped droplets. On addition of SDS to water, the relative permeabilities improve and oil phase residual saturations decreases. The two phase flow experiments reveal that the dominant finger created in the SDS+water-oil system enlarges due to formation of an emulsion at the interface and due to creation and merging of the small fingers on the main channel. For the water-only case, single fingers evolve in the cell that flow in their separate channels without engulfing or mobilizing more oil. This implies that the oil recovery from fracture reservoirs could be raised by adding surfactant to the injected water.

4.2. Introduction

There are many systems with co-current flows of two liquid phases where the liquid interfaces are unstable and as a consequence, complex flow patterns result. One such system is fractured carbonate rocks which host huge oil volumes. Recovery of oil from fractured reservoirs have challenges due to the nature of multiphase flow, that of oil and water, heterogeneity of the reservoir rock, and the capillary interaction between flow within the relatively high permeability fractures and the lower permeability rock that bounds the fractures (Bourbiaux, 2010).

The use of surfactants for fractured reservoirs may improve oil recovery. The addition of surfactant reduces the amount of energy required to deform oil-water interfaces due to reduction in the interfacial tension (Tcholakova et al., 2008) and alters wettability of the reservoir rock by von der Waals forces between the surfactant molecules and rock surfaces (Rosen and Kunjappu, 2012). Surfactant molecules bridge between the oil and water phases with the non-polar part in oil and polar part in water. Thus, negative charges create on oil droplets cause mutual repulsion that consequently results in dispersion of the oil droplets in water and mobilize oil in the fractured rock (Porter, 1991; Leonce, 2012; Kianinejad et al 2013). In the most cases, fractured carbonate rock systems are oil to mixed wet (Hirasaki, 2004). In separate studies, Standnes et al., (2000); Chen et al., (2000), and Hirasaki et al., (2011) reported incremental increase in oil recovery as a result of using surfactants.

Hele-Shaw cells, glass micromodels, or single fractures created in a rock sample have been used to investigate impact of surfactants on flows in the context of oil recovery from the fracture. Razmi et al., (2012) investigated heavy oil recovery in glass micromodels. They flooded sodium dodecyl sulfate (SDS), linear alkyl benzene sulphonate (LABS), and water through the micromodels and concluded that surfactants, especially SDS, yields higher oil recovery than that of water and LABS. Ferno et al., (2012) experimentally examined the wettability of an oil-wet 1 mm aperture fracture in limestone. The oil saturated rock was first flooded with water and then with surfactant before a second water flood. They showed that with water, a capillary threshold pressure must be achieved before flow started through the fracture. When surfactant was added, the threshold pressure was negligible. They concluded that the surfactant

changes wettability of the fracture surface by altering it hydrophilic. They also observed that the recovery and sweep efficiency from the oil-wet fractured rock enhances by adding surfactant to the injected water.

Hele-Shaw cells or glass micromodels have also been used to investigate the onset of instabilities created when surfactants are used. Park et al., (1996), in 0.9 and 1.8 mm gap (Hele-Shaw cells), experimentally examined the effect of surfactant on air bubble and water droplets (1.3 to 2.1 cm plan-form diameter) with and without surfactant driven in silicon oil (97 cP). They concluded that the surfactant did not significantly affect the shape and movement of the air bubbles. However, on adding SDS, the translational velocity and shape of the water droplets changed significantly. Fernandez et al., (2005), in an open-sided 310 micron gap in a vertical Hele-Shaw cell, experimentally examined instability and fingering created in dipping and withdrawal of a Hele-Shaw cell in and out of the surfactant solution at a constant speed. They observed drifting fingers at a surfactant solution (C) = 2.8×10^{-3} mol/l, dipping speed (V) = 1.52 cm/s and withdrawal speed (V_d) = 0.635 cm/s, merging of fingers at c = 0.67 and V = 1.65 cm/s, and bubble ejection phenomenon at V=3.3 cm/s and c = 0.34, in unsteady conditions. They also observed different steady patterns for various surfactant concentrations greater than 67%, different dipping and withdrawal speeds. They concluded that the fingering depends upon the cell withdrawal and dipping velocities and concentrations of the surfactant solution. Similarly, Hashimoto et al. (2008), in a 2 to 5 mm gap Hele Shaw cell, also observed dynamic instabilities and flow patterns of a water droplet in hexadecane (3.032 cP at 25°C) in the presence of a surfactant. They used Tween 20 (2%) surfactant in the aqueous phase and Span 80 (3%) surfactant in the oil phase resulting in low interfacial tension (~0.01mN/m). They observed that the shape of the droplet first expanded sideways with subsequent disintegration into small circular droplets due to a shear-based instability. They also observed that a high concentration of surfactant (3%) is needed to keep the water droplets separate because at low surfactant concentrations, the water droplets coalesce.

For multiphase flow within a fracture, the impact of interfacial tension and wettability effects using surfactants on the relative permeabilities and its consequent effect on oil recovery remained unclear. In this work, we examined multiphase flow of a 20 cP

mineral oil and water with and without surfactant on multiphase flow behaviour and relative permeability of each phase. Flow patterns resulted from various injection scenarios in the presence of a surfactant are investigated and compared with the case without surfactants.

4.3. Experimental Apparatus, Materials, and Procedure

The apparatus, displayed in Figure 4.1, consists of a Hele-Shaw cell with the areal dimensions of the fracture 40 cm × 14 cm and 0.397 mm gap between the two Plexiglas plates (set by shim stock). The displaced fluids injection pumps (Two Isco Syringe Pump Model 500D, Teledyne Isco- connected in series and one Gilson peristatic pump - Model 305, Gilson Inc.), CCD camera (Model scA1000-30gc, Basler), thermocouple and two pressure transducers (Model PX 209-015G5V, Omega Environmental Inc.) are connected to a data acquisition system. Saturations of each phase flowing in the cell are calculated from the images acquired by data acquisition system. The actual gap is typically slightly less than the nominal gap set by the shim stock which is determined by single phase flow of water and is found equal to 0.2973 mm. The consequent absolute permeability of the gap is equal to 7.365×10^{-9} m^2. Detail of the apparatus and experimental procedure is given in chapter-3 and elsewhere (Raza et al., 2016). Properties of the Mineral oil, 'Marcol-7', water and the 2 wt.% aqueous phase of the surfactant used in the experiments are presented in Table-4.1. For detailed analysis of the interfaces, the microscopic images of the interfaces and droplets are acquired by Nikon A1R confocal laser microscope.

Different concentrations (0.1%, 0.3%, 0.5% and 2%) of 10% sodium dodecyl sulfate (SDS, VWR, Catalog Number CA97062-964) are added to dyed de-ionized (DI) water before injection into the cell. Viscosity of each surfactant aqueous phase is determined by a Stabinger Viscometer (Model #SVM 3000, Anton-Paar) and the interfacial tensions between each surfactant solution and the mineral oil are measured by using a Du Nouy Ring Tensiometer (TensioCAD, CAD Instruments).

As described in Raza et al., (2016), the hydraulic gap available for the flow is calculated using the planar Poiseuille's equation. A combination of the Planar Poiseuille's

equation and Darcy's equation yields the absolute permeability of the gap. The relative permeabilities of the oil and water phases are then calculated by:

$$k_{rf} = \frac{q_f \mu_f}{A k_{abs}\left(\frac{\Delta p}{L}\right)} \quad (1)$$

where subscript $'f'$ represents oil and water, area '*A'* is equal to the product of the hydraulic gap 'b' and width of the cell '*W'*. The capillary number 'Ca' provides a measure of the ratio of viscous to capillary forces. For multiphase flows, it is defined as:

$$C_a = \frac{\mu_i U_j}{\sigma_{ij}} \quad (2)$$

where μ_i is viscosity of the oil, U_j is velocity of the SDS finger and $\sigma_{ij}$is the interfacial tension between the two phases.

The Hele-Shaw cell is initially saturated with mineral oil. Thereafter, the flow rates of the injectants are raised gradually which after breakthrough are held constant at a prescribed value until the pressure drop and saturations stabilize; this usually takes about 4 minutes. At this point, the flow rates, pressure drops, and images are taken and stored on the data acquisition computer. The data acquisition software analyzes the images to determine saturations of the two phases.

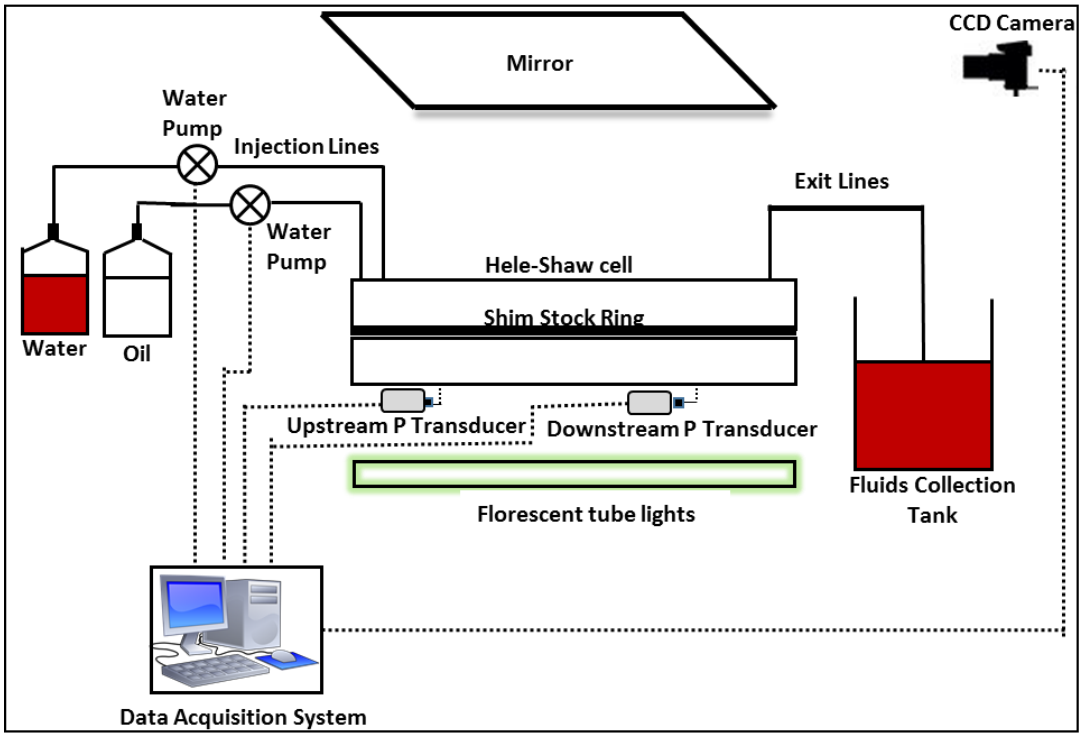

Figure 4.1: Schematic of experimental apparatus

Table 4.1: Properties of the oil, de-ionized water and 2 wt.% aqueous phase of SDS

Property	Oil (Marcol 7)	De-ionized Dyed Water	2 wt.% (20,000ppm) aqueous phase of SDS
Viscosity at 22.46°C (cP)	20.236 ± 0.001	1.100 ± 0.001	1.120 ± 0.001
Density at 22.46°C (kg/m^3)	847.0 ± 0.0002	998.85 ± 0.0002	997.77 ± 0.0002

4.3.1. Fluid Properties

Many previous studies have observed that mixing a surfactant with water not only reduces the interfacial tension (with other phases) but it also raises water viscosity (Seethepalli et al., 2004; Adibhatla et al., 2008; Hashimoto et al., 2008; SyedAkram et al., 2011; Hirsaki, 2011; Ferno et al., 2012; Kianinejad et al., 2013). In our experiments,

we also investigated the SDS concentration dependency of solution viscosity and interfacial tension. The results are displayed in Figures 4.2 and 4.3. Figure 4.2 depicts that the water viscosity slightly increases with increase in the SDS concentration, i.e. the viscosity rises from 1.108 to 1.168 cP when the SDS concentration is increased from 0 to 8 wt.% (0 to 80,000 ppm). Figure 4.3 illustrates the interfacial tension between the mineral oil and water phases versus SDS concentrations. The interfacial tension drops from 44.67 to 9.01 mN/m when the SDS concentration is increased from 0 to 2 wt.% (0 to 20,000 ppm). The greatest reduction of the interfacial tension occurs in the addition of 0.5% SDS to the DI water i.e., the interfacial tension falls from 44.67 to 15.7 mN/m. Further addition of SDS reduces the interfacial tension but at a decreasing slope.

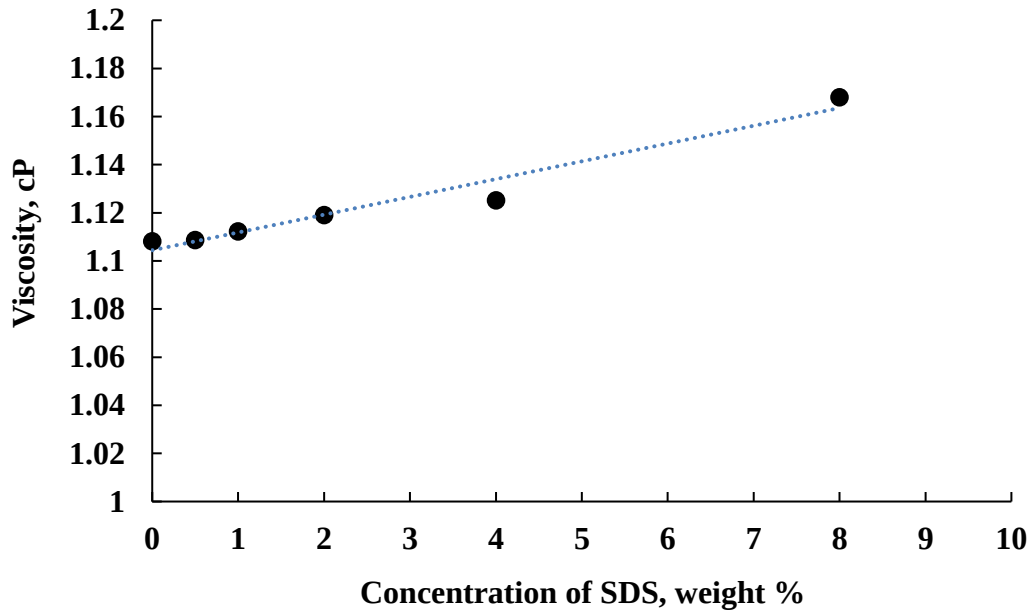

Figure 4.2: Viscosity of SDS+water solutions versus SDS concentration at 22.46°C (instrumental error = ±0.1%). Data shown is average of five measurements (maximum standard deviation is 0.000255 cP)

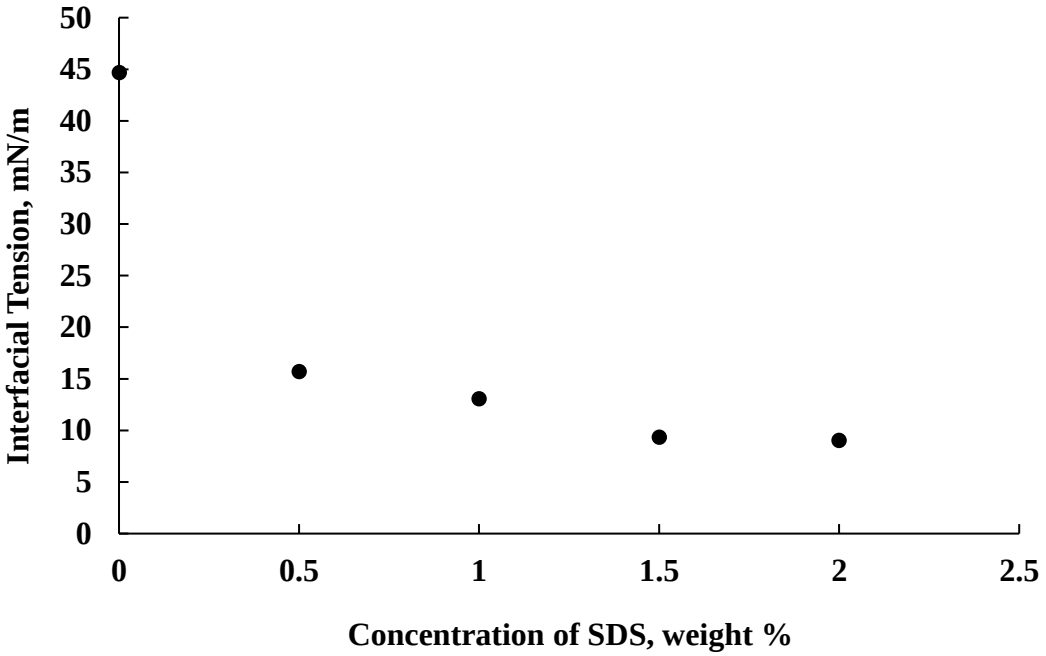

Figure 4.3: Relationship among interfacial tension between oil and aqueous phases and SDS concentration. Instrumental error could be ±0.01 mN/m

4.4. Results and Discussion

As described earlier, initially, the Hele-Shaw cell is completely filled with the mineral oil. Water and oil are then co-injected into the cell with water or SDS aqueous phase injected into the central port and oil into the two offset ports. Table 4.2 displays the results, at the same flow rates and times for the DI water-only (Case 1) and the 2 wt.% SDS + DI water (Case2) experiments. The comparison of relative permeabilities for water-oil and surfactant+water-oil is presented in Figure 4.4. The results suggest that the shapes of the relative permeability curves are almost similar for both cases except a slight increase in the relative permeabilities in the case-2 over case-1. This could be the direct result of decreases in the interfacial tension among the phases that facilitates movement of both liquids within the cell. The biggest difference in the relative permeability vs saturation curves is the residual oil saturation which is lower in the case-2 than case-1. It can be observed from the figure that the residual oil saturation for the case-1 (water-only) is equal to about 0.25 (projected from the water-oil relative

permeability curves) whereas for the case-2 (SDS case), it is equal to about 0.1 (projected from the SDS-oil relatively permeability curves). The surfactant lowers the surface energy of the oil-water interfaces, from 45 to 9 mJ/m^2 by adding 2 wt.% SDS to the water; thus the amount of energy required to deform the oil-water interfaces in the SDS case is one-fifth that of the water-only case. This leads to increase in the phase interference and reduction in the residual oil saturation. The phase interference can also be confirmed from the images of the flow patterns in Table 4.2 and Figure 4.5.

Figure 4.5 displays flow patterns for both the cases at the same saturations of the displacing phases. To recall, the oil is transparent and the water/SDS aqueous phase are shown in the red color. The comparison of the images reveals that the SDS aqueous phase engulfs the oil droplets that move out with the displacing phase, but in case of water-only minimum number of oil droplets form, which are mostly immobile. For example, a droplet of oil is engulfed by water at time 1658 second in the case-1 which is shown encircled in Table 4.2. Similarly, in the images of water-oil flow patterns shown in Figure 4.5, a droplet of oil is encircled (Figure 4.5(a)). It can be observed in the images at the subsequent steps, that in both the cases, the oil droplets did not move (encircled in the last images). On the other hand, in the case of surfactant-oil flow shown in Figure 4.5(h), a droplet of oil is encircled which is divided into small droplets and flew out of the cell that can be observed in the following images shown in Figure 4.5. This suggests that in the SDS+water case, the mineral oil enclosed within the host water phase flows at the same speed as that of the water. Even at higher water saturations, the nature of the flow is different with significantly more oil droplets hosted within the case-2 than case-1. The results also show that at low water flow rates, the flow channels are more dispersed and irregular especially in the case-2. This phenomenon is more prominent due to the low interfacial tensions and consequent capillary forces, which resulted formation of oil droplets and their movement in the cell. Due to reduction in the interfacial tension, there is a greater tendency for the SDS+water phase to engulf oil droplets. This can also be confirmed from the microscopic images, displayed in Figures 4.6 and 4.7, of the water-only and oil interface and the SDS+water-oil cases, respectively. The comparison shows that in case of water-only oil system (Figure 4.6), the water makes an irregular interface with the oil which is highly curved and has no or very few oil droplets engulfed in the water phase. The water-oil interfaces

show the dominancy of the capillary forces in the system. On the other hand, in the SDS+water case (see Figure 4.7), the SDS aqueous phase first penetrates the oil phase in the form of narrow channels which evolves into a network of channels with SDS droplets within the network. Larger SDS drops further split into small round-shaped droplets forming the emulsion zone.

4.4.1. Flow Pattern Analysis

As discussed earlier that Table 4.2 represents images of the evolution of interfaces in oil-water and SDS-water injection into the Hele-Shaw cell at the same flow rates. The images reveal that a finger of water/SDS+water is fed from the inlet port at the center of the cell, which displaces the oil linearly. In the case-1, the linear behaviour of the finger exits at water flow rates less than 0.3 ml/minute, while in the case-2 the linear nature of the finger exits until its flow rate reaches 0.45 ml/minute. Under these flow rates the SDS+water phase displaces oil with a comparatively stable interface due to low interfacial tension between oil and the aqueous phases, while due to higher interfacial tensions/capillary forces, the water finger is relatively narrow and penetrates the oil phase with one or two branches at the front end. It can be observed that at these flow rates, the saturation of the aqueous phase in case-2 is 22.3% while in the case-1, it is 5.8 % only. With further increase in the flow rates, the displacing phases become unstable at the tip of the fingers and start flowing with a comparatively higher speed than earlier in the process. This phenomenon is observed in case-1 at flow rates from 0.3 ml/minute to 0.55 ml/minute while in the case-2, this behaviour continues until its breakthrough occurs at 0.65 ml/minute flow rate. At this stage, it can be seen that the surfactant finger is wider and takes longer time (2,295 seconds) to reach the exit while the water finger is comparatively narrower and takes about 1,981 seconds to reach to the other end. During this time, a few small fingers develop in the interfaces which get combine with the main channels.

After breakthrough, the SDS aqueous phase finger narrows towards the exit (on the left side) as the flow evolves (from time 2,694 to 3,889 seconds) and the aqueous phase saturation drops (Table-4.2). In the time period of 2,845 seconds to 7,850 seconds, the saturation of SDS aqueous phase falls below the water saturation. At its flow rate ranging from 1.6 ml/minute to 7.5 ml/minute, the SDS aqueous phase flows in the form

of a complicated, irregular and unstable flow channels which cannot be seen in the water-oil case at this stage. There is a cyclic creation and distortion of fingers, and formation of the oil droplets (mostly circular shaped), due to trapping by the unstable interfaces. As a result of this unstable condition (creation and distortion of the droplets) the saturations of the phases fluctuate greatly. After this fluctuation in the saturations (at flow rate >1.6 ml/minute), the SDS+water saturation remains higher than that of water until the end of the experiments. During this period, the water flows in separate channels (both in main and secondary fingers), while the SDS+water phase flows in the form of a single channel that expands to the sides and engulfs more oil droplets than that of the water-only case. It can also be seen from the images that some small fingers develop on the body of the SDS main channel and merge with it which further enlarges its area. In contrary, in the case of water, single, narrow fingers develop at the sides of the cell that flow in their separate paths and rarely combine with the main finger. The residual finger at time 4,614 seconds, contains many oil droplets that flow with the aqueous phase of SDS.

The water-only case exhibits fingering and engulfment of large oil droplets within the water phase as the flow evolves. The morphology of the oil droplets within the SDS aqueous phase are different from those of the water case. In the SDS+water case, the droplets tend to be small and appear to be created at the interface through a shear-mode instability. The interface appears to be more rugose than that of the water-only case. In the water-only case, the oil droplets that are hosted in the aqueous phase are largely due to engulfment events where finger splitting and merging result in trapping a larger-scale oil droplet.

Table 4.2: Comparison of water-oil and SDS (2wt.%) + water-oil flow patterns acquired at the same time and flow rates. The mineral oil is shown transparent whereas the aqueous phase is red in colour. Inlet is on the right side of the cell

Time, s	Rates, ml/min		Water-Oil	SDS+Water-Oil
	Water	Oil		
365	0.3	0.5	S_w = 0.044	S_w = 0.015
420	0.3	0.5	S_w = 0.058	S_w = 0.023
504	0.35	0.5	S_w = 0.079	S_w = 0.045
659	0.35	0.5	S_w = 0.119	S_w = 0.087
824	0.45	0.5	S_w = 0.206	S_w = 0.125
898	0.45	0.5	S_w = 0.206	S_w = 0.181
981	0.55	0.5	S_w = 0.233	S_w = 0.223
219	0.65	0.5	S_w = 0.254	S_w = 0.361
295	0.65	0.5	S_w = 0.256	S_w = 0.385

Time, s	Rates, ml/min		Water-Oil	SDS+Water-Oil
	Water	Oil		
2694	0.85	0.5	S_w = 0.275	S_w = 0.315 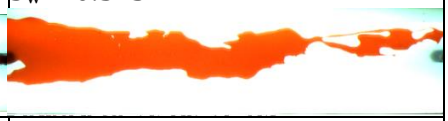
3083	1	0.5	S_w = 0.222 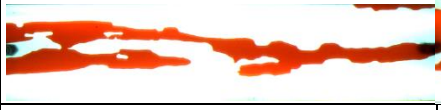	S_w = 0.258
3331	1.15	0.5	S_w = 0.275	S_w = 0.164 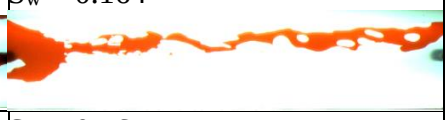
3889	1.6	0.5	S_w = 0.265	S_w = 0.161 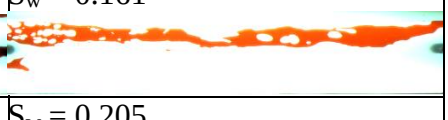
4614	2.25	0.5	S_w = 0.228	S_w = 0.205 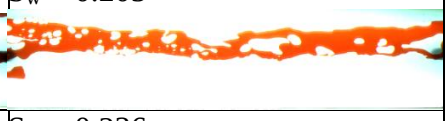
5086	3	0.5	S_w = 0.237	S_w = 0.236
5712	4	0.5	S_w = 0.335 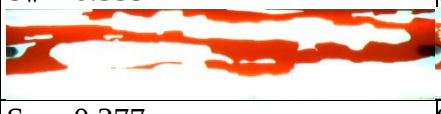	S_w = 0.277
6665	6	0.5	S_w = 0.377	S_w = 0.321
7456	8	0.5	S_w = 0.384	S_w = 0.372
8180	9	0.4	S_w = 0.381	S_w = 0.445
8515	9	0.3	S_w = 0.399	S_w = 0.508
8822	9	0.2	S_w = 0.450	S_w = 0.548

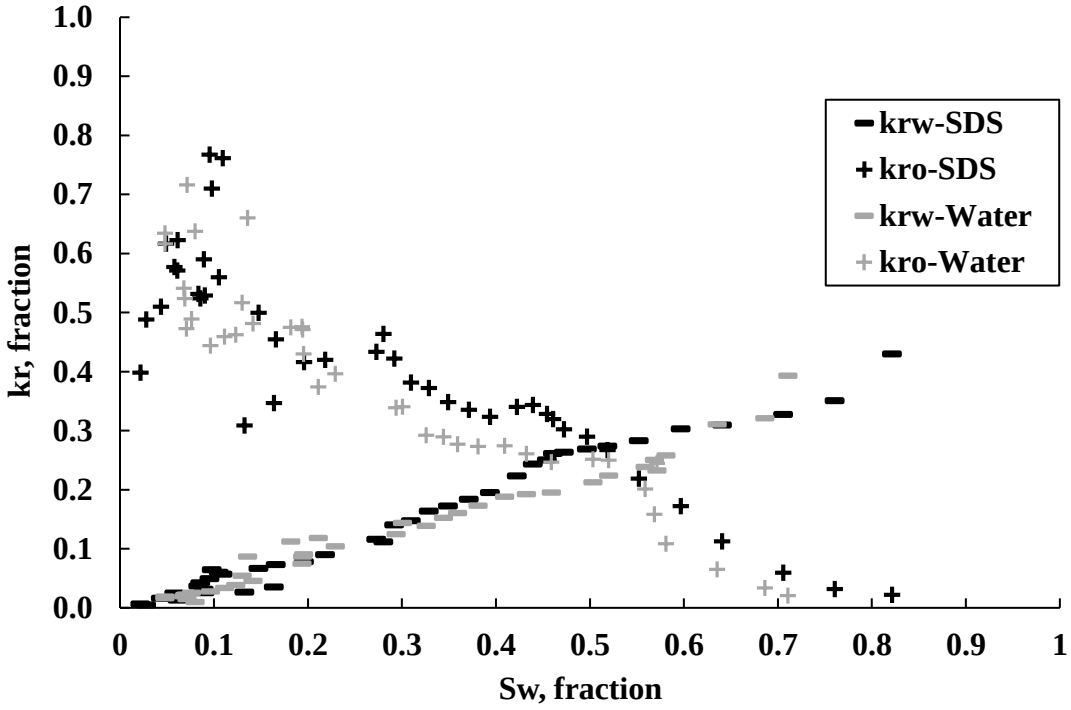

Figure 4.4: Relative permeability curves for water-oil and 2 wt.% SDS+water-oil flow in the drainage process

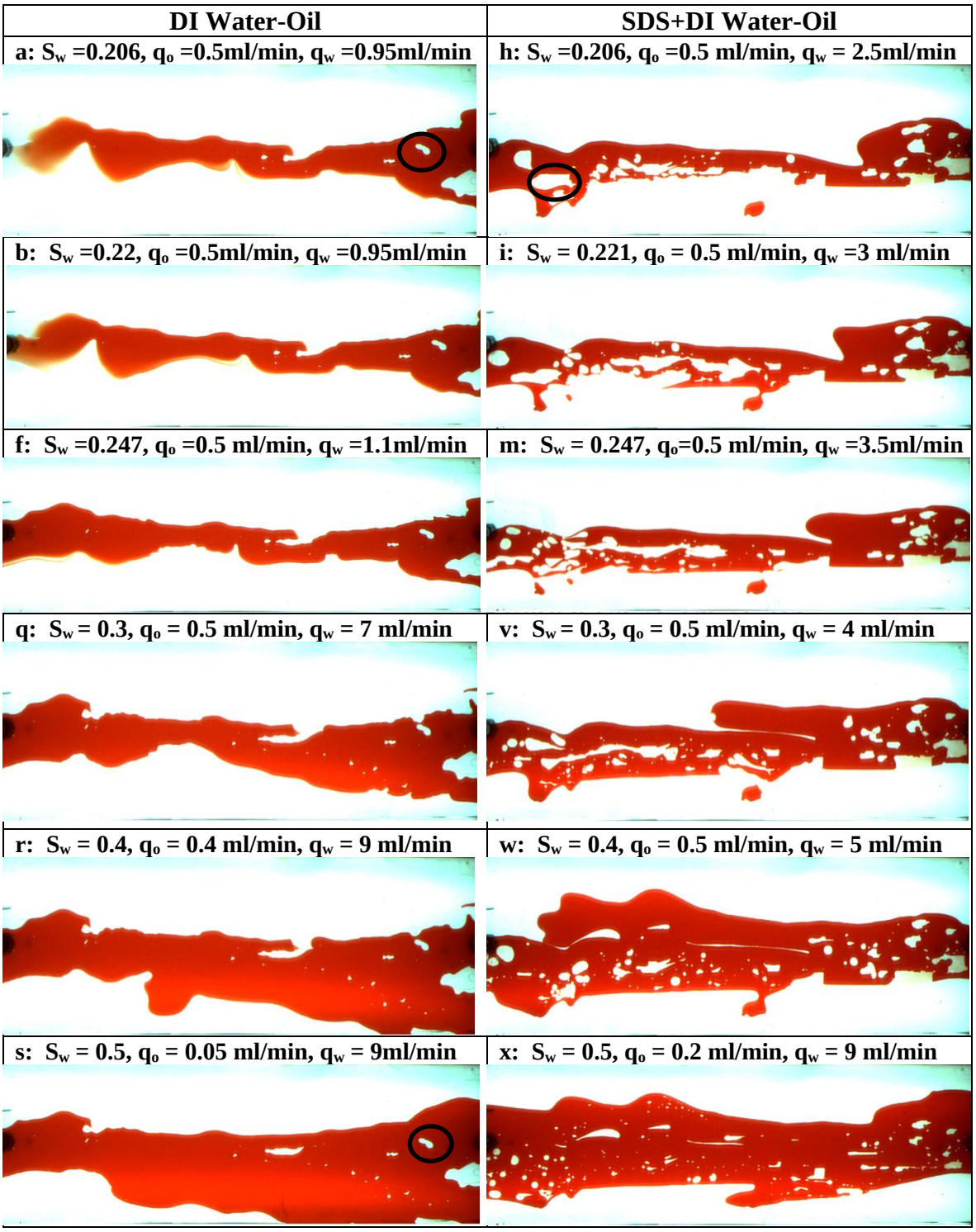

Figure 4.5: Comparison of flow patterns of de-ionized water and surfactant (2 wt.%SDS) flooding with oil at the same saturations. The red colour shows the aqueous phase of the surfactant whereas the transparent phase is the mineral oil

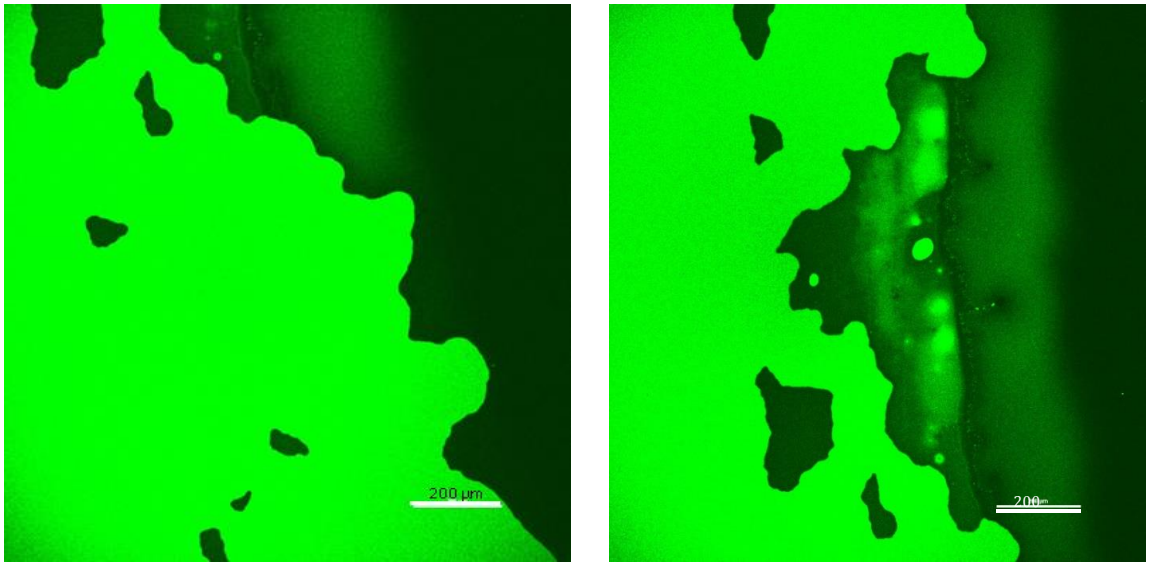

Figure 4.6 Microscopic images of the interfaces developed in water-oil system. The light green color shows water while dark green is oil

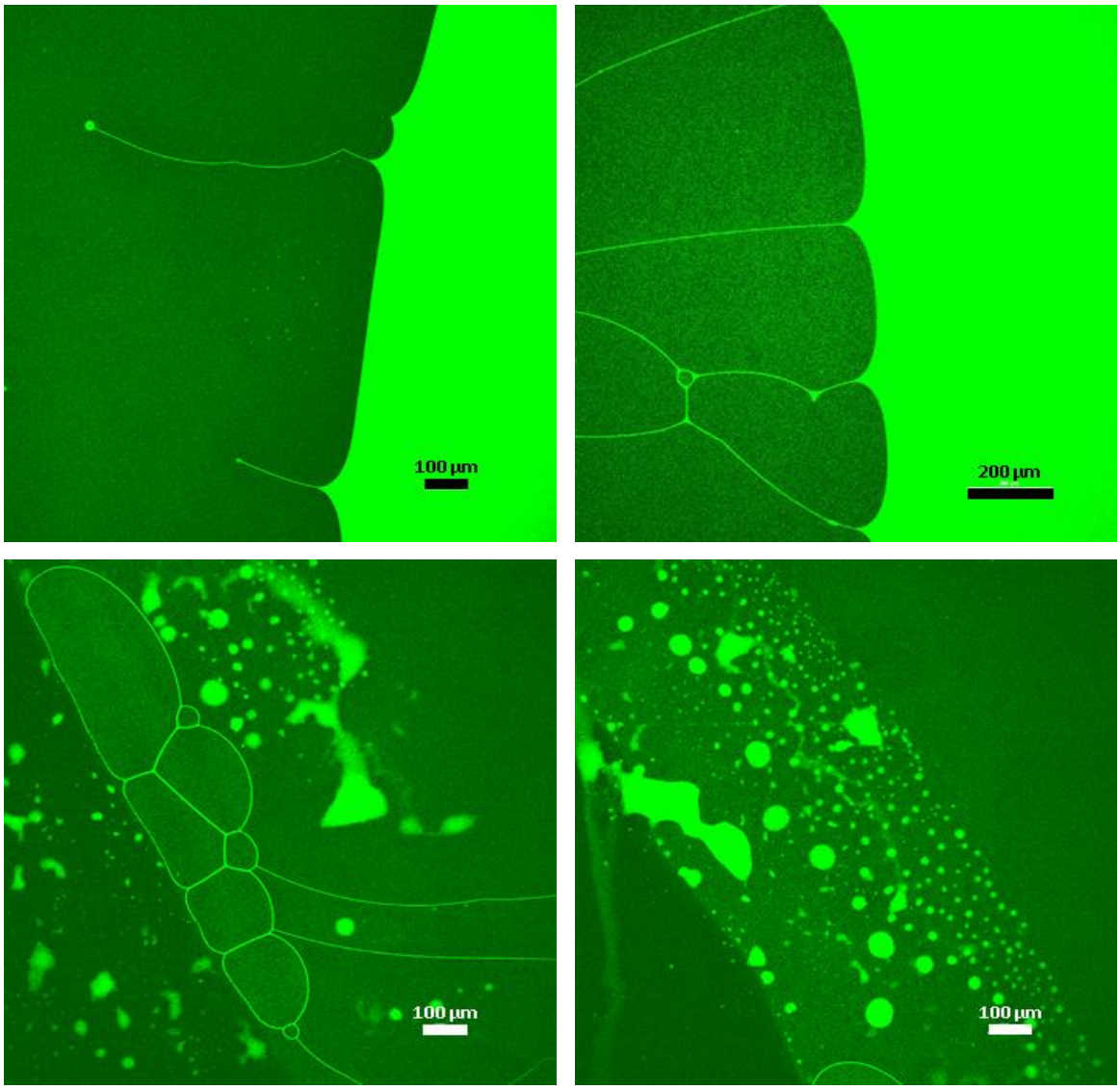

Figure 4.7: Lenses of Surfactant solution and interfaces created in water + SDS - oil systems. Light green shows surfactant while the dark green is the oil solution

4.4.2. Effect of Surfactants on the Capillary Number

The capillary number measures the relationship between viscous and the capillary forces. The capillary number in our experiments for both systems (water-oil and SDS+water-oil) is calculated by using Equation 2 and the results are displayed in Figure 4.8. It can be observed from the figure that the capillary numbers for both the systems are less than unity, indicating that the interfacial tension or capillary forces dominate over viscous forces. However, the relationship also reveals that on raising the aqueous phase saturation, the capillary number increases up to a peak value and then drops. This behaviour is due to the viscous forces that rise with the flow rates. The comparison of the capillary numbers further indicates that the surfactant (2wt.% SDS) increases the value of the maximum capillary number from 0.000189 to 0.000936 reflecting the impact of the reduction of the interfacial tension with the addition of SDS.

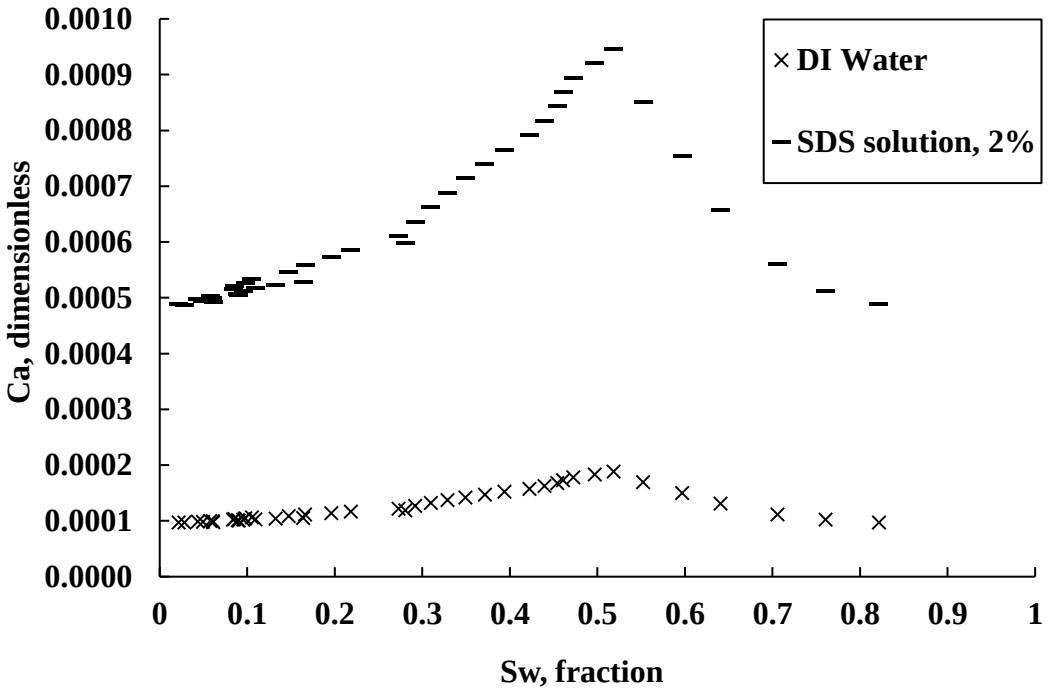

Figure 4.8: Comparison of capillary numbers (Ca) vs saturation obtained from de-ionized water and SDS 2 wt.% solution flooding with the oil through the fracture

4.5. Conclusion

The addition of SDS to water reduces interfacial tension between the surfactant aqueous and oil phases and lowers the residual oil saturation in the Hele-Shaw cell. The increase in breakthrough time and saturation at the breakthrough also increases with the addition of SDS to the water. The capillary number in both water and SDS+water experiments is less than unity demonstrating that capillary forces are more dominant than viscous forces within the system. After breakthrough, the SDS+water finger narrows and traps oil droplets along its periphery due to instabilities of the interface. For the water-only case, the water fingers split and merge leading to relatively large elongated oil droplets trapped in the aqueous phase, most of them are less movable or immobile. Microscopic analysis demonstrated that the SDS aqueous phase penetrates into the oil phase in the form of droplets which further splits to small round shaped droplets and form an emulsion of the aqueous phase in the oil phase while in the case of water-oil, there is no formation of emulsion at the interfaces and the interfaces mostly irregularly shaped droplets. The relative permeability curves for both the cases are same in the shape but different in the sizes, i.e. saturation of the SDS (2 wt.%) displacing phase is 11% more than the saturation of water in the case-1, which means that the surfactant recovered 11% more oil than water.

List of symbols

k_r = Relative permeability

k_{rw} = Relative Permeability of Water

k_{ro} = Relative permeability of Oil

k_{abs}= Absolute Permeability (m^2)

q = volumetric flow rate of the fluid (m^3/sec)

q_w = volumetric flow rate of water (m^3/sec)

q_o = volumetric flow rate of fluid (m^3/sec)

μ = viscosity of the liquid (Pa.s)

μ_m= Mean viscosity (Pa.sec)

μ_o= viscosity of oil

μ_w= viscosity of water

L = length of the cell (m)

W = width of the cell (m)

Δp = differential pressure between the transducers (Pa)

A = cross sectional area of the flow =b W (m^2)

V_m= Mean volumetric flux (m/sec)

b= Hydraulic Diameter (m)

IFT = σ = Interfacial tension, dyne/cm

C_a = Capillary Number, dimensionless

SDS = Sodium Dodecyl Sulfate

References

Adibhatla, B., & Mohanty, K. (2008). Oil recovery from fractured carbonates by surfactant-aided gravity drainage: Laboratory experiments and mechanistic simulations. SPE Reservoir Evaluation & Engineering, 11(1), pp: 119–130. http://doi.org/10.2118/99773-PA

SayedAkram, N. I., Aramco, S., & Mamora, D. (2011). Simulation study on surfactant-polymer flood performance in fractured carbonate reservoir. In SPE Enhanced Oil Recovery Conference 2011 - "From Science to Success: More, Faster, Greener, Cheaper", EORC 2011 (Vol. 2, pp. 1635–1646). http://doi.org/10.2118/149106-MS

Bourbiaux, B. (2010). Fractured reservoir simulation: a challenging and rewarding issue. Oil & Gas Science and Technology – Revue de l'Institut Français Du Pétrole, 65(2), pp: 227–238. http://doi.org/10.2516/ogst/2009063

Chen, H. L., Lucas, L. R., Nogaret, L. A. D., Yang, H. D., & Kenyon, D. E. (2000). Laboratory Monitoring of Surfactant Imbibition Using Computerized Tomography. In Proceedings of the 2000 SPE International Petroleum Conference and Exhibition in Mexico (pp. 271–284). http://doi.org/10.2118/59006-MS

Dukler, A.E., Wicks, M., Cleveland, R.G. (1964). Frictional pressure drop in two phase flow: Comparison of existing correlation for pressure loss and hold-up. AIChE J., (10)1. pp: 38 – 43.

Fernandez, J., Krechetnikov, R. and Homsy, G.M., (2005). Experimental study of a surfactant driven fingering phenomenon in a Hele-Shaw cell. J. Fluid Mech, (2005), vol. 527, pp. 197-216.

Ferno, M.A. (2012). Enhanced oil recovery in fractured reservoirs, introduction to enhanced oil recovery (EOR) processes and bioremediation of oil contaminated sites, Dr. Laura Romero-Zeron (Ed.), ISBN: 978-953-51-0629-6. pp:89-110.

Hashimoto, Michinao; Garstecki, Piotr; Stone, Howard A.; Whtesides, George M. (2008). Interfacial instabilities in a microfluidic Hele-Shaw cell. Soft Matter, 2008, Royal Society of Chemistry Journal 2008.4, pp: 1403 – 1413.

Hirasaki, G., Zhang, D.L., 2004. Surface chemistry of oil recovery from Fractured, oil-wet, carbonate formations. SPE 88365. June 2004 SPE Journal, 9(2), pp:5-8.

Hirasaki, G.J., Miller, C.A., Puerto, M. (2011). Recent advances in surfactant EOR. SPE 115386. SPE Journal 16 (4), 3-5.

Kianinejad, A., Ghazanfari, M. H., Kharrat, R., & Rashtchian, D. (2013). An Experimental Investigation of Surfactant Flooding as a Good Candidate for Enhancing Oil Recovery from Fractured Reservoirs Using One-Quarter Five Spot Micromodels: The Role of Fracture Geometrical Properties. Energy Sources, Part A: Recovery, Utilization, and Environmental Effects, 35(20), 1929–1938. http://doi.org/10.1080/15567036.2010.525591

Leonce, D. (2012). Synthesis and properties of soap. University of Dar Es Salaam. Fluid Flow Simulation in Fractured Reservoirs Mon., Vol. 19, 1954, pp. 38-41.

Park, C.-W., Maruvada, S. R. K., & Yoon, D.-Y. (1996). The influence of surfactant on the bubble motion in Hele–Shaw cells. Zhonghua Fu Chan Ke Za Zhi, 31(1994), 409–411. http://doi.org/10.1063/1.868059

Porter, M. R. (1994). Handbook of Surfactants. Handbook of Surfactants. http://doi.org/10.1007/978-94-011-1332-8, Glasgow, Blackie.

Raza, S., Hejazi, H., Gates, I.D., (2016). Two phase flow of liquids in a narrow gap: Phase interference and Hysteresis. Physics of Fluids, vol. 28, 074102 (2016); doi: 1063/1.4953238. http://dx.doi.org/10.1063/1.4953238

Razmi, R., Sedghat, M.H., Janamiri, R. and Hatampour, A. (2012). Application of SDS/LABS in recovery improvement from fractured models. World Academy of Science, Engineering and Technology, Vol 6, pp: 12-27.

Rosen, M. J., & Kunjappu, J. (2012). Surfactants and Interfacial Phenomena, 3rd Edition. Section Title Surface Chemistry and Colloids. http://doi.org/10.1002/0471670561 pp:34 - 46

Seethepalli, A., Adibhtla, B. and Mohanty, K.K., (2004). Physicochemical interactions during surfactant flooding of fractured carbonate reservoirs. SPE 89423. SPE Journal, 9(4), pp:17 -21 http://doi.org/10.2118/89423-PA

Tcholakova, S., Denkov, N. D., & Lips, A. (2008). Comparison of solid particles, globular proteins and surfactants as emulsifiers. Physical Chemistry Chemical Physics: PCCP, 10, pp:1608–1627. http://doi.org/10.1039/b715933c

Chapter Five: Impact of Polymer on Flow Behaviour, Phase Interference, and Displacement in a Hele-Shaw Cell

5.1. Abstract

It is well known that polymer additives to water for oil displacement in porous media improves displacement by regulating mobility ratio of the phases. This has not been examined for oil displacement in fractures through relative permeabilities, flow behaviour analysis and microscopic observations. The interfaces between phases also play a vital role in improving oil recovery which needs to be analysed in fractured media. The research documented here shows experimental evaluation of oil displacement using polymer additives to water in a Hele-Shaw cell. A series of experiments are conducted to examine how aqueous polymer (polyethylene oxide) solution changes the behaviour of oil displacement in a narrow gap. Unlike the case of co-current oil and water flow where after the breakthrough, complex fluid distribution patterns with engulfed oil drops resulted, we report that in the case of polymer, the aqueous solution dominant finger expands and completely occupies the cell. Thus, a high oil recovery is resulted.

5.2. Introduction

When a more viscous phase (oil) is displaced by a less viscous one (water), the fluid interface becomes unstable and the displacing fluid fingers into the displaced phase (Hill et al., 1952; Saffman and Taylor, 1958; Chouke et al., 1959). Consequently, an early breakthrough of the displacing phase to production wells is resulted where a large volume of oil remains unrecovered. Decreasing the viscosity difference or mobility ratio of the displacing and displaced phases, minimizes instability of the interfaces. In the case of displacing a viscous phase with a less viscous phase, the viscosities difference among the phases could be reduced by adding polymer additives to the displacing phase. Polymer solution flooding through core samples extracted from reservoirs or glass micromodels has been experimentally and numerically examined for the past four decades. Donaldson (1985) examined the impact of polymer solutions on oil recovery and found that oil displacement improves because polymers tend to increase the viscosity of the displacing aqueous phase. He further described that the polymer adsorbs on the rock surface causing concentration reduction.

Mungan, (1971) studied different rheological properties, adsorption and transport characteristics of water and oil by injecting different concentrations of polymer solution (polymer molecular weights ranged from 2 to 7 million Daltons). Adsorption studies are carried out on silica samples whereas dynamic adsorption experiments were performed on 20-inch-long and 2-inch diameter sand packs. For fingering analysis, Mungan used a Hele-Shaw cell (dimensions 26.8cm x 26.8cm x 0.006cm) and a porous media sample of Berea sandstone block (dimensions 12" × 12" × 1"). He concluded that viscosity of the polymer is mainly dependant on the flow rate, molecular weight, and the composition of the solvent and that of oil recovery is increased by injecting a small volume of different concentrations of the polymer before water flooding. He observed a breakthrough recovery factor of 84% for viscosity ratio of 0.03 (polymer solution to oil) while 28% for viscosity ratio of 30. Mungan further explained that the interface in case of the lower viscosity contrast is more stable than the higher viscosity ratios and proposed that polymer slug before water injection is more economical and creates a stable front.

Abrams, (1975) examined changes of the interfacial tension, fluid viscosity and flow velocity in case of a polymer aqueous phase flooding through a short water-wet core. He concluded that the oil recovery rises with a drop of the interfacial tension. Abrams proposed a factor 'F' which defines the efficiency of the polymer flooding process in terms of increase in oil recovery from the core:

$$F = (^{v_m \mu_w}/_{\sigma_{ow}})(^{\mu_w}/_{\mu_o})^{0.4} \quad (1)$$

where v_m is the homogeneous/combined velocity of both the phases and μ is the viscosity and subscripts 'w' and 'o' refer to the water based phase and oil phases, respectively. Abrams explained that if '*F'* is greater than 10^{-4}, the residual oil saturation will be low and the oil recovery will be high whereas in case of smaller values of *F*, the efficiency of the process will be low. The results implied that for getting maximum oil recovery, the value of '*F'* should be increased by raising viscosity of the water and reducing interfacial tension between the phases.

Donaldson et al., (1985) and Grillet et al., (2012) investigated the use of polymers for oil recovery. They concluded that it is very costly to inject the polymer solution for the entire oil recovery process, therefore, a small quantity of the polymer should be flooded followed by water flooding as studied by Mungan, (1971) and Daripa and Pasa, (2004, 2005). Gorell and Homsy, (1983) examined numerically three layers flow with the more viscous layer (of displaced phase), intermediate layer of variable viscosity and less viscous layer of the displacing phase, for flow in Hele-Shaw cell where the interfaces are considered as contact discontinuities. Following that, Daripa and Pasa (2004, 2005) also studied three-layers flow in Hele-Shaw cell. They theoretically proposed an optimal viscosity profile for aqueous phase of polymer (polysolution) flooding ahead of water in a Hele-Shaw cell. They concluded that with the use of viscosity profile, the viscosity jump reduces and viscous fingering can be eliminated. In another research, Daripa and Pasa (2005) estimated minimum concentration of polymer and length of the intermediate layer of the polymer aqueous phase. They concluded that with the use of the estimated concentration and length of the polymer layer, instabilities in the interface could be reduced and oil recovery can be increased, experimentally and on field scale.

Hematpour, (2011) studied the effects of different types of polymers for displacing low viscosity oil from two simplified glass micromodels (quarter five-spot pattern) with different porosities. The oil saturated cells were flooded with three different types of polymers at a constant flow rate of 0.0008 cc/min. They reported that the polymer reduces mobility of water and improves oil recovery. Their results showed that the hydrolyzed polyacrylamide (HPAM 25%) solution yields more recovery than other types of polymers. The results showed that increasing the flow rate of water or polymer solution raises the effective permeability of the phase, reduces breakthrough time, and lowers oil recovery. Therefore, for higher oil recovery, they recommended lowest feasible injection rate of the displacing phase (polymer aqueous phase).

Clemens et al., (2012) experimentally and by computational fluid dynamics (CFD) simulation, analyzed fingering in a displacement process of oil by water and polymer flooding in micromodels with area of 25 cm^2, permeability 950 mD, and porosity 47% which was initially saturated with a 450 cP crude oil. They flooded both the cells separately with water and polymer solution (16 cP). They observed that the polymer creates more fingers but shorter in length than the fingers created by water. The polymer yielded higher oil recovery than water. The results of the CFD simulations were consistent with those obtained from the experiments.

Ying-Jie et al., (2013) studied effects of pore structures on the oil recovery by polymer and synthetic reservoir brine flooded through synthetic oil (1.78 cP) saturated glass micromodels (dimensions 3cm × 2cm with channels 1 to 100 μm) etched represented properties typical of the pore structure of the Shuanghe oil field in China (600 mD). The water cut of the reservoir after extensive water flooding was 95%. To achieve greater oil recovery, polymer (400×10^4 Daltons) was tested in the experiments. The micromodel had single injection and single exit ports at opposite ends. Four models were prepared on the basis of different pore throat ratio (PTR) and coordination number (CN). After drying and evacuating the models for 2 hours, they saturated them with water for 2 days and then flooded with oil for 3 days. The oil was displaced by polymer flooding after water injection at a constant flow rate of 2 μl/min. They noticed that water flowed through the larger channels, bypassed narrow pore throats, resulted oil entrapped due to higher capillary forces. They also observed that the PTR effected recovery more than the coordination number and explained that the higher PTR

implies more heterogeneity. Ying-Jie et al. concluded that the polymer significantly increased oil recovery from all micromodels tested.

In the research documented here, the dynamics of polymer solution and its concentration on multiphase flow and oil-polymer interactions in a narrow gap is examined.

5.3. Experimental Apparatus and Methodology

Figure 5.1 depicts the equipment used for the co-current flow of polymer solution with oil. The set up consists of a Hele-Shaw cell made of Plexiglas plates with a 1/64-inch gap thickness. The gap is initially saturated with oil and then fluids are injected with a step wise changes in their flow rates.

The polymer used in the experiments is polyethylene oxide (PEO). Different concentrations solutions of the polymer are prepared by adding its different quantities with de-ionized water. The colourless mineral oil (20.236 cP at 22.46°C) used in the experiments is Marcol 7 provided by Imperial Oil with density of 847.0 kg/m^3 at 22.46°C.

The aqueous phase (with dissolved PEO) is injected through the middle port and the mineral oil is injected through the adjacent ports. The fluids are produced through three exit ports. Two pressure transducers are connected to the gap through the lower plate and the area between them is considered as the area of observation. After breakthrough and on reaching the steady state conditions, the differential pressure, time, saturations and images of the flow patterns are collected by the data acquisition system over a 4-minutes time interval at each flow rate. A series of experiments are conducted for each polymer solution concentration (0.5 wt. %, 1 wt. %, 1.5 wt.%). The data and images are analysed to evaluate the relative permeabilities and flow patterns. This analysis is carried out for each step of the flow rate. The relative permeability calculation is started as soon as the flow channels/fingers of both phases extend across the zone of observation. The absolute permeability of the Hele-Shaw cell is obtained from the planar Poiseuille's law by using water flow through the gap at different flow rates. The absolute permeability of the cell is equal to 10,923 D. The relative permeability of

each phases is calculated using extended Darcy's equation for multiphase flow through the gap. The average values of Reynolds number in all the experiments is ranging from 0.08 to 0.42 indicating laminar flow of the fluids. Considering no slip conditions and steady state, laminar flow in the cell, Darcy's and the planar Poiseuille's equations for the flow can be used to calculate the relative permeabilities of the phases.

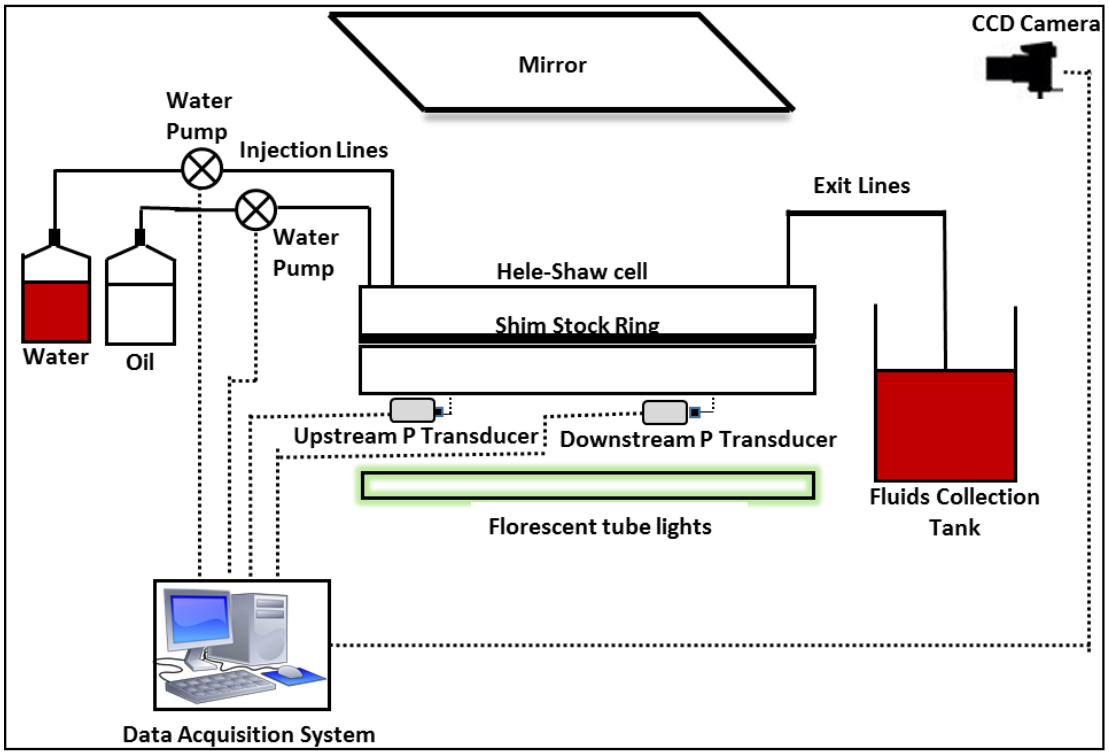

Figure 5.1: Schematic of the experimental set up (adapted from Raza et al., 2016)

5.4. Results and Discussion

5.4.1. Impact of Polymer on Viscosities and Interfacial Tensions of the Fluids

Figure 5.2 shows the effect of polymer concentration on viscosity of the aqueous phase. Aqueous phase viscosity is an increasing function of polymer concentration. Figure 5.2 depicts that with the addition of 0.5 wt. % polymer to the water, its viscosity increases from 1.07 to 2.97 cP. Similarly, 1 wt. % of the polymer raises the water viscosity to 6.89 cP and 1.5 wt. % PEO to 11.4 cP. By raising concentration of the

polymer more than 1.5 wt. %, the polymer aqueous phase viscosity exceeds the viscosity of the oil. At 2 wt. % PEO, the aqueous phase viscosity reaches 30.26 cP while for 5 wt. % PEO this value raises up to 392 cP. The highest concentration of the polymer solution used in this study is 1.5 wt. %.

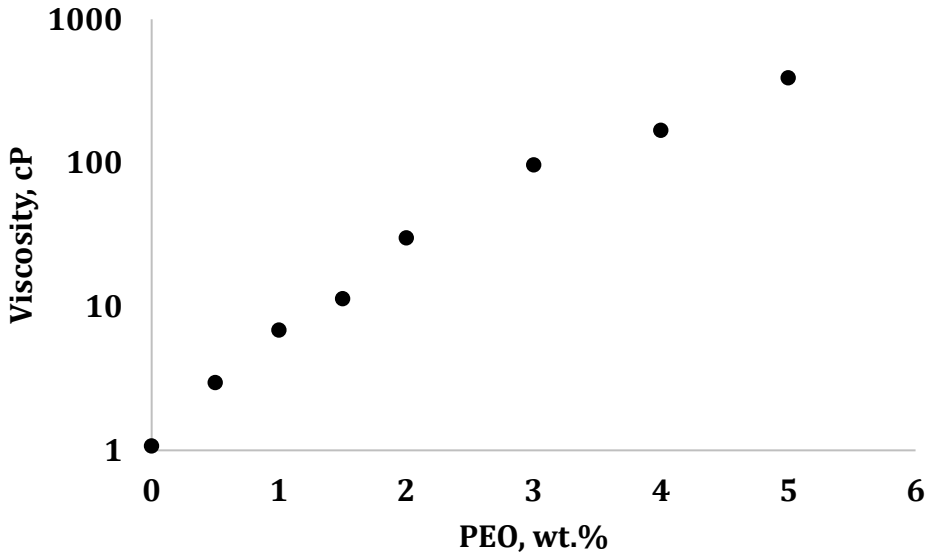

Figure 5.2: Relationship of viscosity of the polymer (PEO) aqueous phase to its concentration

Figure 5.3 shows the reduction in interfacial tension, measured by the Du Noüy Ring method using a TensioCAD tensiometer. The interfacial tension falls from 45.7 to 28.62 mN/m by adding only 0.5 wt.% of the polymer to the water but further increase of the concentration (from 0.5 wt.% to 5 wt.%) did not reduce the interfacial tension significantly and its values varied between 26.77 to 28.62 mN/m. The viscosity and interfacial tension data show that the main impact on the properties of the polymer solution over 0.5 wt.%, PEO is due to viscosity of the aqueous phases.

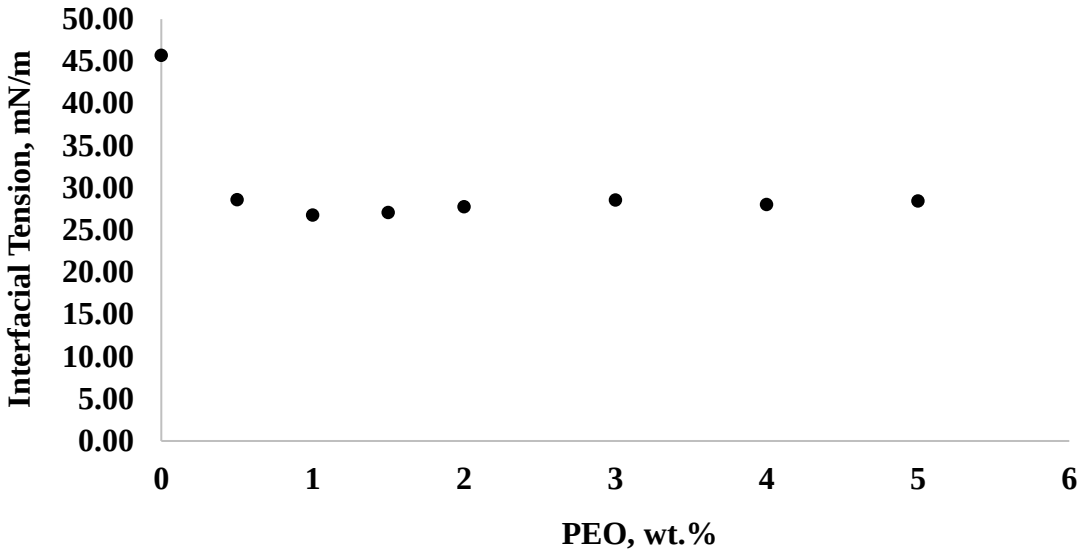

Figure: 5.3. Interfacial tension between oil and polymer aqueous phase versus concentration of PEO

5.4.2. Phase Flow Patterns Analysis

Table 5.1 shows a comparison of the water-oil and polymer solution (1.5 wt.%) -oil flow results in the Hele-Shaw experiments. The differential pressure, phase saturations, and images of the phases (red is aqueous phase and clear is oil phase) are acquired before breakthrough for each step of flow rate that is run for 4 minutes, while after breakthrough, the data and images are recorded at steady state conditions of the differential pressure and saturations. As the flow evolves, the water channel on reaching to the centre of the cell, splits into two parts and then merge, engulfing oil droplets hosted in the water phase as shown at time 1706 seconds. The polymer solution exhibits similar behaviour as shown at times 1706 and 1947 seconds. Thereafter, water tends to flow in a straight path through the dominant finger although a secondary finger emerges at about time 2183 seconds. It takes roughly 813 seconds (13 minutes) for the water to reach the end of the observation area with an average velocity of 2.95 cm/minute and water saturation equals to 23.3% at breakthrough. In the case of the polymer solution, it enters the cell in the form a finger, initially narrower than the water finger and then widens, especially at the upstream end of the flow. At the time of exit from the zone of observation the width of the PEO solution finger

becomes greater than the finger created in the water-oil flow. For the polymer solution case, breakthrough occurs after about 1473 seconds (23.5 minutes) with polymer solution saturation at breakthrough is equal to 43% whereas the average volumetric flow rate of 1.63 ml/minute. Thus, in period before breakthrough, the polymer solution case achieves higher recovery of oil. A comparison at time 2663 seconds reveals that the saturation of the polymer solution phase is 70% greater than that of the water case. These observations confirm that the increase in viscosity of the solution by adding polymer, leads to wider and uniform channel of the aqueous phase as the flow evolves to breakthrough.

Thereafter, as can be seen from the time 2909 to 3639 seconds, the aqueous phase saturation and pressure drop increase for both the cases but the width of the displaced zone in the polymer solution case remains always greater than that of the water-only case. For the polymer solution case from time 3639 to 4614 seconds, a secondary finger emerges at the top of the aqueous phase which extends across the cell. The results clearly show that the aqueous phase in the polymer solution case occupies more area of the cell than the area occupied by the water finger. The pressure drops are greater, over most of the time: the polymer solution case has pressure drop roughly double that of the water case. This is due to the greater viscosity of the polymer solution. By the time 5579 seconds, the saturation of the polymer solution within the observation area is greater than 85% and this persists for the remainder of the experiment. In the water case, the saturation is below 30% at this time. Beyond time 7499 seconds, over 90% of the cell is occupied by polymer solution and the oil flows in the form of a narrow channel from one side of the domain to the other side.

One important difference that is observed between the water-oil and polymer solution-oil floodings, is the widening and narrowing of the displacing phase after the breakthrough. In the water-oil case, the water channel is initially wider before breakthrough but it stretches and becomes narrow after the breakthrough and its saturation drops down from 29% to 22.7%. In the case of the polymer solution, the aqueous phase continues to grow wider as the flow evolves and it is due to the adsorption of the polymer on the surface, which will be discussed in the following paragraphs with details.

Table 5.1: Comparison of water-oil and polymer (1.5 wt. %) solution-oil data and images

Time	q_w,	q_o,	Water-Oil			Polymer Solution-Oil		
s	ml/min	ml/min	dp, psi	S_w	Image	dp, psi	S_w	Image
1222	0.25	0.5	0.0485	0.012	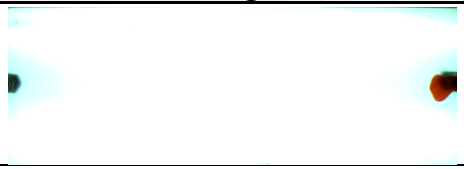	0.044	0.008	
1457	0.3	0.5	0.0445	0.058		0.045	0.032	
1706	0.35	0.5	0.0485	0.12	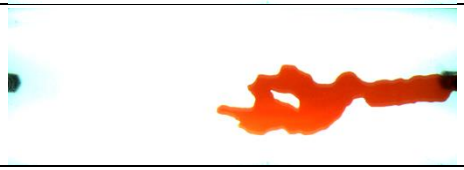	0.047	0.076	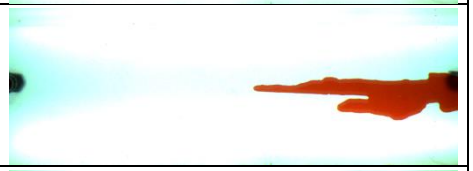
1947	0.45	0.5	0.0395	0.206	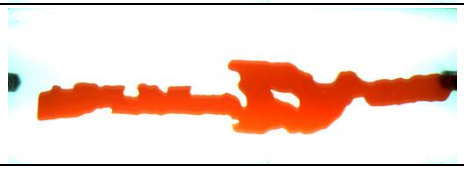	0.052	0.134	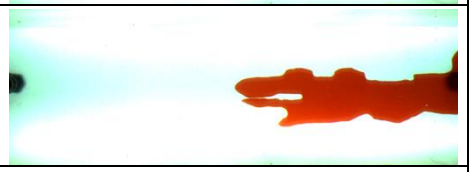
2183	0.55	0.5	0.0435	0.249	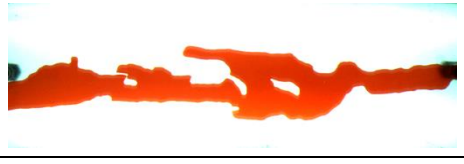	0.055	0.215	

Time	q_w,	q_o,	Water-Oil			Polymer Solution-Oil		
s	ml/min	ml/min	dp, psi	S_w	Image	dp, psi	S_w	Image
2422	0.65	0.5	0.0305	0.252	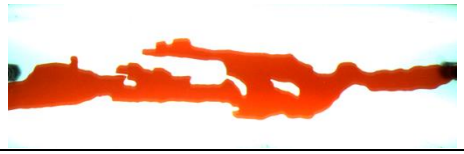	0.059	0.322	
2663	0.75	0.5	0.0415	0.261	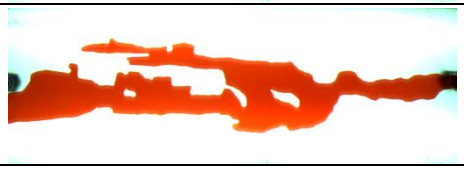	0.062	0.446	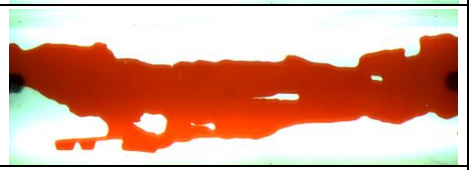
2909	0.85	0.5	0.0325	0.29		0.05	0.517	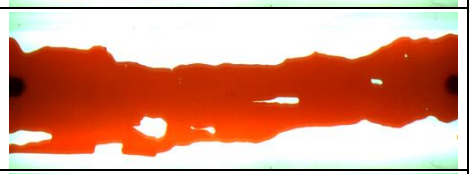
3146	1	0.5	0.0465	0.257	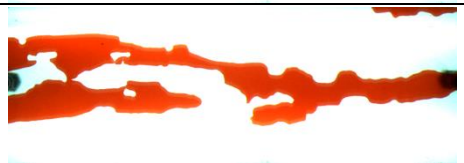	0.057	0.545	
3397	1.15	0.5	0.0515	0.275		0.06	0.556	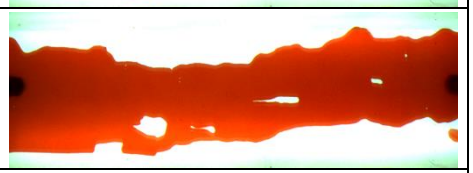
3639	1.3	0.5	0.0475	0.275	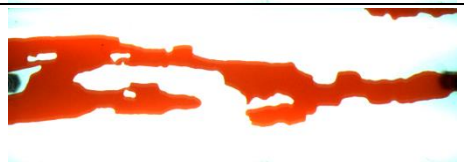	0.066	0.585	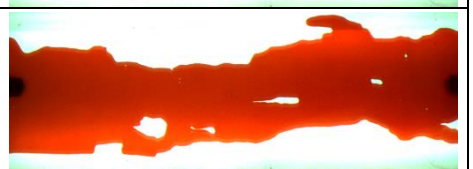

Time	q_w,	q_o,	Water-Oil			Polymer Solution-Oil		
s	ml/min	ml/min	dp, psi	S_w	Image	dp, psi	S_w	Image
3883	1.45	0.5	0.0445	0.269	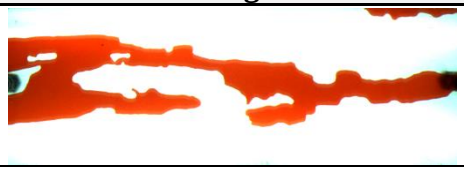	0.065	0.62	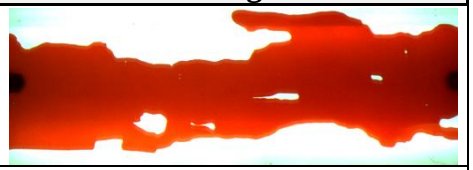
4125	1.6	0.5	0.0445	0.256		0.074	0.668	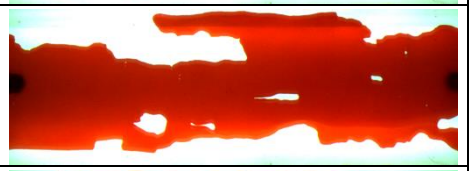
4371	1.75	0.5	0.0435	0.241	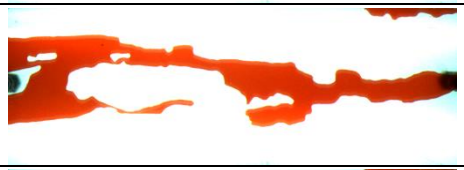	0.078	0.721	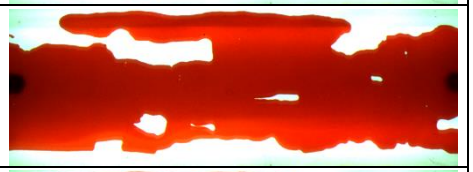
4614	2	0.5	0.0445	0.230	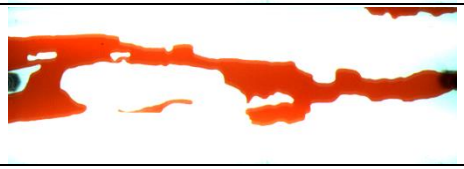	0.086	0.743	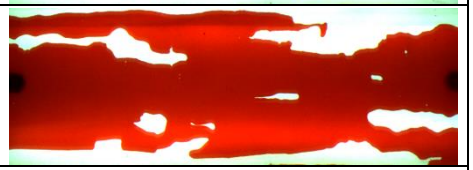
4857	2.25	0.5	0.0505	0.227	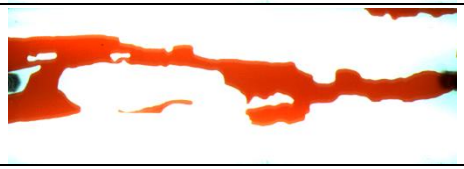	0.100	0.744	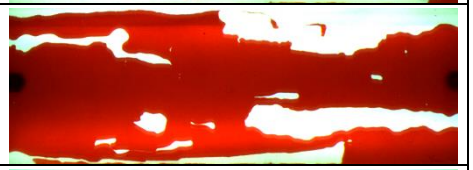
5099	2.5	0.5	0.0485	0.233	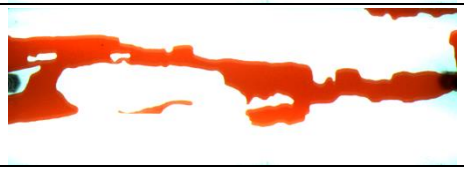	0.098	0.7	

Time	q_w,	q_o,	Water-Oil			Polymer Solution-Oil		
s	ml/min	ml/min	dp, psi	S_w	Image	dp, psi	S_w	Image
5342	3	0.5	0.0545	0.245	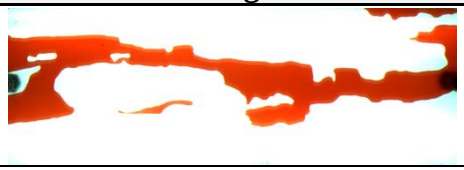	0.112	0.746	
5579	3.5	0.5	0.0585	0.269		0.114	0.867	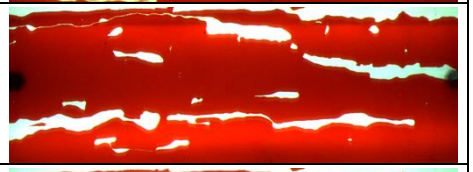
5815	4	0.5	0.0615	0.335		0.143	0.863	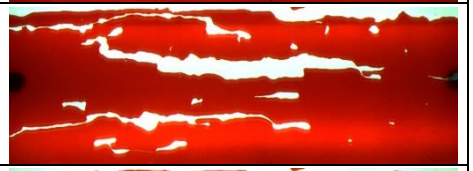
6053	4.5	0.5	0.0315	0.398		0.155	0.868	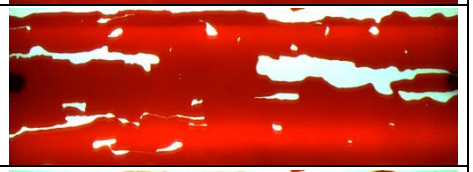
6305	5	0.5	0.0375	0.39		0.169	0.874	
6546	5.5	0.5	0.0455	0.382		0.177	0.914	

Time	q_w,	q_o,	Water-Oil			Polymer Solution-Oil		
s	ml/min	ml/min	dp, psi	S_w	Image	dp, psi	S_w	Image
6788	6	0.5	0.0505	0.377	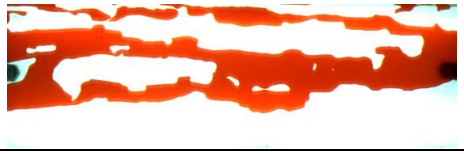	0.192	0.909	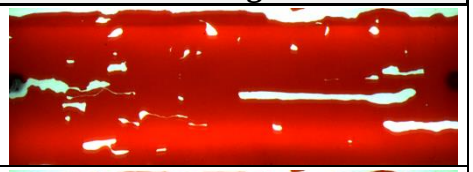
7022	6.5	0.5	0.0485	0.371	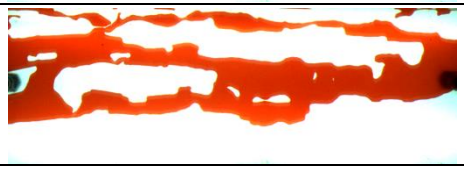	0.217	0.902	
7265	7	0.5	0.0525	0.367		0.219	0.914	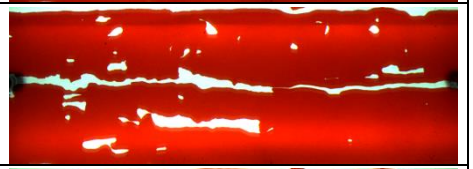
7499	7.5	0.5	0.0535	0.374		0.241	0.942	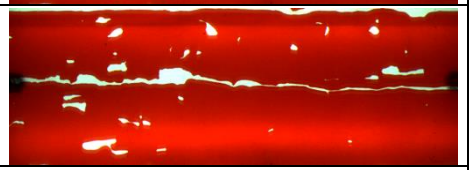
7743	8	0.5	0.0585	0.406	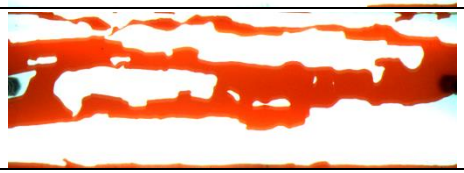	0.248	0.939	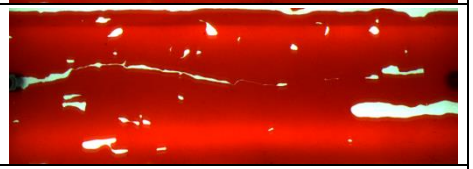
7984	8.5	0.5	0.0655	0.399		0.246	0.931	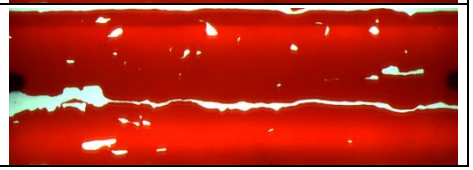

Time	q_w,	q_o,	Water-Oil			Polymer Solution-Oil		
s	ml/min	ml/min	dp, psi	S_w	Image	dp, psi	S_w	Image
8225	9	0.5	0.0675	0.387		0.256	0.944	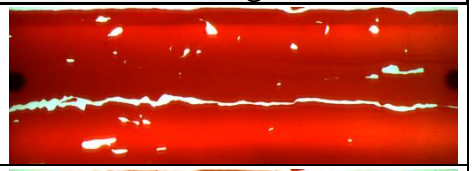
8487	9	0.4	0.0645	0.385		0.245	0.956	
8755	9	0.3	0.0665	0.412		0.237	0.964	
8984	9	0.2	0.0685	0.45		0.241	0.969	
9224	9	0.1	0.0585	0.476		0.241	0.966	
9470	9	0.05	0.0535	0.501		0.235	0.981	

Time	q_w,	q_o,	Water-Oil			Polymer Solution-Oil		
s	ml/min	ml/min	dp, psi	S_w	Image	dp, psi	S_w	Image
9719	9	0.025	0.0435	0.517		0.234	0.985	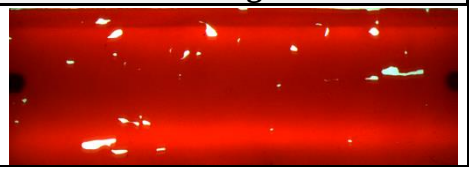

As discussed earlier that the flow rates are changed step wise and kept constant for at least 4 minutes to stabilize the flow before taking the saturation and differential pressure readings. The maximum and averaged values of the properties are calculated from the acquired data and is presented in Table 5.2. This procedure is repeated for each set of the fluids i.e., for oil-water and for all concentrations of polymer and oil during their flow through the gap.

It can be observed from the differential pressure listed in Table 5.2 that in the case of a single finger movement before breakthrough, the differential pressure in the polymer solution flooding case is higher than that of the water and it increases as the channel moves forward. This is due to the enhanced viscosity of the polymer solution although some part may be due to the shift of wettability of the plates (shown in Figure 5.8-will be discussed later) that in turn lowers the effective mobility of the aqueous phase due to adsorption of polymer that resists their flow. In the water flooding case, the differential pressure fluctuates due to disconnection and reconnection of the water channels and each time the pressure difference rises when a new channel is moving and then declines at the exit of the channel from the cell. In the polymer solution flooding case, the continuous increase of the differential pressure and relatively low fluctuations is due to no disconnection of channels or reduction of its size after the finger reaches the end of the cell.

The rise in viscosity of the polymer aqueous phase, shown in Figure 5.2, and decrease in the interfacial tension, displayed in Figure 5.3, results in an increase of the capillary number (Figure 5.4) and factor, *F* (Figure 5.5) introduced by Abrams (1975). In the case of reduced capillary forces associated with the rise of the capillary number, the interference between the phases enlarges with tip splitting and small droplets of oil form near the interface (as observed under microscope). These oil droplets hosted in the aqueous phase are then carried out with the aqueous phase from the system. Figures 5.4 and 5.5 also reveal that although the capillary numbers and factor 'F' increase with the addition of the polymer,

they are still less than unity, which shows that the flow in any case is dominated by capillary forces.

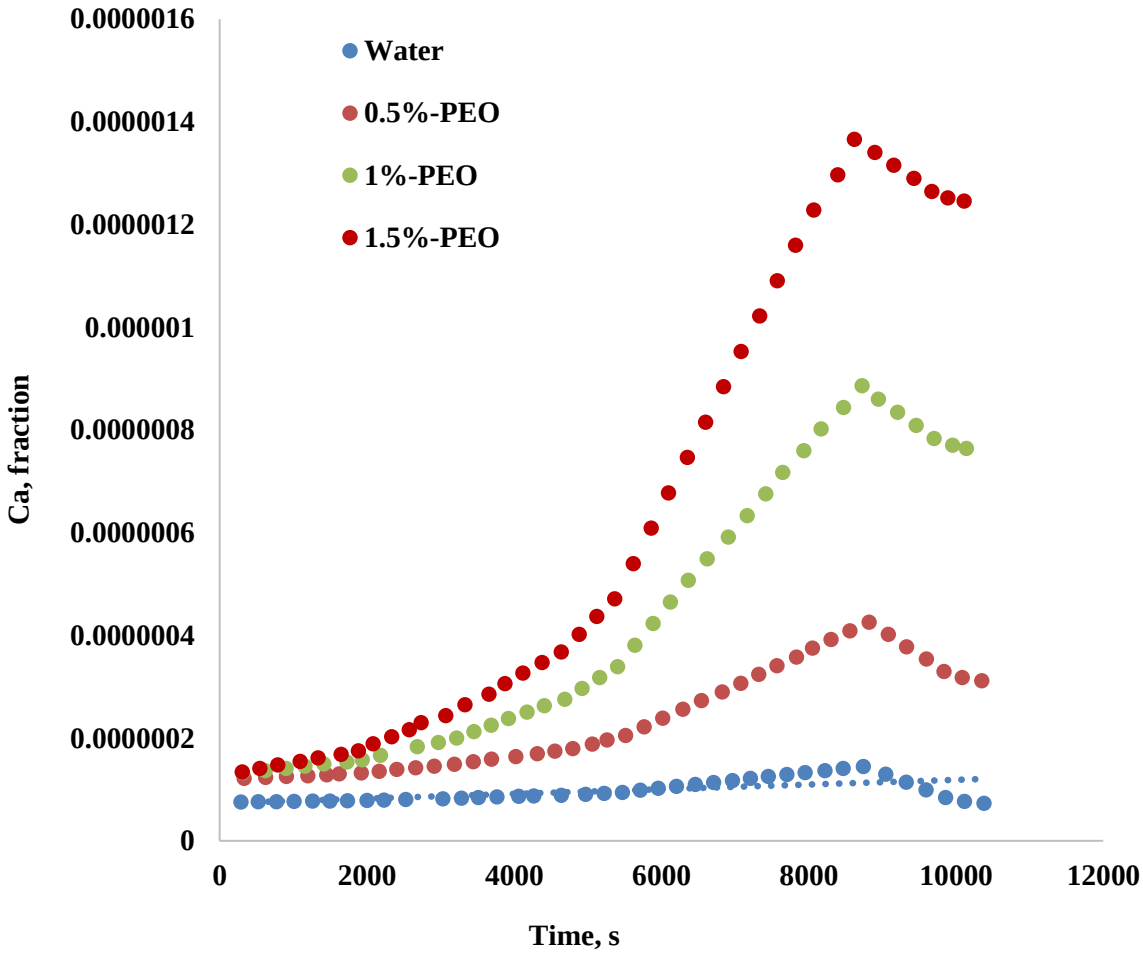

Figure 5.4. Relationship of capillary numbers of water and different concentrations of PEO

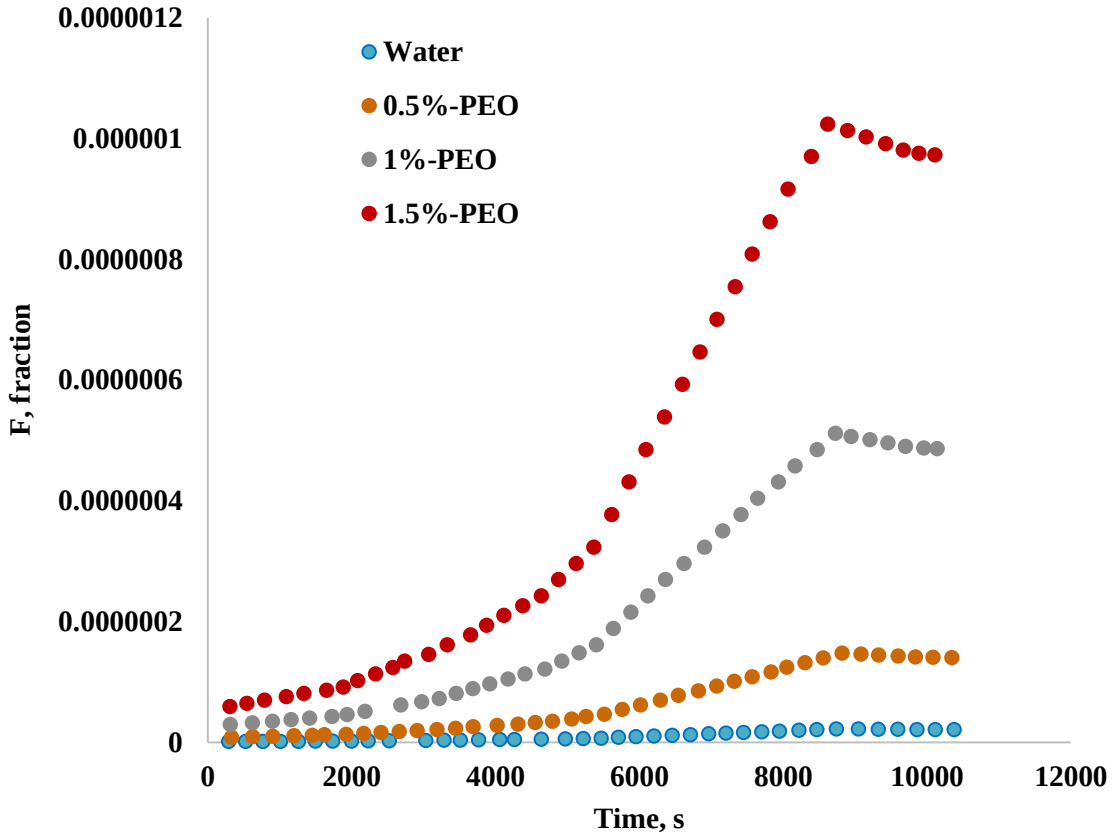

Figure 5.5: Comparison of the factor *F*, introduced by Abrams (1975) for different concentrations of PEO

As shown in Figures 5.6 and 5.7, the mobilities of both the phases dropped with increase in the concentration of the polymer. The reduction of the aqueous phase mobility is mainly linked to the enlargement of its viscosity and adsorption of the polymer aqueous phase on the surface altering wettability of the surface. Thus, after each experiment, there is a thin layer of polymer adhered to the surface of the plates, since the polymer solution uniformly displaces the oil from the gap, the deposited polymer is nearly uniform throughout the gap. The polymer thin layer can also be depicted from the reduction in absolute permeability by

642D. The polymer changes wettability of the Hele-Shaw cell from less water-wet to more water-wet. It can be observed in Figure 5.8 which shows spreading of the water droplets on the Hele-Shaw plate both in the original state (prior to exposure to PEO) and after the polymer coats the surface. The images reveal that the polymer coating raises wettability of the surface with respect to water. The polymer coating adds a resistance to the flow of the aqueous phase which in turn lowers its mobility leading to improved displacement of the oil phase. This behaviour was also observed by Donaldson (1985); Jennings et al., (1971); Domingues et al., (1977), and Needham et al., (1987), and Hendraningrat et al., (2012).

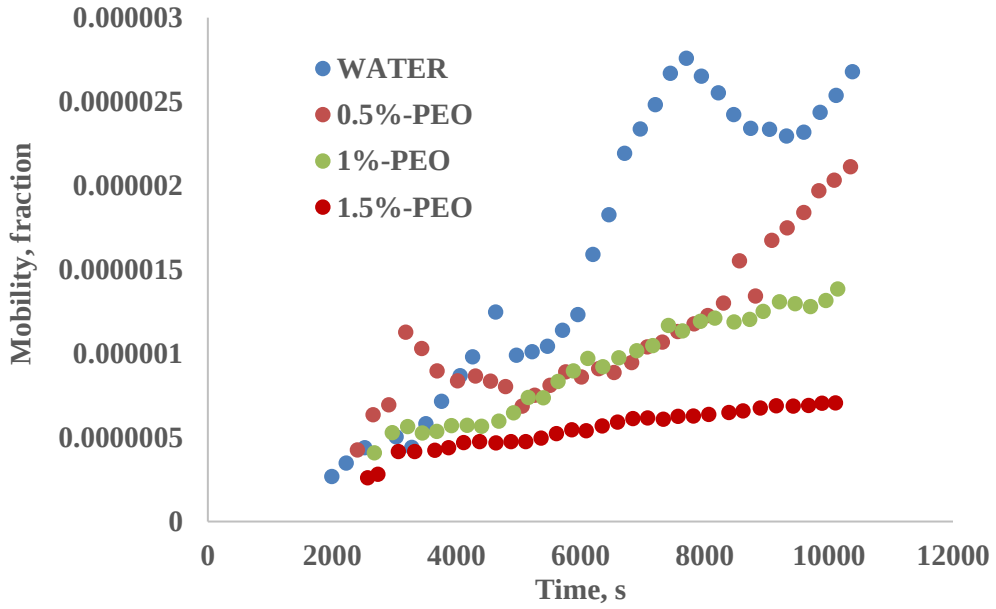

Figure 5.6: Mobility of the water changes with different concentrations of the polymer (PEO)

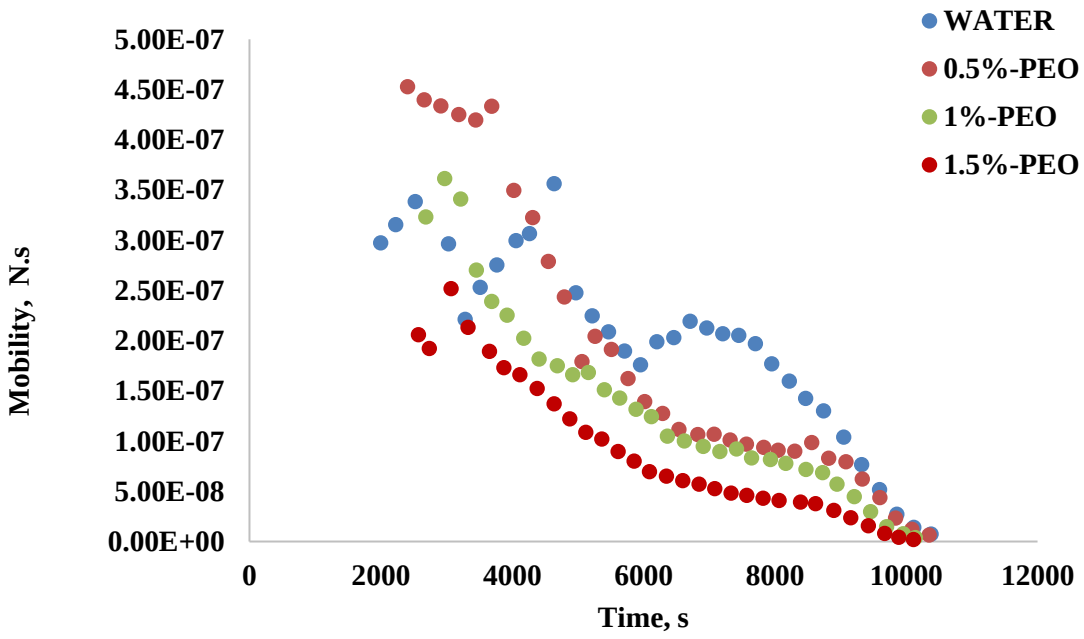

Figure 5.7: Changes of mobility of oil with different concentrations of polymer

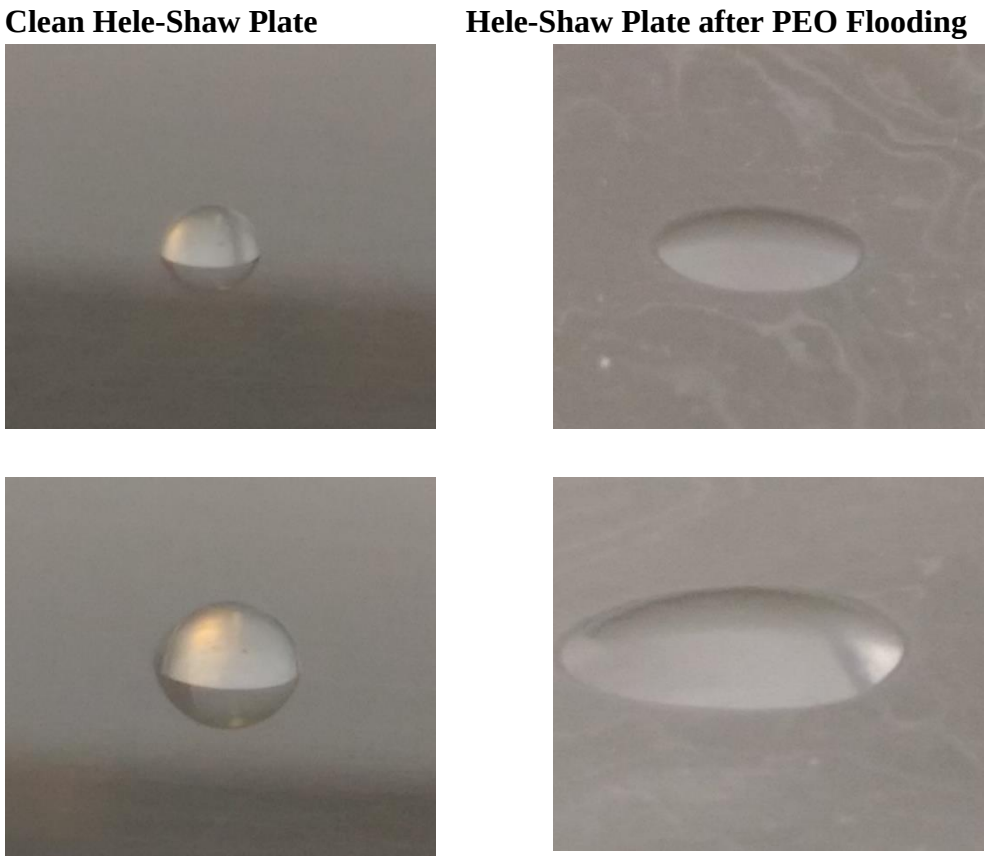

Figure 5.8: Examples of 0.1 ml water droplets placed on the Hele-Shaw plates before PEO flood and after PEO flood

5.4.3. Impact of Polymer on Relative Permeabilities, Saturations of the Phases, Reynolds Numbers and Mobility Ratios

As described in the last subsection that polymer alters the surface of the cell from being less hydrophilic to more hydrophilic. Figure 5.9(a) shows the relative permeability curves of the oil and aqueous phases for 0, 1, and 1.5 wt. % PEO polymer concentrations. The water-oil curves are relatively straight with the cross-over point equal to about 0.6. The

irreducible water saturation in the case of oil water flow is equal to about 0.1 and residual oil saturation is about 0.17. In the case of 1 wt. % polymer solution, the relative permeability curves become less straight and the residual oil saturation lowered to about 0.08. In case of 1.5 wt.% polymer solution, the residual oil saturation is further reduced to about 0.03. In general, the addition of polymer to the aqueous phases raises the aqueous phase relative permeability curve. On the other hand, the oil relative permeability curve follows the same trend as the polymer solution concentration is increased.

Figure 5.9(b) displays a comparison of the water-oil relative permeability curves for the case where the Hele-Shaw plates are clean (no PEO) and the case after the PEO has coated the plates (experiment conducted after flooding 1.5 wt. % polymer solution). The results show that the polymer coating on the plates significantly changed the relative permeability curves – both their shape and endpoints. The mobile phase region between the endpoints is narrow in the case with the polymer coating. This reveals that the presence of the polymer film lowers mobility of the water within the cell.

(a)

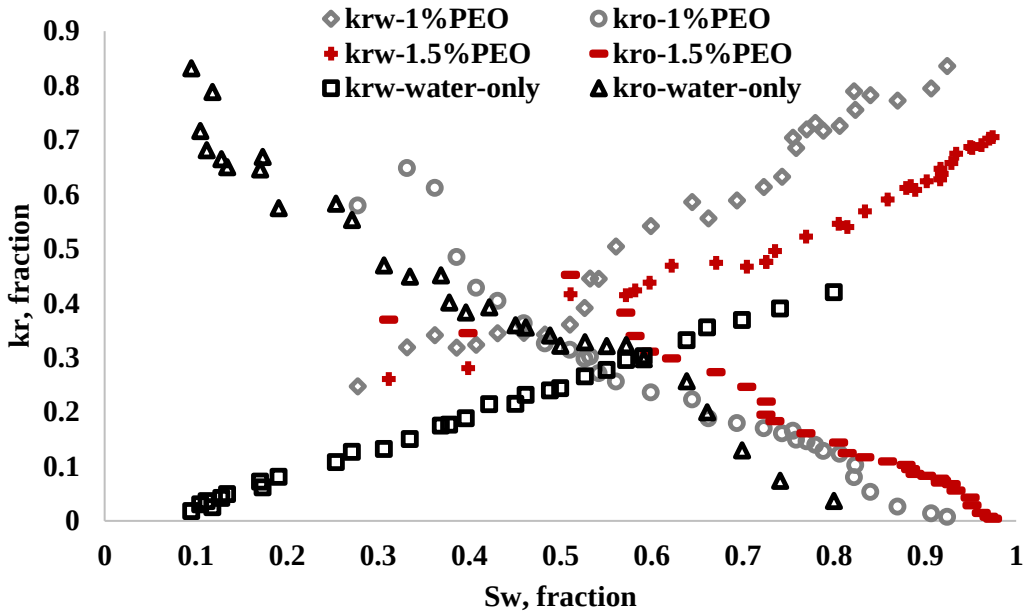

(b)

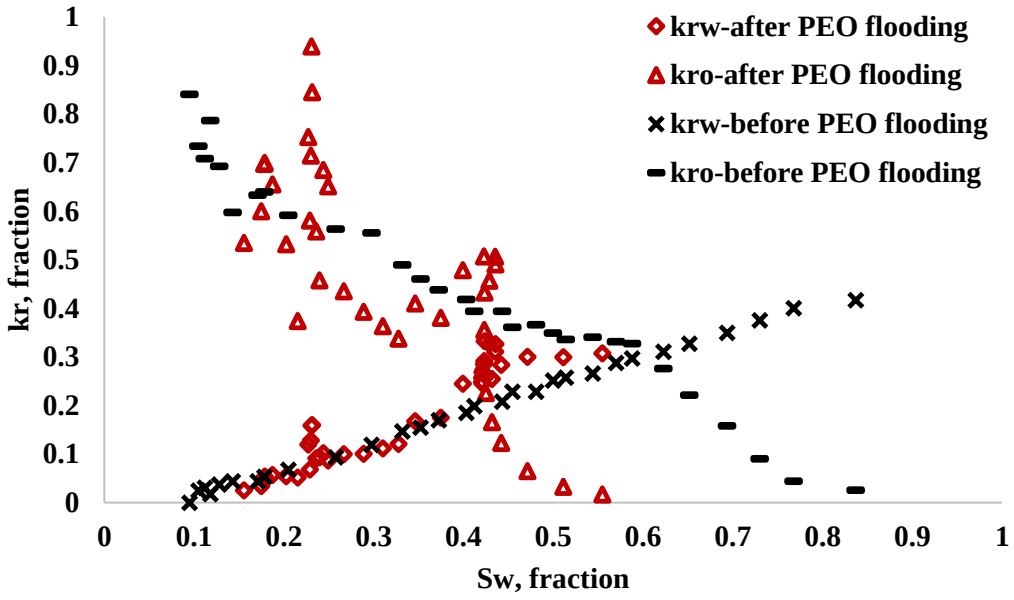

Figure 5.9: (a) Relative permeabilities of oil with water and 1 and 1.5 wt.% polymer solution and (b) comparison of relative permeability curves for water (before PEO flood) and water (after PEO flood with thin layer of PEO on Hele-Shaw plates)

We further quantify the relative permeability data for various cases, polymer solutions with different concentrations, as presented in Table 5.2. From a comparison of the averaged values in the Table 5.2, it can be observed that the end point saturation of water rises with increase in the concentration of the polymer (as discussed earlier). The table shows that the water saturation increases from 58% to 81.7% by adding 0.5 wt.% polymer and to 97% by adding 1.5 wt.% polymer to the water. It is expected that this value could drop with roughness of the surface or in the actual rock sample of a reservoir but our results at least gave an indication that the oil recovery could be raised with an increase in the concentration of the polymer. Also, as noticed earlier, the viscosity of water increases with polymer addition and to flood the viscous fluid through the cell, higher differential pressure is needed. Also from the Darcy's equation for relative permeability, the viscosity of a phase has a linear relationship with differential pressure and relative permeability. Results in co-current flow of oil and polymer depict that the average differential pressures increased from 295 Pa to 521 Pa when the polymer concentration is increased from 0 to 1.5 wt. % PEO. As a result of this increase in the water relative permeability, the averaged mobility ratio also increased slightly from 28.70 (water) to 29.61 (1.5 wt. % PEO), but the individual mobilities of water and oil phases dropped. This reduction in the values of mobility are also noticed by Donaldson (1985). In the same way, the average Reynolds numbers calculated on the basis of homogenous viscosity, velocity and density defined by Delhaye, (1981) reduced from 0.47 to 0.082 by increasing the polymer concentration from 0 to 1.5 wt.%. On the other hand, the capillary number raised from 0.975×10^{-7} to 6.37×10^{-7} due to the increase in viscosity and decrease in interfacial tension between polymer and oil.

Saturation analysis indicates that oil recovery is an increasing function of polymer concentration. This is mainly due to increase in the viscosity of the water and slight decrease in the interfacial tension with the addition of polymer. From the trend lines of the capillary number and factor, *F*, it can also be confirmed that their values rise with an increase in the polymer concentration. Although the values of *F* are less than that of Abrams, (1975) suggested value for efficient oil recovery from reservoir (10^{-4}), the results

show that the polymer significantly improves the effectiveness of displacing oil from the cell.

Table 5.2: Comparison of the data and calculated values obtained during water with 0.5%, 1% and 1.5% PEO experiments. Shaded rows show maximum and unshaded the averaged values for the entire experiment

PEO (%)	Max./ Avg	S_w	dp (Pa)	k_{rw}	k_{ro}	λ_w	λ_o	*M*	N_{re}	Ca	*F*
0	Max	0.581	500.1	0.260	0.655	2.76E-06	3.56E-07	360	1.922	1.44E-07	2.22E-08
	Avg	0.303	295.2	0.154	0.364	1.63E-06	1.98E-07	28.7	0.470	9.75E-08	1.01E-08
0.5	Max	0.817	770.4	0.595	0.833	2.28E-06	4.53E-07	360	0.718	4.26E-07	1.48E-07
	Avg	0.392	392.5	0.314	0.347	1.20E-06	1.83E-07	28.7	0.237	2.37E-07	6.60E-08
1	Max	0.925	954.7	0.857	0.665	1.42E-06	3.61E-07	360	0.314	8.86E-07	5.12E-07
	Avg	0.513	493.3	0.571	0.251	9.46E-07	1.36E-07	29.6	0.128	4.42E-07	2.33E-07
1.5	Max	0.974	1742.4	0.723	0.463	7.24E-07	2.52E-07	360	0.191	1.37E-06	1.02E-06
	Avg	0.617	816.6	0.564	0.168	5.64E-07	9.11E-08	29.6	0.082	6.37E-07	4.57E-07

5.4.4. Microscopic Analysis of the Interfaces Between PEO Polymer and Oil

Figure 5.10 presents microscopic images of the interfaces between 1.5wt. % PEO polymer and oil as viewed in an Nikon Ti-E inverted confocal microscope. Figure 5.10(a-c) display a time sequence illustrating how the interfaces developed just after the two phases contact each other. When zoomed in, as shown in Figure 5.10(d-f), it is observed that the polymer solution forms small, less than 2 μm diameter, droplets in the oil phase just beyond the main interface. These small droplets tend to be irregular in shape and are positioned within 10 to 20 μm of the main interface. The observations show that an aqueous phase in oil microemulsion is created just upstream of the interface. This precursor microemulsion likely aids in displacing oil from the system.

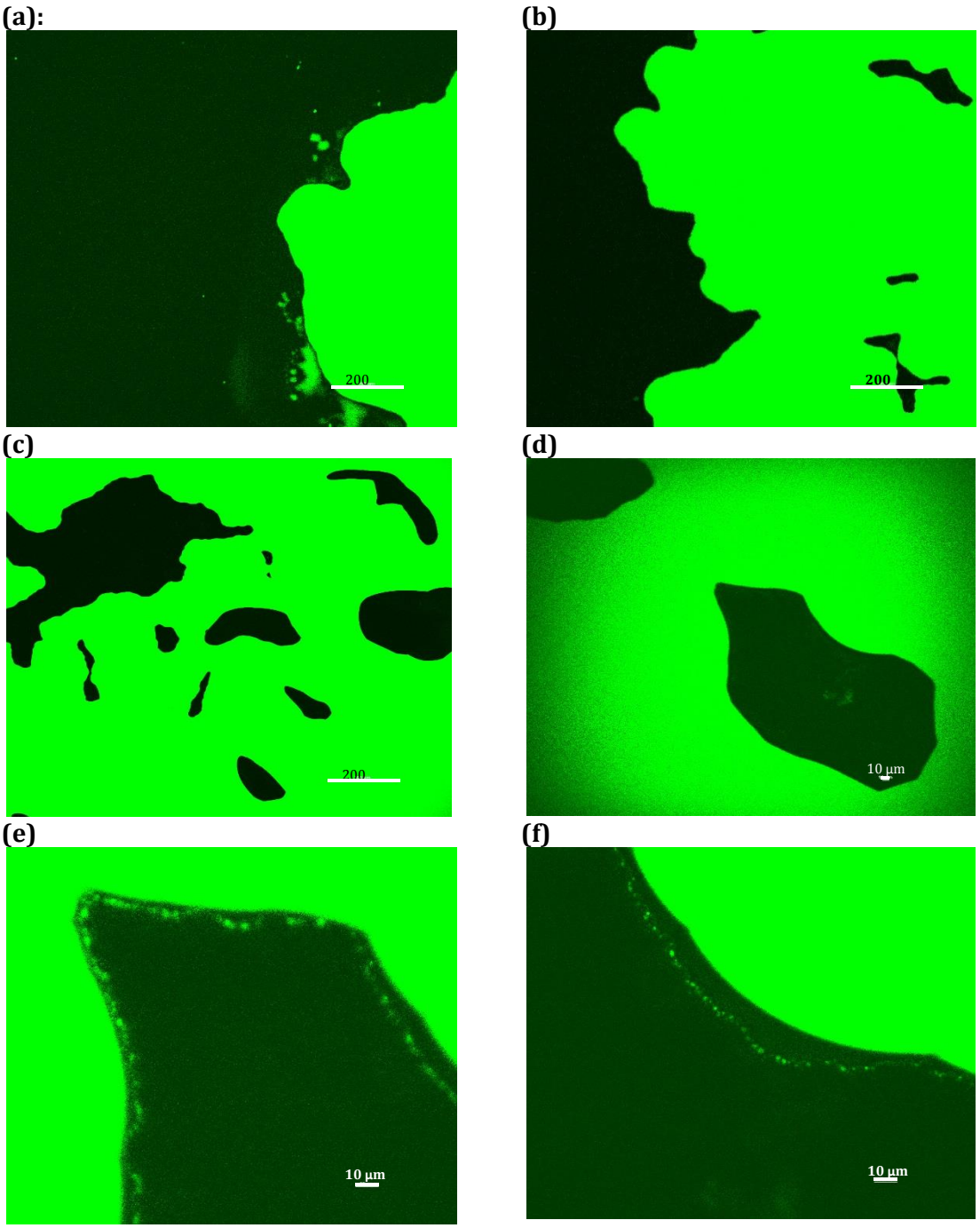

Figure 5.10: Microscopic images of the interfaces between the polymers aqueous phase (light green) and oil (dark green) phase: (a) interface at start of the observation, (b) image after 8 seconds (aqueous phase moves from right to left), (c) image after 16 seconds, (d) zoom in of a trapped oil droplet, (e) zoomed in (closer) view of interface, and (f) zoomed in view of interface

5.5. Conclusions

In the research documented here, co-current flow of polyethylene oxide (PEO) polymer solutions with oil through a Hele-Shaw cell is experimentally investigated. The experiments are repeated for the oil-water phases and their results are compared with different concentrations of the PEO polymer. The results show that due to increase in viscosity of the water and decrease in the interfacial tension with polymer addition to the water phase, the capillary forces relative to the viscous forces drop. The results also show that the interference between phases rises when the concentration of polymer is enlarged. The experiments also show that a thin polymer film adsorbs on the cell plates. This film tends to shift the wettability of the surfaces to be more water-wet which changes the relative permeability behaviour of fluids within the cell. The results suggest that polymer solutions can be used to improve oil displacement from a narrow gap.

List of symbols

μ_o = viscosity of displaced fluid (oil), Pa.s

μ_w = viscosity of displacing phase (water or polymer solution), Pa.s

v_m= homogenous velocity of the phases, m/s

σ_{ow} = IFT = interfacial tension, mN/m

Ca = Capillary number

CFD = computational fluid dynamics

CN = coordination number

cP = centipoise, unit of viscosity

D = Darcy, unit of permeability

dp = differential pressure, psi or Pa

F = ratio of viscous forces to the capillary forces as used by Abrams (1975)

HPAM = Hydrolyzed polyacrylamide

k_r = relative permeability, fraction

k_{ro} = relative permeability of displaced phase (oil), fraction

k_{rw} = relative permeability of displacing phase (water or polymer aqueous phase), fraction

$M = {}^{k_{rw}\mu_o}/_{k_{ro}\mu_w}$, mobility ratio, dimensionless

N_{re} = Reynolds number, fraction

P = pressure, Pa

PEO = Polyethylene oxide

PTR = pore throat ratio

q = volumetric flow rate of fluid, m^3/s

q_o = volumetric flow rate of displaced phase (oil), m^3/s or ml/minute

q_w = volumetric flow rate of displacing phase (water or polymer aqueous phase), m^3/s or ml/minute

S_w= saturation of displacing phase (water or polymer aqueous phase), fraction

$\boldsymbol{\lambda}_o = k_{abs}k_{ro}/\mu_o$, mobility of oil, kg.m/s

$\boldsymbol{\lambda}_w = k_{abs}k_{rw}/\mu_w$, mobility of water or polymer aqueous phase, kg.m/s

µm = micrometer, unit of length

References

Abrams, A. (1975). The influence of fluid viscosity, interfacial tension, and flow velocity on residual oil saturation left by waterflood, SPE 5059, presented at the SPE-AIME 49th Annual Fall Meeting, held in Houston, Oct. 6 – 9, 1974, pp: 437 - 447

Chouke, R. L., van Meurs, P., van der Poel, E. (1959). The instability of slow, immiscible, viscous liquid-liquid displacements in permeable media. Trans. AIME 216, pp:188-194

Clemens, T., OMV, Tsikouris, K., Buchgraber, M. (2012). Pore-scale evaluation of polymers displacing viscous oil – Computational Fluid Dynamics simulation of micromodel experiments. SPE 154169. 2012. Presented at the Eighteenth SPE Improved Oil Recovery Symposium held in Tulsa, Oklahoma, USA, 14 – 18 April 2012.

Daripa, P., Pasa, G. (2005). New Bounds for Stabilizing Hele-Shaw flows. Applied Mathematics Letters 18 (2005) pp: 1293-1303

Delhaye, J.M. (1981). Composite-averaged equations. In Delhaye, J.M., Giot, M. and Riethmuller, M.L. Two phase flow and heat transfer in power and process industries. Hemisphere Publishing Corporation, New York. pp. 181 – 186.

Dominguez, J. G., & Willhite, G. P. (1977, April 1). Retention and flow characteristics of polymer solutions in porous media. This paper SPE 5835 was first presented at the SPE-AIME Fourth Symposium on Improved Oil Recovery, held in Tulsa, March 22 – 24, 1976. Society of Petroleum Engineers. doi:10.2118/5835-PA, pp: 111 - 121

Donaldson, E., Chilingarian, G.V., Yen, T.F. (1985). Enhanced Oil Recovery: Fundamentals and Analysis. Elsevier Science Publishers B.V. P.O.Box 211, 1000 AE Amsterdam, The Netherlands. pp:199-204

Grillet, A.M., Wyatt, N.B. and Gloe, L.M. (2012). Polymer Gel Rheology and Adhesion. Book edited by Juan De Vicente, ISBN 978-953-51-0187-1.

Hematpour, H., Mardi, M., Edalatkhan, S., Arabjamaloei, R. (2011). Experimental study of polymer flooding in low viscosity oil using one quarter five spot glass micromodel. Petroleum Science and Technology, 29:11, pp: 1163-1175.

Hendraningrat L., Shidong, L., Suwarno., Torsaeter, O. (2012). A glass micromodel experimental study of hydrophilic nanoparticles retention for EOR project. This paper (SPE 159161) was first presented at the SPE Russian Oil and Gas Exploration and Production Technical Conference and Exhibition held in Moscow, Russia, 16 – 18 October 2012.

Hill, S, M.A. and Inst, F.P. (1952). Channeling in packed columns. Chemical Engineering Science 1(6). P: 247-253

Jennings, H. Y., Jr., (1975). A study of caustic solution crude oil interfacial tension. This paper (SPE 5049) was first presented at the SPE – AIME 49th Annual Fall Meeting held in Houston, Oct. 6 – 9. 1974. Soc. Pet. Engineering J. 15, No. 3, pp: 197-202.

Mungan, N. (1971). Improved waterflooding through mobility control. The Canadian Journal of Chemical Engineering, Vol. 49, February, 1971, pp: 32 - 37

Needham, R. B., Co, P. P., & Doe, P. H. (1987). Polymer Flooding Review. Journal of Petroleum Technology, (December), pp: 1503–150

Saffman, P.G., Taylor, G.I. (1958). The penetration of a fluid into a porous medium or Hele-Shaw cell containing a more viscous liquid. Proc. R. Soc. London Ser. A 245: pp: 312 – 329.

Ying-jie, Y., Ji-rui, H., Feng-Ian, Z., Chun-sheng, Y. Feng-min, Z., (2013). Research on influence rules of pore structure on water and polymer flooding using etched glass micro-model. SL, vol. 10, no. 1, pp. 59-70.

Chapter 6: Impact of Cellulose Nanocrystals on the Water-Oil Interfaces and Displacement

6.1. Abstract

Flows of multiple phases within narrow gaps abound in the natural world and industry. One industrial setting is that of oil and water flow in fractures in oil reservoirs. Under water flooding, water injected into a fracture will displace oil hopefully to a production well. However, oil displacement from the fracture is not ideal and at this point, it remains unclear why this is the case. We examine the impact of the cellulose nanocrystals (CNC) addition to the aqueous phase, i.e. nanofluid, on the displacement of oil as well as the behaviour of the interfaces between the aqueous and oil phases. The results show that the nanofluid creates stable interfaces with oil due to the reduced interfacial tension and increased viscosity of the aqueous phase. Microscopic analysis of the interface among 1 wt.% CNC and oil, reveals that the nanofluid penetrates the oil phase forming a microemulsion upstream of the main interface.

6.2. Introduction

Nanocellulose, also referred to as cellulose nanocrystals (CNC) or nanocrystal cellulose (NCC), derived from cellulose of wood pulp by mechanical, chemical or combination of both processes (Cheragian et al., 2013). Due to its low density, biodegradability, high strength, good adhesion properties, unique chemical and physical properties, abundance and sustainability, nanocellulose is widely used as a rheology modifier, coating constituent, optical filler, stabilizer for multiphase systems, and strengthening agent in medical, cosmetic, electronic, sensing applications, and more recently, in the petroleum industry (Salas et al., 2014). Nanoparticles are widely used for improving heat transfer of fluids (Kakac et al., 2009), for in situ measurement of temperature and pressure in reservoirs (Alaskar et al., 2011; Engeset et al., 2011) for improving penetration and decreasing wear and tear of oil drilling equipment and for efficient cooling of the drill bits due to its thermal conductivity (Amanullah, 2011; Kasiralvalad, 2014). Nanoparticles have also been shown to improve oil displacement efficiency in porous media after mixing it with injected water (Suleimanov et al., 2011).

The viscosity of CNC aqueous phase (nanofluids) increases with increase in the concentration of CNC because it easily makes hydrogels structure which create a network of cellulose chains that are self-organized and can easily flow with the fluids (Salas et al., 2014). As a result of this self-assembly of nanoparticles to each other and to the host fluid, the stability to the interfaces is enhanced and there is evidence that the wettability of solid surfaces can be changed with polymer (Salas et al., 2014).

Kalashnikova et al., (2011) by using scanning electron microscopy (SEM), analyzed the interface between oil (hexadecane) and water in the presence of cellulose nanocrystals. They added CNC to a water (70%) and oil (30%) volume and observed that the CNC provided stability to the oil-in-water emulsion. Kalashnikova et al. added different concentrations (0.5, 1 and 5 g) of CNCs to one liter of water and observed that stability of the interfaces increases with increase in concentration of the nanoparticles.

6.3. Background

Nanotechnology has been applied in oil recovery in the form of nanoparticles (NPs) added to a fluid phase, in most cases, water. Nanofluids are obtained by mixing nanoparticles (nanofibers, nanotubes, nanowires, nanodrops) in the fluid phase (Wu et al., 2012). Nanoparticles affect oil-water systems in several ways that can improve the oil recovery from reservoir rock:

1. Reduction of the interfacial tension,
2. Viscosification of the aqueous phase,
3. Adsorption of nanoparticles on solid which changes wettability of the solid, and
4. Alteration of the relative permeability of both phases.

Rodriguez et al., (2013) injected different concentrations (18 to 42 wt.%) of silica nanoparticles (5 and 20 nm size) coated with a polyethylene glycol polymer (to keep the particle dispersed in the water phase) through cores of limestone and sandstones with flow rates of 1 to 4 ml/minute. The viscosity of the solution enlarged with greater concentration of nanoparticle in the water phase; the maximum viscosity reached was 3 cP. It was observed that the amount of the nanoparticles retained on the pore throats within the core after post flush was small (from 1 to 10%) due to smaller sizes of nanoparticles than the pores throats and the coating of the particles with the polymer which kept the particles separate from each other. They concluded that the nanoparticles increased the van der Waals forces and wet the pores surfaces. The ionic strength can also be increased by adding saline material to the solution. They observed that the surface treatment of the particles, i.e., polymer coating, increased slippage of the particles on the solid surface.

Roustaei et al., (2012) used three types of polysilicon nanoparticles to investigate their effects on the interfacial tension between water and oil and recovery of oil from the reservoir core samples collected from an Iranian oil reservoir. They concluded that the nanoparticles reduced interfacial tension of oil and water from 26.3mN/m to 1.72 to 2.55mN/m. As a result, oil recovery from the cores increased by 28 to 32%.

Alaskar et al., (2012) studied the effect of size, shape, distribution and surface action of nanoparticles on their mobility through core samples of porous and fractured media, for sensing temperature inside the core. They concluded that spherical shaped nanoparticles easily pass through the porous media with 25% recovery (of nanoparticles) while the rod/wire like nanoparticles trap on the inlets of the cores and are unable to flow through the core, resulting in low recovery. Apart from the shape, surface charges of the particles also affect transport of the particles. They found that the particles coated with surfactant achieved 23% recovery whereas the particles without the surface treatment were trapped at the inlet of the cores by bridging and plugging. Similarly, particles with sizes greater than 200 μm trapped at the inlet while smaller sized particles passed through the cores.

Cheraghian et al., (2013) injected two types of nanoparticles, i.e., titanium dioxide and fumed silica, both in water, into reservoir rock. They proposed that oil recovery and formation scale control can be improved by using nanoparticles as it changes wettability of the surface and improves mobility ratio of the phases. The purpose of using nanoparticles in drilling mud was to reduce the velocity of mud layers and to push out the particles into the reservoirs (Cheraghian et al., 2013).

Apart from the use of nanoparticles in enhanced oil recovery, nanoparticles are widely used in the oil industry for reducing friction losses through casings and for supporting geological formations (Westland et al., 1994). It is also used to enhance rheological properties of drilling fluids (Lenk et al., 1992) to increase strength of the cement and viscosity of the fluids for fracturing and packing (Rincon et al., 2013) and to replace polymer for oil recovery (Lafitte et al. 2013). Wasan and Nikolov, (2003) concluded that nanoparticles improved oil-water flow through small channels and therefore, they can be efficiently used to increase oil recovery from tight porous media.

In general, nanoparticles appear to improve oil recovery from reservoir rock, in particular, sandstone. There have not been any studies in the literature on its impact in fractured rock or that in a Hele-Shaw cell. This is the focus of the research reported here.

6.3.1. Capillary Number and Relative Permeability

Capillary number plays a vital role on stability of an interface between the displacing and displaced phases. Capillary number describes the relative role of viscous and capillary forces in the system i.e., greater capillary number means more viscous and less capillary forces and maximum oil recovery. To investigate the capillary number, a number of equations can be used.

In one method, Delhaye, (1981) suggested calculation of capillary number calculated on the basis of mean/homogeneous values of velocities and viscosities of the phases in the two phase co-current flow (same like our case), and explained that this capillary number incorporates the effect of both the phases which can be calculated by:

$$C_a = \frac{\mu_m U_m}{\sigma_{o-w}} \tag{1}$$

where μ_m is the mean viscosity of the mixture, U_m is the mean mixture characteristic velocity of the flow and σ_{o-w} is the interfacial tension between the two phases.

$$\mu_m = \frac{\mu_o q_o + \mu_w q_w}{q_o + q_w} \tag{2}$$

and the homogeneous pseudo velocity of the two phases, is given by:

$$U_m = \frac{q_o + q_w}{A} \tag{3}$$

where A is the cross-sectional area of the zone of interest where the flows of the phases take place and is equal to the product of the hydraulic gap *(b)* and width of the channel *(W)*.

In the other method, the capillary number is calculated on the basis of individual velocity and viscosity of the displacing fluid and interfacial tension between the two phases and is given by (Moore et al. 1955):

$$C_a = \frac{\mu_w U_w}{\sigma_{o-w}} \quad (4)$$

μ_w is viscosity of the displacing fluid (water or CNC aqueous phase) and U_w is the actual velocity of the finger.

In the third method, the capillary number is calculated by incorporating differential pressure between the two points i.e., inlet and outlet of the zone of observations. Tabir et al. (1969) carried out a number of experiments to recover the residual oil from a reservoir rock samples and concluded that the maximum recovery (close to 100%) can be obtained by adjusting the term $\frac{\Delta P}{L\ \sigma_{o-w}}$. This relationship can be make dimensionless by multiplying it with effective permeability which yields the same results as equation (4) (Folleso, 2012). The equation is given as:

$$C_a = \frac{\Delta P.k_{eff.}}{L\ \sigma_{o-w}} \quad (5)$$

ΔP is the differential pressure across the ends of the sample having length L and K_{eff} is the effective permeability of the displacing fluid (water or CNC aqueous phase in our case). Folleso (2012) described that in a system with a Ca $<10^{-5}$, the capillary forces will be significant and will dominate the viscous forces i.e., the interface will be unstable and vice versa.

The relative permeabilities are calculated with the help of Darcy's equation for multiphase flow through porous media and planar Poiseuille's law.

$$k_{rf} = \frac{q_f \mu_f}{A k_{abs}\left(\frac{\Delta p}{L}\right)} \quad (6)$$

where the subscript "f" represents the fluid either oil or the nanofluids.

6.4. Methodology

The experimental apparatus, shown in Figure 6.1, consists of a Hele-Shaw cell of Plexiglas with the dimensions of the zone of observation 40cm×14cm×0.039cm. The cell is connected with two injection pumps through three injection ports. The dyed phases of nanocrystals are injected through the central injection port by two syringe pumps (Model 500D Isco, Teledyne Isco)- connected in series and the mineral oil (Marcol 7, provided by Esso Chemical) is injected through the adjacent outer injection ports by Gilson 307 pump (supplied by Gilson Inc.). Images of the flow patterns are collected by CCD camera (Model scA1000-30gc, Basler) which are processed by the data acquisition system to get the sequential saturations of the phases. Two pressure transducers (Model PX 209-015G5V, Omega Environmental Inc.) are connected to the ports in the lower cell located at the inlet and outlet of the zone of observations. For clear visibility of the interfaces, lights are placed under the cell and the displacing phases are dyed by adding super red food color (Chefmaster, Product No. C5001-SR), which increases contrast in color with the mineral oil (transparent). The sequential phase saturations are the areal fraction of the image occupied by each phase.

Suspensions of cellulose nanocrystals (Batch number: 150814UOC, supplied by Alberta Innovates - Technology Futures) of different concentrations are used as displacing fluids. Both 1 wt.% and 2 wt.% concentrations of CNC suspensions in the aqueous phase is prepared by dissolving the nanocrystals in de-ionized water. The Hele-Shaw cell is initially saturated with the oil followed by injecting cellulose nanocrystals suspension at gradually increasing flow rates up to 9 ml/minute which is then kept constant and the oil injection rate is gradually reduced (from 0.5 to 0.025 ml/minute).

The differential pressure, flow rates and images of the flow patterns are collected by the data acquisition system which are further processed for calculations of differential pressure, saturation of each phase, relative permeabilities, capillary number, and Reynolds number.

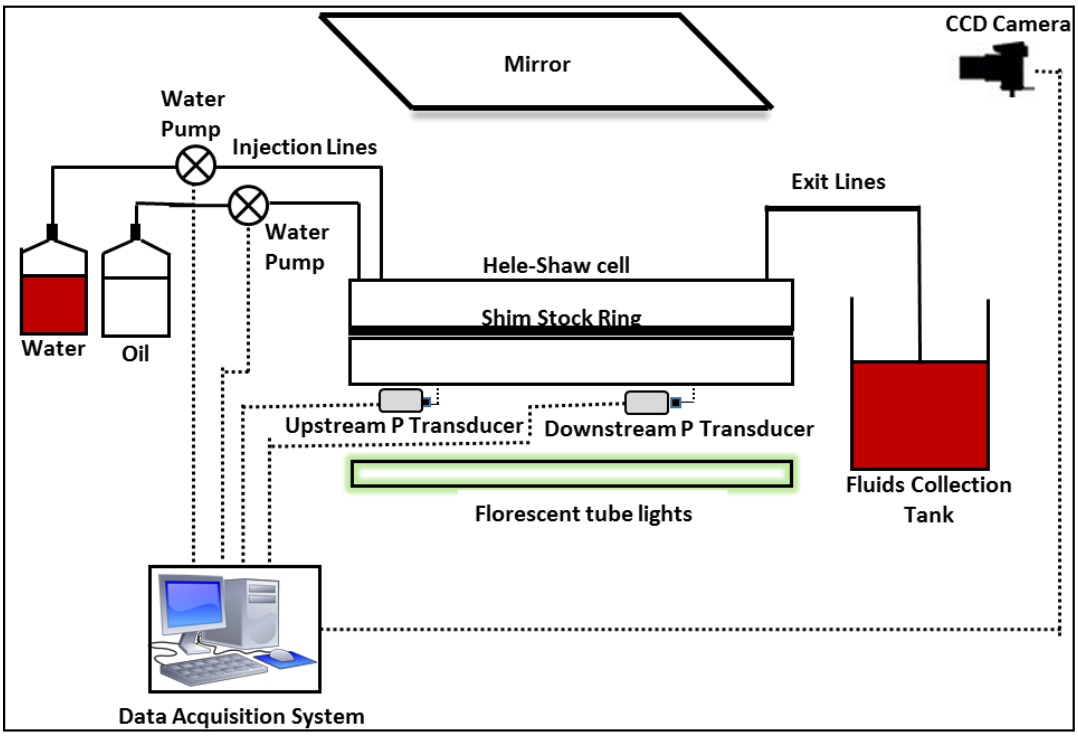

Figure 6.1: Experimental set shows the injection pumps, Hele-Shaw cell, data acquisition system, camera, and pressure transducers etc

6.5. Results and Discussion

We analyzed the change in viscosity, interfacial tension, mobility ratios, capillary numbers, relative permeabilities and instabilities in the two phase co-current flow after adding different concentrations of cellulose nanocrystals to the injected water for displacing oil from the Hele-Shaw cell.

6.5.1. Variation of Viscosity and Interfacial Tension with Nanocrystals

As described by Rincon et al., (2013); Rodriguez et al., (2013), and Salas et al., (2014) that viscosity of water increases by adding nanoparticles to the water. We also investigated

variation of viscosity with the concentration of the CNC using a Stabinger Viscometer (Model #SVM 3000, Anton-Paar). Table 6.1 shows results of the viscosity variation with the concentration of the nanocrystals. It can be observed from the data that the viscosity of the solution rises with increase in concentration of the CNC: the viscosity grows from 1.108 cP to 8.500 cP by adding 2 wt.% of the nanocrystals, which is less than half of the viscosity of the mineral oil that we used (20cP). Moreover, the table depicts that viscosity of the suspension becomes almost the same as that of the mineral oil when 3 wt.% of the nanocrystal is added to the water, which suggests that further increase in concentration of the nanocrystals (>3 wt.%) may increase in the interfacial tension, which can be depicted from Table 6.1 but this needs to be investigated in the future research work.

To investigate the change in interfacial tension of the phases, we determined the interfacial tensions between oil and different suspensions of the nanocrystals by using a Dy Nouy Ring Tensiometer (TensioCAD model, CAD Instruments) and the results are presented in Table 6.1. The results revealed that the interfacial tension drops with increases in the CNC concentration up to 2 wt.% but at 3 w.%, the interfacial tension becomes greater than the interfacial tension obtained for 2 wt.%. The possible reason could be the increase in viscosity and formation of microemulsion near the interface that we observed microscopically and will be discussed in the following sections.

On observing the viscosity and interfacial tension values in Table 6.1, it can be concluded that the nanocrystals can be used both for viscosity increase and interfacial tension reduction simultaneously. As a result of this dual action of CNC, we got results that were different than the results we obtained in our experiments by using de-ionized water, PEO polymer and SDS surfactant as a displacing phase.

Table 6.1: Viscosity and interfacial tension variation with different concentrations of CNC suspension

Concentration of CNC (wt.%)	Viscosity at 23 °C, (cP)	Interfacial Tension at 23 °C, mN/m
0.0	1.1082	44.1002
0.5	1.9558	39.2925
1.0	3.5462	35.6959
2.0	8.4923	32.1352
3.0	19.9333	33.4181

6.5.2. Mobility Ratios

The mobility ratios in case of 1 wt.% and 2 wt.% CNC suspension co-current flow with oil through the cell are listed in Table 6.2. Two methods were applied in the calculation. In one of the methods, called the 'end point mobility ratio', was calculated at the maximum relative permeability of the displacing phase or minimum relative permeability of the displaced fluid. In the other method, called the 'averaged mobility ratio', the mobility ratio was calculated at each step of the flow rates and were then averaged for the entire experiment. The mobility ratios calculated with both the equations are presented in Table 6.2. It can be observed from the table that the end point mobility ratios for water and 1 wt.% CNC suspension are same (360), whereas this value for the 2 wt.% CNC suspension is equal to 12. The averaged mobility ratios are reduced from 28.70 to 22.51 by increasing CNC concentration from 0 to 1 wt.% and to 4.65 for 2 wt.% CNC nanofluids. It can be concluded from the data that in the case of the 2 wt.% suspension, the end point mobility ratio is slightly above the stability range suggested by Folleso, (2012), i.e., 10 for porous media but in the case of the average mobility ratio, it is within the stability range i.e., 4.65, which predicts the stability on the basis of the mobility ratios reasonably good because a stable interface is observed in the case of the 2 wt.% CNC aqueous phase (Table 6.2). Generally, the table suggests that the mobility ratio can be controlled by adding

nanocrystals to the displacing phase which ultimately reduces the viscous fingering and increases the oil displacement from the cell.

Table 6.2: Mobility ratios of the oil-aqueous system examined

Type of mobility ratio	Mobility ratio of water-oil	Mobility ratio of CNC (1 wt.%)-oil	Mobility ratio of CNC (2 wt.%)-oil at Maximum k_{rw}
End point	360.0	360	12.00
Averaged	28.70	22.51	4.65

6.5.3. Effects of Nanocrystals on the Capillary Number

The capillary numbers are calculated by using all the three methods described in Equations 1, 4, and 5 and the results are listed in Table 6.3. It can be observed from the data that the values of the capillary numbers are significantly less than unity which reveals that the interfacial forces are much larger than viscous forces. The table reveals that the capillary number can be raised with increase in concentration of the CNC and the relative role of the interfacial tension could be increased but it does not increase the viscous forces high enough to dominate over the capillary forces. The averaged capillary number calculated by homogeneous flow equations (Equation 1) is increased from 0.000097 to 0.00037 by adding 2 wt.% of CNC to water. The capillary numbers calculated by Equations 4 and 5 are also listed in the table and show the same pattern but their values are not the same as that calculated by Equation 1. This difference in the values of the capillary numbers depict that considering the two phase flow as homogenous flow (as assumed in the Equation 1) is not a suitable assumption to be implemented and should be further investigated.

As per Folleso, (2012), the finger will be unstable if the capillary numbers calculated by Equations 4 and 5 are less than 0.00001. The table shows that the values of Ca for water-

oil system are comparatively closer to 0.00001 but for the CNC (2wt.%)-oil system, the Ca values are larger than 0.00001 which shows that the finger in the former will be more unstable than the latter. The capillary numbers also confirm the conclusion derived in the last section i.e., the inverse relation of the concentration of the nanocrystals with the mobility ratio. The capillary number raised and stability of the CNC aqueous phase increased with increase in its concentration and as a result the oil displacement from the cell increased. At higher capillary numbers, the curvatures of the interfaces also reduced, which will be discussed in the following sections.

Table 6.3: Capillary number calculated for each set phases system.

Phases	Ca from equation 1	Ca from Equation 4	Ca from Equation 5
Water-oil	0.000097	0.00004	0.00004
CNC 1wt.%-oil	0.00018	0.000119	0.00119
CNC 2 wt.%-oil	0.00037	0.00012	0.00012

6.5.4. Macroscopic and Microscopic Flow Patterns and Relative Permeability Analysis

As the experiments are conducted for examining the co-current flow of 1 wt.% and 2 wt.% CNC aqueous phases with oil through the gap, therefore, the results will be analysed for each set of the fluids.

6.5.4.1. 1 wt. % CNC Suspension

6.5.4.1.1. Flow Patterns Observations

Figure 6.3 shows images acquired during oil-CNC (1 wt.%) co-current flow through the cell. It can be observed that a couple of fingers enter into the cell, one of them, usually the central one, dominates over the others and penetrates into the oil ahead of the others. The other fingers join the dominant finger and increases its size. The saturation of the 1 wt.% CNC phase rises up to 18.8% as it reaches to the exit end of the area of observations which regularly increases with increase in the flow rates whereas in the case of water-oil, the water finger contracts due to higher capillary forces after the breakthrough and then widens with increase in the flow rates. On the other hand, in the case of CNC, after the CNC solutions passes through the cell, it stays there and keep on raising its saturation in the cell instead of dropping (as seen in water oil flow). The images also depict that with further increase in the nanofluids injection rate, more separate secondary fingers create and combine with the main finger, which further enlarges its size. The oil droplets evolve in between fingers in the form of irregular shapes. The nanofluids finger size increases gradually with the passage of time and its saturation rises up to about 85% at the end of the experiment. On the basis of the results, it can be concluded that the 1wt.% CNC aqueous phase flows in separate channels, merge with each other and displaces oil from the cell. As a result of merging, oil droplets trap in the CNC suspension which are immobile and can be seen in Figure 6.2 (encircled). The results show that 1 wt.% CNC increases the oil recovery from the cell.

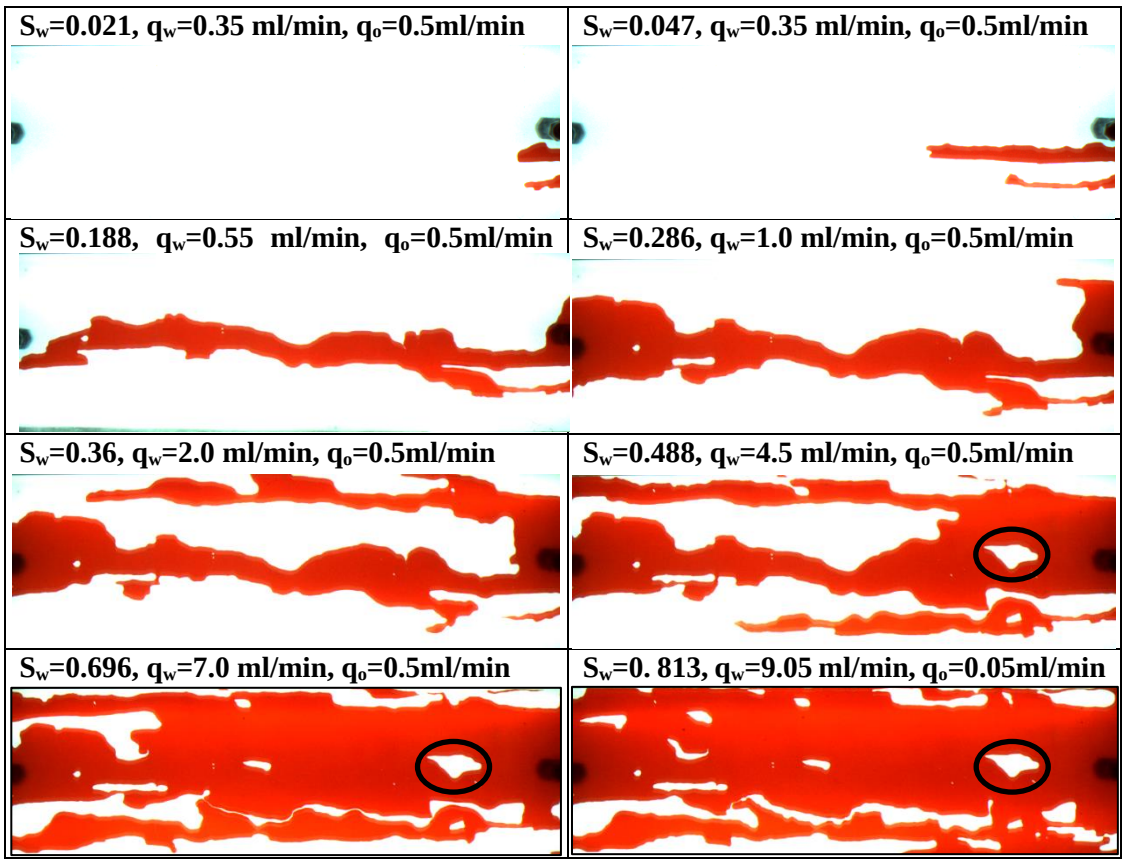

Figure 6.2. Images retrieved during 1wt.% CNC suspension (red color) and oil (white color) phases flow through the cell.

6.5.4.1.2. Microscopic Analysis of the Interfaces

Microscale images of the interfaces among 1 wt.% CNC nanofluids and mineral oil, acquired by a microscope (Nikon A1R), are presented in Figure 6.3. The dark green color in the figures shows the oil phase whereas the light green color is CNC 1wt.% suspension. Figure 6.3(a)acquired at 200 µm scale, represents a comparatively smaller view of the interfaces. It shows some irregular shaped oil droplets dispersed in the CNC phase. Stable interfaces of the CNC aqueous phase with the oil observed in the images of the two phases

flow patterns (Figure 6.3). Enlarging the image up to 100 µm scale, a closer view of a portion of the image shown in Figure 6.3(a) can be seen in Figure 3(b) which also displays stable and irregular shaped interfaces of both the phases with no emulsion. On further increasing the image size to 20 µm scale we get further enlarged views of Figure 6.3(b) shown in Figures 6.3 (c, d, e, f). These images reveal that the CNC suspension accumulates in the oil phase in the form of a micro-emulsion close to the interface.

A detailed microscopic structure of the interfaces developed in between the 1 wt.% CNC aqueous phase and oil is displayed in Figure 6.4. It can be observed that four layers of different structures are found inside the oil phase. The outer most layer (layer-1) of the oil phase is darker in color than the next two layers and consists of mainly oil phase with few CNC droplets. This layer forms a sharp interface with the CNC phase. The second layer (layer-2) is lighter in color as compared to layer-1 and consists of micron sized droplets of the CNC phase hosted in the oil phase. The next layer, referred to as layer-3, consists of more CNC droplets than emulsion layer-1 and 2. In this layer, the droplets are larger in size and mostly circular in shape. The fourth layer (layer-4) has no or very few CNC droplets, and is actually the oil droplet surrounded by the CNC and emulsion phase.

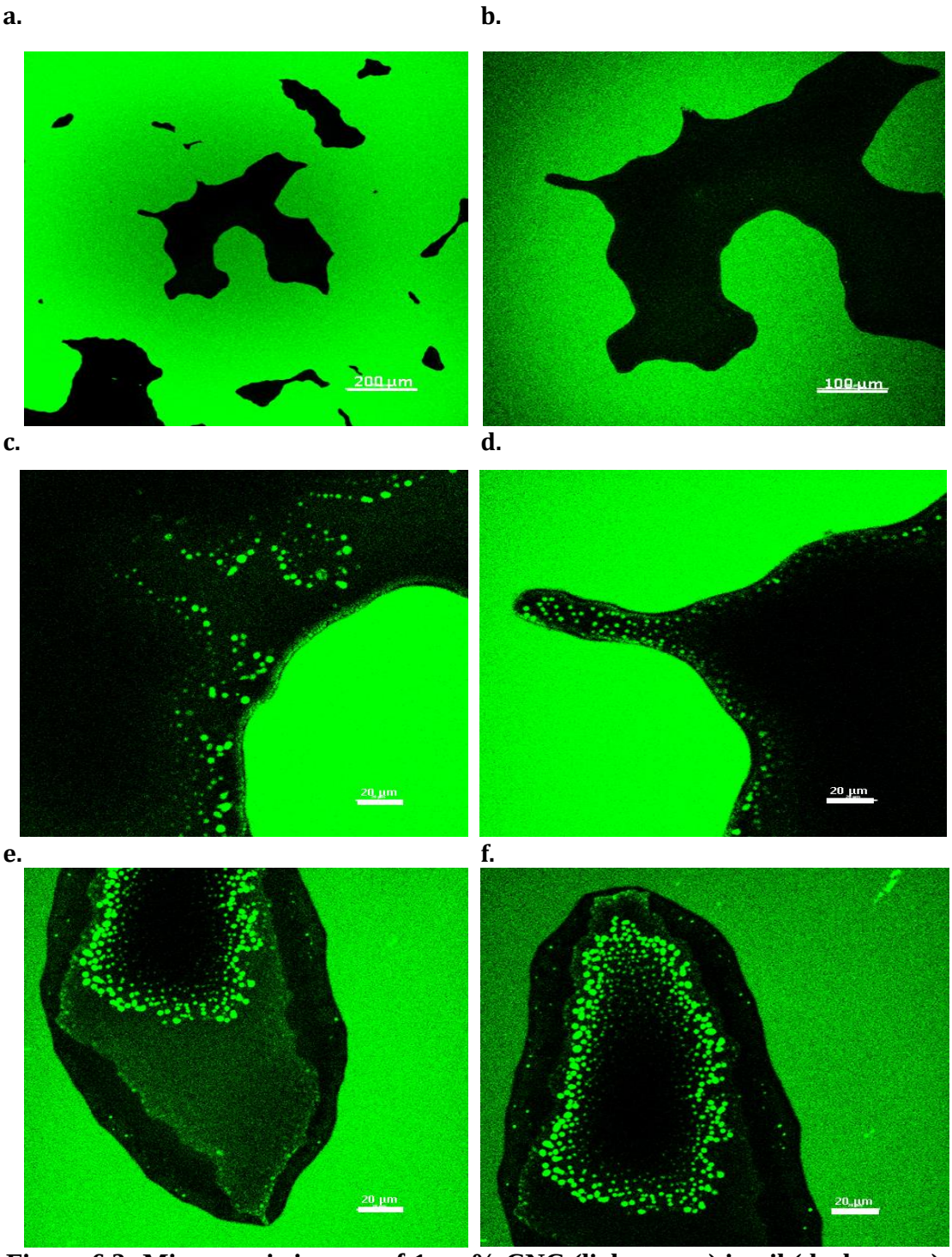

Figure 6.3: Microscopic images of 1 wt.% CNC (light green) in oil (dark green). (a). CNC solution droplets in the oil phase, size 200 µm, (b). A portion of the (a), size 100 µm, (c, d, e, f) larger scale images (20 µm) of different portions of the image in part (b)

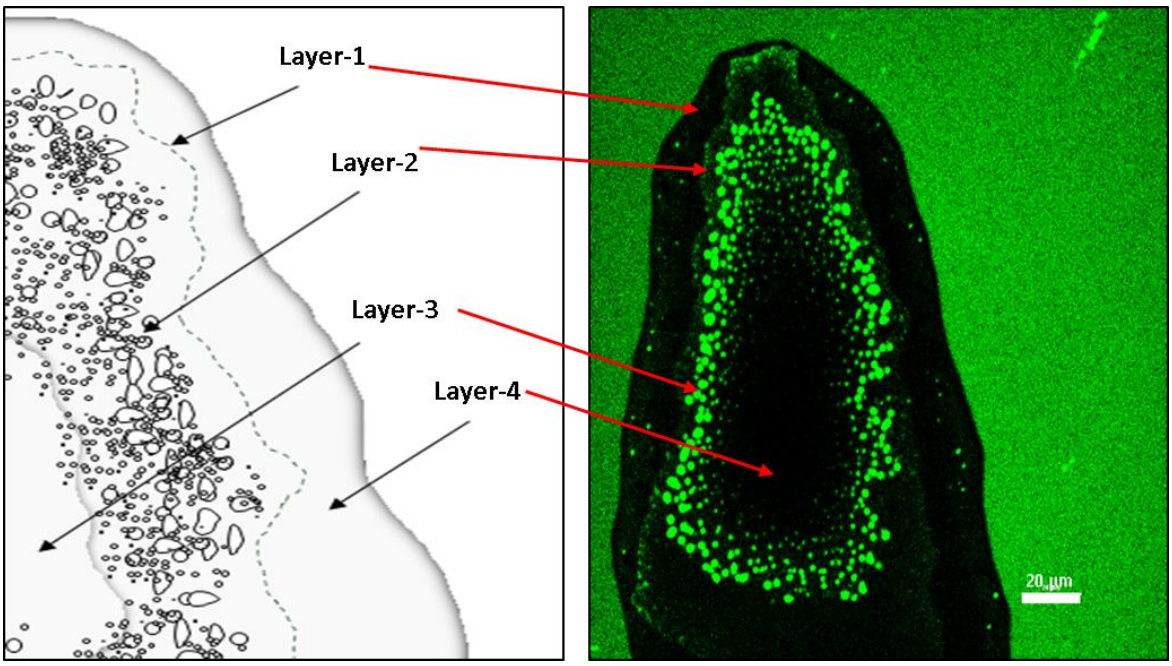

Figure 6.4: Microscopic schematic of interface among the mineral oil and 1% CNC suspension and various layers inside the oil phase. Dark green in the microscopic image shows the oil while light green is the CNC phase

6.5.4.1.3. Relative Permeabilities

The relative permeability values for each phase and each step of the flow rates are calculated from the averaged data obtained at steady state differential pressure and saturations of the phases. The cell is initially saturated with oil and the plates are oil-wet. The results, displayed in Figure 6.5, show that the relative permeability curve of the CNC nanofluids is concave upward and is higher than the relative permeability curve of the oil. The maximum residual oil saturation in case of 1 wt.% CNC phase is 25%. The relative permeability curves exhibit a relatively quick drop of the oil saturation and rise of the displacing phase saturation after the CNC saturation equals 0.70. This is due to the changes in the injection rates of the phases. At this point and beyond this, the CNC flow rate is kept constant at maximum while the oil flow rate is gradually reduced. It can be concluded from this behaviour that for consistent oil recovery from the fracture or fractured media, the

displacing phase flow rate should be increased continuously. The results also suggest that the overall oil recovery could be further enhanced if the flow rate of oil is reduced.

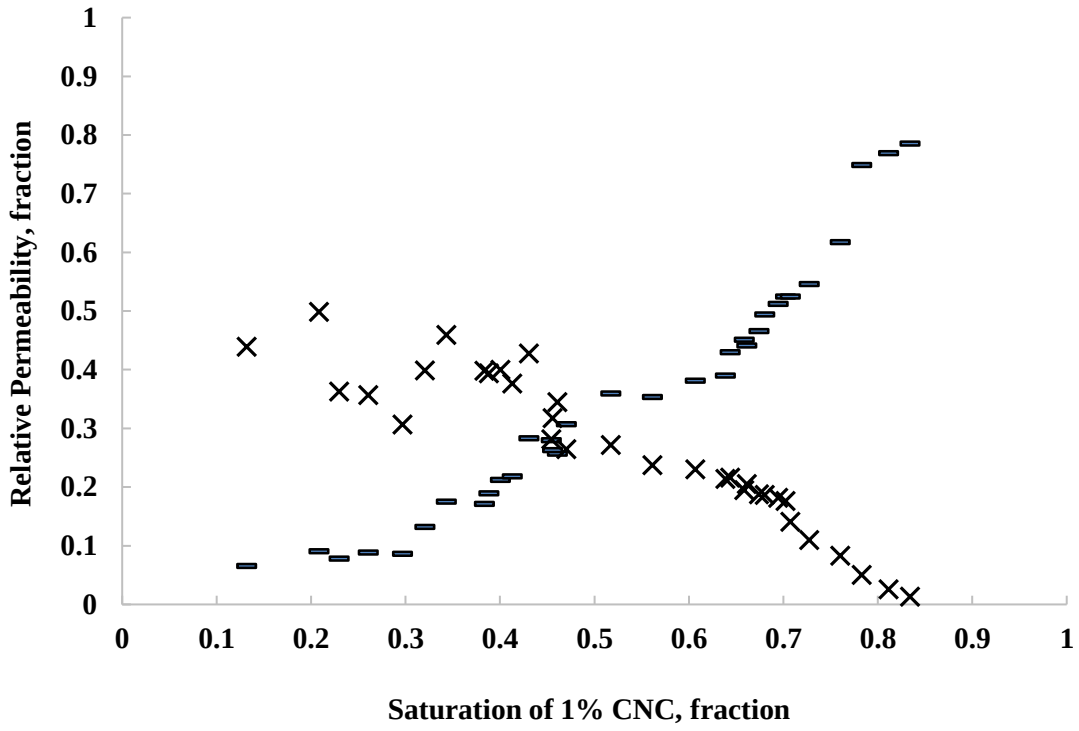

Figure 6.5: Relative permeability curves for 1 wt.% CNC aqueous and oil phases flowing through the Hele-Shaw cell in the case of drainage

6.5.4.2 2 wt. % CNC Suspension

6.5.4.2.1. Flow Patterns Analysis

The 2 wt.% CNC suspension-oil interface behaviour is completely different than the interfaces developed in the flow of 1 wt.% CNC-oil. Figure 6.6 shows images of the flow patterns created in the flow of 2 wt.% CNC nanofluid and oil. The results shown in the figure represents the images and saturations of the CNC phase acquired at different flow rates of each phase. The 2 wt.% CNC suspension travels through the cell in the form of a

stable and straight interface normal to the direction of the flow. The aqueous phase more or less completely displaces the oil after 1 hour of the commencement of the experiment at injection rate of 1.45 ml/minute and 0.5 ml/minute of CNC and the oil phases, respectively. The saturation of the aqueous phase reaches 92% at this stage. The maximum oil recovered is 98% at a flow rate of 1.6 ml/minute (CNC suspension) and 0.5 ml/minute of the oil phase. This degree of oil recovery is not achieved with the water flood or 1 wt.% CNC flood even at higher flow rates. The possible reasons for this stable interface and enormous oil displacement can be deduced from the microscopic observations shown in Figures 6.3 and 6.4. As discussed earlier that the CNC suspension forms a microemulsion in the oil phase, which results in possible decrease in the interfacial effects (need further investigation) and improvement in the effectiveness of the flood. Thus, the CNC suspension displaced the oil as a piston. This behaviour of the CNC suspension shows that it can be efficiently used to increase oil recovery from the gap.

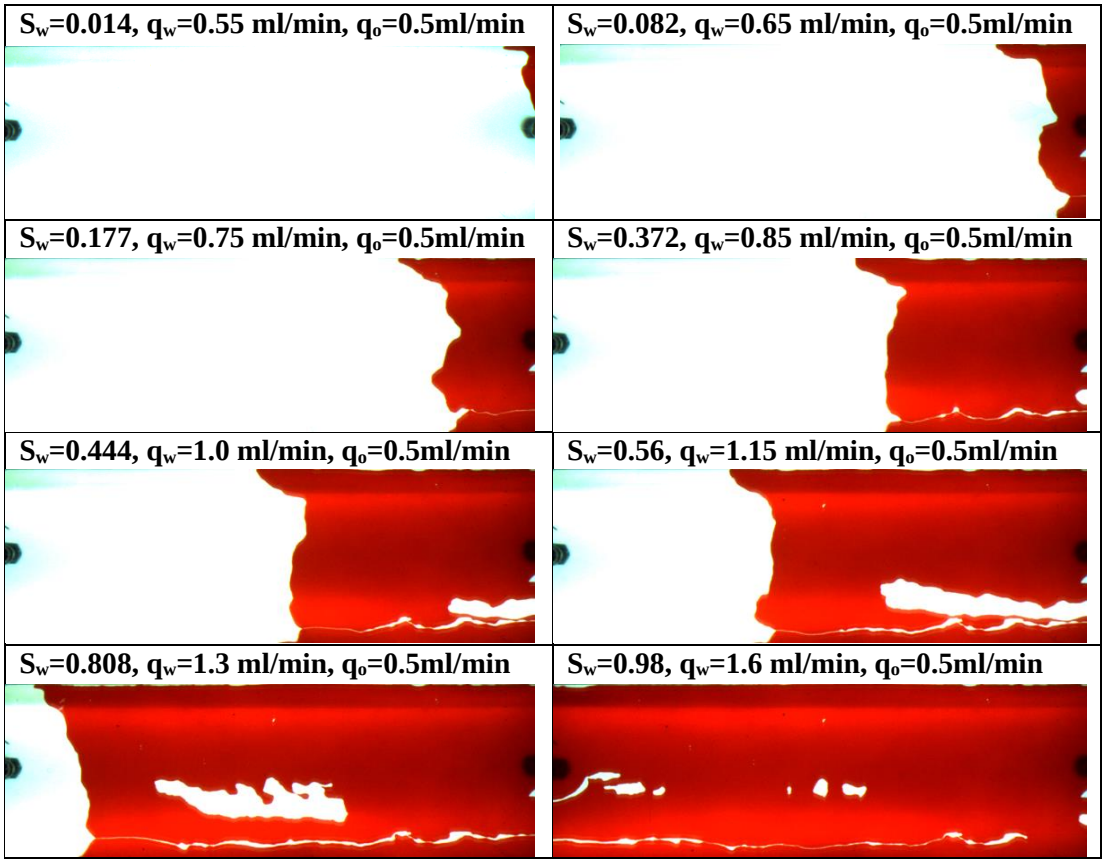

Figure 6.6. Images acquired during 2wt.% CNC suspension (red color) co-current flow with oil (white color) through the Hele-Shaw cell

6.5.4.2.2 Relative Permeability in the Case of 2 wt.% CNC Suspension

As observed in the last section that the 2 wt.% CNC finger expands to the sides of the channel and completely fills the gap except a narrow channel of oil and a few mobile droplets of the oil moving with the aqueous phase (see Figure 6.6). On reaching the CNC channel to the exit end of the area of observation, its saturation raised to 92% and the relative permeability calculation is commenced after this saturation because the relative permeability is calculated for continuous flow of both the phases in between the pressure transducers. The relative permeability curves obtained are shown in Figure 6.7. It can be observed that the relative permeability for both the phases is under 0.2 which is relatively lower than the typical relative permeability curves reported in the literatures for the other fluids such as water and surfactant solutions. The possible reasons for this low relative permeability could be the presence of the emulsion at the interface of the phases that we observed in the microscopic examination (Figures 6.3 and 6.6), which possibly reduced the overall interfacial effects within the system leading to lower phase interference and maximum displacement, but this needs further investigation.

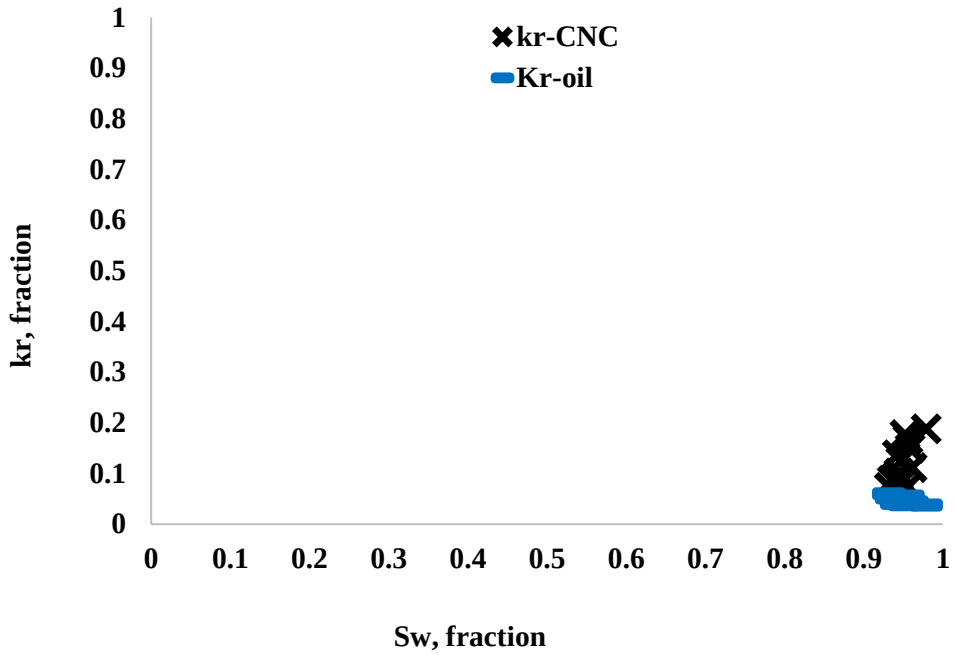

Figure 6.7: Relative permeability curves (k_r) for oil and 2 wt.% CNC suspension vs saturation of the aqueous phase (S_w)

6.5. Conclusions

Cellulose nanocrystals (1 wt.% and 2 wt.%) dissolved in the de-ionized water had duel action i.e., it raised viscosity of the aqueous phase and lowered the interfacial tension with oil. Each suspension of the nanofluids, was injected with oil in the Hele-Shaw cell at different flow rates. It was observed that the nanocrystals raised the saturation of water and reduced the residual oil saturation in the cell. In the case of 1 wt.% CNC suspension flow with oil, it was observed that the phases flow in their separate flow paths which then merged with each other and displaced the oil from the cell by expanding width of the finger normal to the direction of the flow. Many oil droplets engulfed during merging of the phases. Microscopic examination of the interfaces revealed that micro sized 1 wt.% CNC droplets penetrate into the oil phase and form an emulsion along the interface with in the oil phase. The emulsion formation further reduces interfacial tension between the phases

and causes engulfment and mobilization of the oil phase in front of the CNC suspension. As result of this mobilization, we observed a piston like displacement in the case of using 2 wt.% CNC aqueous phase as a displacing phase. The microemulsion formation and decrease in the interfacial tension yielded a complete displacement of the oil with the CNC phase which has a viscosity two times less than the oil viscosity. The local changes in the viscosities and interfacial tensions between the 2 wt.% CNC phase and oil need further investigation. The 1 wt.% CNC suspension flow with oil through the gap could be analysed by typical relative permeability curves but the 2 wt.% CNC could not be examined effectively by the typical relative permeability curves as in this case the saturation rate of the displacing phase is high and a complete displacement of the oil occurs. Therefore, the regular channels of both the phases developed between the two ends of the area of observation (required for relative permeability calculations) at a saturation of 92%, which did not yield typical relative permeability curves. This suggests that the phase interference is reduced as compared to the water injection and 1 wt.% CNC case. With respect to oil recovery, the results demonstrated that CNC suspension can be effectively used for oil displacement from the fractures.

References

Alaskar, M., Ames, M., Liu, C., Connor, S., Horne, R., Li, K., Cui, Yi. (2011). Smart nanosers for in-situe temperature measurement in fractured geothermal reservoirs. Australian Geothermal Energy Conference, 2011.

Amanullah, M., Al-Arfaj, M.K., Al-Abdullatif, Z. Preliminary test results of nano-based drilling fluids for oil and gas field application. SPE/IADC 139534, Drilling Conference, Proceedings, 1(1965), pp:112–120

Blunt, M., King, P. (1991). Relative permeabilities from two and three dimensional pore-scale modeling. Transport in Porous Media, vol. 6, Nov.4, P. 407

Cheraghian, G., Hemmati, M., Masihi, M. and Bazgir, S. (2013). An experimental investigation of the enhaced oil recovery and improved performance of drilling fluids using titanium dioxide and fumed silica nanoparticles. Journal of Nanostructure in Chemistry 2013, 3:78.

Chevalier, C., Amar, M.B., Bonn, D. and Liner, A., (2006). Intertial effects on Saffman-Taylor viscous fingering. Journal of Fluid Mechanics (2006), vol. 552, pp. 83-97.

Collins, R.E. (1961). Flow of fluids through porous materials. Reinhold publishing corporation, New York.PP: 196, 197

Fairbrother, F., Stubbs, A.E. (1935). The bubble tube method of measurement. Journal of Chem. Soc. 1, pp: 527 – 530.

Engeset, B. (2011). The use of nanotechnology in the petroleum industry. Thesis, Norwegian University of Science and Technology.

Folleso, H.N. (2012). Fluid Displacements during multiphase flow visualized at the pore scale using micromodels. Master thesis in Reservoir Physics, University of Bergen.

Hill, S., M.A and Inst, F.P. (1952). Channelling in packed columns. Chemical Engineering Science 1(6), p. 247-253.

Kakac, S., and Pramuanjaroenkij. (2009). Review of convective heat transfer enhancer with nanofluids. International Journal of Heat and Mass Transfer, vol. 52, No. 13-14, pp. 3187 – 3196, 2009.

Kalashnikova, I., Bizot, H., Cathala, B. and Capron, I. (2011). New Pickering emulsions stabilized by bacterial cellulose nanocrystals. UR 1268 Biopolymeres, Interactions et Assemblages, INRA, F-44316 Nantes, France. ACS Publications, 2011.

Kasiralvalad, E. (2014). The great potential of nanomaterials in drilling and drilling fluid applications. Int. Journal of Nano Dimension. 5(5): pp:463 – 471 (Special Issue).

Lafitte, V., Lee, J.C., Ali, S.A., Sullivan, P.F. (2013). Fluids and methods including Nanocellulose. US Patent US 20130274149 A 1.

Lenk, D.A., Penny, G.S., Westland, J.A., (1992). Drilling mud compositions. Patent W01992022621 A1.

Lenorman, R., Touboul, E. and Zarcone, C. (1988). Numerical models and experiments on immiscible displacements in porous media. Journal of Fluid Mechanics. Vol. 189, pp:165-187.

McLean, J.W. and Saffman, P.G., (1981). The effect of surface tension on the shape of fingers in a Hele-Shaw cell. Journal of Fluid Mechanics (1981), vol. 102, pp: 455 – 469.

Nittmann J., Daccord, G., Stanley, H.E. (1986). When are viscous fingers fractal? Fractals in Physics, Elsevier Science Publications B.V.

Park, C.W., Gorell, S. and Stanley, H.E. (1984). Two phase displacement in Hele Shaw cell: experiments on viscously driven instabilities. Journal of Fluid Mechanics. 314, pp:141 - 144

Rincon-Torres, M.T.and Hall, L.J.,(2013). Cellulose nanowhiskers in well services. US Patenet US 20130196883 A1.

Rodriguez, E., Roberts, M.R., Yu, H., Huh, C., and Bryant, S.L. (2013). Enhanced migration of surface treated nanoparticles in sedimentary rocks. SPE 124418. SPE Annual Technical Conference and Exhibition

Saffamn, P.G. (1986). Viscous fingering in Hele-Shaw cells. Journal of Fluid Mechanics. (1986), vol. 173. Pp. 73-94.

Salas, C., Nypelo, T., Rodriguez-Abreu, C., Carrillo, C., Rojas, O.J. (2014). Nanocellulose properties and applications in colloids and interfaces. Current Opinion in Colloid & Interface Science 19 (2014) 383-396.

Suleimanov, B., Ismalov, B., Veliyev, E. (2011). Nanofluid for enhanced oil recovery. Journal of petroleum Sci. Engineering 78, 431 (2011).

Taber, J.J. (1969). Dynamic and static forces required to remove a discontinuous oil phase from porous media containing both oil and water. SPE 2098.

Tabeling, P., Zochi, G., Libchaber, A. (1986). Film draining and the Saffman-Taylor problem. Phy. Rev. A33, pp: 794 - 796

Wasan, D.T. and Nikolov, A.D. (2003). Spreading of nanofluids on solids. Letters to Nature, 423 (6936), pp. 156-159 (8 May 2003).

Westland, J.A., Penny G.S., Stephens, R.S. and Winslow, A.R. (1994). Method of supporting fractures in geological formations and hydraulic fluid composition for same. US Patent US 5350528 A.

Westland, J.A., Penny, G.S., Lenk D.A. (1994). Drilling mud compositions. US Patent US 5362713 A.

Wu, J., He, J., Torsaeter, O., Zhang, Z. (2012). Effect of nanoparticles on oil-water flow in a confined nanochannel: a molecular dynamics study. SPE 156995.

Zolotukhin, A.B., Ursin, J.R. (2000). Introduction to petroleum reservoir engineering. Hoyskoleforlaget, Norweigian Academic Press, 2000

Chapter 7: Conclusions and Future Work

In this work, we studied flow structures of co-current flow of two immiscible phases through a narrow gap, i.e. Hele-Shaw cell. Four sets of experiments were performed, co-current injection of oil-water, oil-surfactant added water, oil-polymer added water, and finally oil- cellulose nanocrystals suspension. Marcol 7 is used as the oil phase for all experiments. For each scenario, snapshots of flow structures were captured for qualitative and quantitative analyses as summarized below.

7.1. Co-current Flow of Oil and Water

In the co-injection of water and oil, various flow regimes were distinguished. It was observed that at low water injection rate, a dominant finger grow in time. Thus, a water channel connecting the inlet to outlet is formed. As the water flow rate increases, the channel width expands which is associated with oil droplet formation and engulfment. Furthermore, in measuring relative permeability curves, the hysteresis of the oil relative permeability and its dependency on the direction of saturation change was disclosed

7.2. Co-current Flow of Oil and Surfactant Solution

Co-current flow of oil and various concentrations of sodium dodecyl sulfate (SDS) surfactant aqueous phases was investigated. It was shown that after the surfactant solution breakthrough, the surfactant phase entraps oil in the form of circular droplets and this is due to the instabilities created at the interfaces. The oil droplets flowed to the exit with the surfactant phase. Microscopic investigation reveals that on contacting oil with surfactant phase, the SDS aqueous phase appears to penetrate into the oil phase in the form of a network of narrow channels which accumulate inside the oil phase in the form of droplets, thus forming emulsions. Such emulsion flow postponed the breakthrough time and

decreased the residual oil saturations, hence, oil recovery was increased by 11% as compared to the non-surfactant case.

7.3. Co-current Flow of Oil and Polymer Solution

Co-current flow of oil and different concentrations of polyethylene oxide (PEO) polymer through the gap was evaluated for analysis of the flow patterns and their impact on the properties of the surface, interfaces of the phases and oil recovery. The results showed that the polymer increases viscosity of the water and as a result, the phase interference of the phases, saturation rate of water and oil recovery from the fracture increase. The major difference, observed in the flow patterns of water-oil and polymer-oil cases, was the formation of fingers which were more stable and had regular interfaces. Polymer retention was also reported. The retention of the polymer solution on the Hele-Shaw cell surfaces resisted the fluid's flow which in turn reduced the mobilities of both the phases.

7.4. Co-current Flow of Oil and Cellulose Nanocrystals Suspension

One and two wt.% of cellulose nanocrystals suspensions (called nanofluids) were used as the oil co- injectants. It was reported that with the addition of nanocrystals, water viscosity increased while the interfacial tension between the phases decreased. Thus, stable interfaces formed.

Microscopic analysis of interfaces revealed that small CNC droplets penetrate into the oil near the interfaces and form an emulsion zone with various droplet size distributions.

7.5. Recommendations for Future Work

The conducted research was enlightening in terms of co-current flow structures for oil and various solutions another immiscible phase, i.e. water. This work can be continued in many directions including the following recommendations:

- A thorough parametric studies is required to disclose variations in many effective factors. For example, the effect of surfactants, polymers and nanocrystals concentration variation, type and viscosity of mineral oil, Hele-Shaw cell surface property and inclination can be analyzed.

- Despite the fact that CNC aqueous phase is less viscous than oil in the bulk phase, the 2 wt.% CNC aqueous phase yielded a piston like flow. Thus, it is interesting to evaluate the local viscosity of this phase. Such examination could be performed by using Thioflavin T (ThT) – a dye molecule used as a viscosity sensor to the fluids (Ponjavic et al., 2015).

- Nonlinear simulations can be performed to disclose some structures that were not fully understood through the experiments.

References

Abadli, F., (2012). Simulation study of enhanced oil recovery by ASP (Alkaline, surfactant and polymer) flooding for Norne field C-segment. Master thesis, NTNU-Trondheim, Norwegian University of Science and Technology, Norway.

Abrams, A. (1975). The influence of fluid viscosity, interfacial tension, and flow velocity on residual oil saturation left by waterflood. Society of Petroleum Engineers Journal, 15(05), pp: 437–447.

Adibhatla, B., Mohanly, K.K. (2008). Oil recovery from fractured carbonates by surfactant-aided gravity drainage: Laboratory experiments and mechanistic simulations. SPE 99773, Reservoir Evaluation & Engineering, 11(1), pp:119–130

Agada, S., Geiger, S., & Doster, F. (2016). Wettability, hysteresis and fracture-matrix interaction during CO2 EOR and storage in fractured carbonate reservoirs. International Journal of Greenhouse Gas Control, 46, 57–75.

Aguilera, R. (1995). Naturally fractured reservoirs (2nd Edition). Pennwell.

Aguilera, R. (2003). Geologic and engineering aspects of naturally fractured reservoirs, CSEG Recorder, Feb. 2003. Vol. 28, No. 2.

Ali, M.I., Sadatomi, M., Charles, M.E. Kawaji, M. (1991). Effect of gap width and orientation on two phase flow in narrow passage between two flat plates. Proceeding of Int. Conf. on Multiphase Flows, 91- Tsukuba, Japan.

Al-Turki, A. A., Maini, B.B., Gates, I.D. (2013b). The effect of fracture aperture and flow rate ratios on two phase flow in smooth-walled single fracture. J. Petroleum Explor. Prod. Tech. (2013), 3: 119-132.

Al-Turki, A.A.B., (2012a). Two Phase Flow in Smooth and Rough Walled Single Fracture. PhD Thesis, University of Calgary.

Angeli, P. and Hewitt, G.F. (1999). Flow structure in horizontal oil-water flow. Int.J. of Multiphase Flow, 26.

Ansari, A., Sylvester, N., Sarica, C., Shoham, O., Brill, J. (1994). A comprehensive mechanistic model for upward two hase flow in wellbores. SPE Production and Facilities, pp: 104 – 113.

Ayatollahi, M.R. and Zanbibaf, A. (2005). Path of crack growth under pure shear, IUST International Journal of Engineering Science, Vol. 16, No. 2, pp: 75 – 83.

Azizi Samir, M.A.S., Alloin, F., Dufresne, A. (2005). Review of recent research into Cellulosic Whiskers, their properties and their application in nanocomposite field. Biomacromolecules, Vol. 6, No. 2, 2005.

Babadagli, T. (1995). Fracture network characterization of geothermal reservoirs. First Trabzon International Energy and Environment Symposium (TIESS-96), Trabzon, Turkey, Vol. 1, Proc. pp: 71 – 77, July 29-31m 1995.

Babadagli, T. (2001). Scaling of co-current and countercurrent capillary imbibition for surfactant and polymer for injection in naturally fractured reservoirs. SPE J. 6:465 – 478.

Babadagli, T. (2002). Dynamics of capillary imbibition when surfactant, polymer, and hot water are used as aqueous phase for oil recovery. J Colloid Interface Sci. 2002 Feb 1; 246(1):203-13.

Baker, O. (1957). Discussion on how uphill and downhill flow affect pressure drop in two phase pipelines in hilly country. Oil and Gas J., pp: 150-152

Bear, J. (1972). Dynamics of Fluids in Porous Media. Soil Science, 120(2), pp:162–163. http://doi.org/10.1097/00010694-197508000-00022

Bear, J. and Bachmat, Y. (1991). Introduction to modeling of transport phenomena in porous media. Kluwer Academic Publishers.

Benham, A.L. and Olson, R.W. (1963). A model study of viscous fingering. SPE 513. Society of Petroleum Engineers Journal, pp: 138 - 144

Boggs, S.Jr. (2006). Principles of sedimentology and stratigraphy. Pearson Prentice Hall, US

Bourbiaux, B. (2010). Fractured Reservoir Simulation: a Challenging and Rewarding Issue Oil & Gas Science and Technology – Rev. IFP, Vol. 65 (2010), No. 2, pp. 227-238 Copyright © 2010, Institut français du pétrole DOI: 10.2516/ogst/200906

Brauner, N., Moalem, M.D. (1992). Flow pattern transitions in two phase liquid-liquid flow in horizontal tubes. Int. J.of Multiphase Flow. Vol. 18, No. 1, pp: 123 – 140.

Brennen, C. (2005). Fundamentals of Multiphase Flows. Cambridge University Press, 128, 368. P:20, http://doi.org/10.1007/s11214-006-9083-0

Brill, J.P. and Beggs, H.D. (1991). Two phase flow in pipes, sixth edition. January 1991.

Brooks, R.H., and Corey, A.T. (1964). Hydraulic properties of porous media; Hydrol. Pap. 3, Civ. Eng. Dep., Colo. State Univ., Fort Collins, 1964

Broseta, D., Medjahed, F., Lecourtier, J., and Robin, M. (1995). Polymer adsorption/retention in porous media: Effects of core wettability on residual oil. SPE Advanced Technology Series, 3, 1, 103-112

White, J. L., Goddard, J. E., Philips, H.M, (1973). Use of polymers to control water production in oil wells. SPE 3672, Journal of Petroleum Technology, pp : 143-150.

Charles, M.E., Govier, G.W., Hodgson, G.W. (1961). The horizontal pipeline flow of equal density oil-water mixtures. The Canadian J. of Chemical Engineering. Vol. 39, Issue 1, Feb. 1961. Pages 27-36.

Chen ,H.L., Lucas, L. R., Nogaret, L, a. d., Yang, H.d., and Kenyon, D. E., 2000. Laboratory monitoring of surfactant imbibition using computerized tomography. SPE/DOE International Petroleum Conference and Exhibition, Willahermosa, Mexco., February 2001

Chen, C., Horne, R.N., Fourar, M. (2004). Experimental study of two-phase flow structures effects on relative permeability in a fracture. Proceedings, 29th Workship on Geothermal Reservoir Engineering Stanford University, Stanford, California, January 26 – 28, 2004.

Chen, C.-Y. (2005). Liquid –Gas relative permeabilities in Fractures: Effects of flow structures, phase transformation and surface roughness. Stanford Geothermal Program Interdisciplinary Research in Engineering and Earth Sciences, Stanford University Stanford, California. SGP – TR-177

Chen, C.-Y., Li, K., & Horne, R. (2007). Experimental study of phase-transformation effects on relative permeabilities in fractures. SPE Reservoir Evaluation & Engineering, 10(5), pp: 514–526.

Cheraghian, G., Hemmati, M., Masihi, M. and Bazgir, S. (2013). An experimental investigation of the enhanced oil recovery and improved performance of drilling fluids using titanium dioxide and fumed silica nanoparticles. Journal of Nanostructure in Chemistry 2013, 3:78.

Chima, A., Geiger, S. (2012). An analytical equation to predict gas-water relative permeability curves in fractures. SPE Latin American and Caribbean Petroleum Engineering Conference held in Mexico City, Mexico, 16-18 April, 2012. SPE 152252.

Chisholm, Hugh, ed. (1911). Petroleum. Encyclopaedia Britannica (11th ed.). Cambridge University Press.

Chouke, R. L., van Meurs, P., van der Poel, E. (1959). The instability of slow, immiscible, viscous liquid-liquid displacements in permeable media. Trans. AIME 216, pp:188-194

Chown, J.C., (1994). The influence of upward water flow on downward DNAPL migration through vertical rough-walled fractures. M.Sc. Thesis, Queen's Univ., Kingston, Canada, 1994.

Clemens, T., OMV, Tsikouris, K., Buchgraber, M. (2012). Pore-scale evaluation of polymers displacing viscous oil – Computational Fluid Dynamics simulation of micromodel experiments. SPE 154169. 2012

Collins, R.E. (1961). Flow of fluids through porous materials. Reinhold Publishing Corporation, New York. pp: 196 - 197

Corey, A. T. (1954). "The interrelation between gas and oil relative permeabilities," Prod. Mon., 1954, pp. 19, 38

Craft, B.C., Hawkins, M.F., Revised by Terry, R. E., and Rogers, J.B. (2014). Applied Petroleum Reservoir Engineering (Third Edition), Prentice Hall PTR PRENTICE-Hall, Inc. A Simon & Schuster Company Englewood Cliffs, New Jersey 07632

Daripa, P., Pasa, G. (2005). New bounds for stabilizing Hele-Shaw flows. Applied Mathematics Letters 18 (2005), PP:1293-1303

Delhaye, J.M. (1981). Composite-averaged equations. In Delhaye, J.M., Giot, M. and Riethmuller, M.L. Two phase flow and heat transfer in power and process industries. Hemisphere Publishing Corporation, New York. pp. 181 – 186.

Dindoruk, B. and Firoozabadi, A. (1995). Computation of gas-liquid drainage in fractured porous media recognizing fracture liquid flow. J. of Can. Petrol. Tech. 34(10), pp: 39 - 49

Diomampo, G. P. (2001). Relative Permeability through fractures. Stanford Geothermal Program Interdisciplinary Research in Engineering and Earth Sciences, Stanford University Stanford, California. SGP – TR-170

Donaldson, E., Chilingarian, G.V., Yen, T.F. (1985). Enhanced oil recovery: Fundamentals and analysis. Elsevier Science Publishers B.V. P.O.Box 211, 1000 AE Amsterdam, The Netherlands. pp:199-204

Doughty, C. (2007). Modeling geologic storage of carbon dioxide: Comparison of non-hysteretic and hysteretic characteristic curves. Energy Conversion and Management, 48(6), pp:1768–1781.

Dukler, A. E., Wicks, M. & Cleveland, R. G. 1964 Frictional pressure drop in two-phase flow: comparison of existing correlation or pressure loss and hold-up. AIChE J-l 10, pp:38-43.

Dushin, V.R., Nikitin, V.F., Phylippov, Yu.G., Legros, J.C. (2010). Two-component fluid convective flow in thin gaps. Acta Astronautica, 66 (2010), pp:742 – 747.

EIMofty, Omar. (2012). Surfactant enhanced oil recovery by wettability alteration in Sandstone reservoirs, Missouri, Curtis Laws Wilson Library, Missouri University of Science and Technology.

Fernandez, J., Krechetnikov, R. and Homsy, G.M., (2004). Experimental study of a surfactant driven fingering phenomenon in a Hele-Shaw cell. J. Fluid Mech, (2005), vol. 527, pp: 197-216.

Ferno, M.A. (2012). Enhanced oil recovery in fractured reservoirs, introduction to enhanced oil recovery (EOR) processes and bioremediation of oil contaminated sites, Dr. Laura Romero-Zeron (Ed.), ISBN: 978-953-51-0629-6.

Firoozabadi, A. (2000). Recovery mechanisms in fractured reservoirs and field performance. Journal of Canadian Petroleum Technology, Vol. 39, No.11, pp:13 - 17

Fleming, K., Gray, D. G., & Matthews, S. (2001). Cellulose crystallites. Chemistry - A European Journal, 7(9), pp: 1831–1835.

Fourar, M., Bories, S. (1995b). Experimental study of Air-Water two-phase flow through a fracture (narrow channel). Int. J. Multiphase Flow, Vol. 21, No. 4, pp. 621 – 637.

Fourar, M., Bories, S., Lenormnd, R., Persoff, P. (1993). Two phase flow in smooth and rough fractures: Measurement and correlation by porous medium and pipe flow models. Water Resource. Res., 29 11, pp: 3699 – 3708.

Fourar, M., Bories, S., Lenormnd, R., Persoff, P. (1993a). Two-phase flow in smooth and rough fractures: Measurement and correlation by porous medium and pipe flow models. Water Resource. Res., 29 11), pp: 3699 – 3708.

Fourar, M; Lenormand R. (1998). A Viscous Coupling Model for relative permeabilities in a fracture, SPE Annual Technical Conference and Exhibition, 27 – 30 September, New Orleans, L Sep/1998uisian. SPE – 49006-MS

Furakawa, T., Fukano, T. (2001). Effect of liquid viscosity on flow patterns in vertical upward two-phase flow in a pipe. International J. of Multiphase Flow, pp: 1109 – 1126.

Gale, J. E. (1975). A numerical field and laboratory study of flow in rocks with deformable fractures. Ph.D. thesis, University of California, Berkeley, 255.

Geogarty, W.G., Surkalo, H. (1972). A field test of micellar solution flooding. SPE, 3439.

Gibson, A.H. (1913). On the motion of long air-bubble in a vertical tube. Phil. Mag. 26, pp: 952 – 965.

Glass, R.J. (1993). Modeling gravity-driven fingering in rough-walled fractures using modified percolation theory. Proceedings of the 4th annual high-level radioactive waste management conference. Las Vegas, Nevada: Society of Civil Engineering.

Govier, G. and Short W. (1958). The upward vertical flow of air-water mixtures II. Effect of tubing diameter on flow patter, holdup and pressure drop. The Canadian Journal of Chemical Engineering, pp: 195 – 202.

Govier, G.W. and Aziz, K. (1972). The flow of complex mixtures in pipes. Van Nostrand Reinhold Company, Canada.

Gutmanis, J., Batchelor, T., Cotton, L., Baker, J. (2012). Hydrocarbon production from fractured basement formations. GeoScience, (2012.)

Habibi, Y., Lucia, L. A., & Rojas, O. J. (2010). Cellulose nanocrystals: Chemistry, self-assembly, and applications. Chemical Reviews, 110(6), pp: 3479–3500.

Hasan, A. and Kabir, C. (1998). A study of multiphase in vertical wells. SPE Production Engineering, pp: 263 – 272.

Hasimoto, Michinao; Garstecki, Piotr; Stone, Howard A.; Whtesides, George M. (2008). Interfacial instabilities in a microfluidic Hele-Shaw cell. Soft Matter, 2008, 4, pp: 1403 – 1413. Royal Society of Chemistry Journal 2008.

Hematpour, H., Mardi, M., Edalatkhan, S., Arabjamaloei, R. (2011). Experimental study of polymer flooding in low viscosity oil using one-quarter five spot glass micromodel. Petroleum Science and Technology, 29:11, pp: 1163-1175

Hewitt, G., Hall-Taylor, N. (1970). Annular two phase flow. Pergamon Press.

Hill, S, M.A. and Inst, F.P. (1952). Channeling in packed columns. Chemical Engineering Science 1(6). P: 247-253

Hirasaki, G., & Zhang, D. (2004). Surface chemistry of oil recovery from fractured, oil-wet, carbonate formations. SPE Journal, 9(2), pp: 5–8.

Hirasaki, G.J., Miller, C.A., Puerto, M. (2011). Recent advances in surfactant EOR. SPE 115386.

Horle, T., Firoozabadi, A. and Ishimoto, K. (1990). Laboratory studies of capillary interaction in fracture/matrix systems, SPE Res. Eng., 5, pp: 353-360.

Hubbert, M.K. (1956). Darcy law and fluid equations for the flow of underground fluids. Trans AIME (1956), Vol. 207, pp. 222-239.

Hughes, R. G., & Blunt, M. J. (2001). Network modeling of multiphase flow in fractures. Advances in Water Resources, 24(3-4), pp: 409–421.

Huitt, J. L. (1956). "Fluid flow in simulated fractures." American Institute of Chemical Engineers Journal. vol. 2, issue 2, pp. 259-264.

Indraratna, B., Ranjith, P.G., Price, J.R., Gale, W. (2003). Two phase (air and water) flow through rock joints: Analytical and Experimental Study, Journal of Geotechnical and Geo-environmental Engineering, 2003, 129 (10), pp: 918-928.

Izadi, M., Shadizadeh, S. R., & Moradi, S. (2012). Experimentally Measurements of Relative Permeability in Fractured Core. International Journal of Science Emerging Tech., 3(1), pp:46–51.

Jensen, T.B., Sharma, M.P., Harris, H.G. and Whitman, U. (1992). Numerical investigations of steam and hot water flooding in fractured porous media. SPE 24172.

Johnson, R.W. (1998). The handbook of fluid dynamics. Published by Springer.

Katsuhiko, I. (1976). Fundamental studies of fluid flow through a single fracture. PhD Thesis, Civil Engineering, University of California, Berkeley.

Kazemi H, Gilman JR. (1993). Multiphase flow in fractured petroleum reservoirs. In: Bear J, Tsang CF, de Marsily G, editors. Flow and contaminant transport in fractured rock. New York: Academic Press.

Keller, A. A., Blunt, M.J., Roberts, P.V. (2000). Behavior of nonaqueous phase liquids in fractured porous media under two-phase flow conditions. Transp Porous Med 2000; 38, pp:189–203.

Khelifa, C., Zeddouri, A., Djabes, F. (2014). Influence of natural fractures on oil production of unconventional reservoirs. The international conference on technologies and materials for renewable energy, environment and sustainability, TMREES 14.

Khosravi, V. (2012). Various methods to determine relative permeability in fractured reservoirs. SPE Asia Pacific Oil and Gas Conference and Exhibition held in Perth, Australia, 22 – 24 October, 2012. SPE 158384.

Kianinejad, A., Ghazanfazri, M.H., Kharrat, R., Rashtchian, D. (2013). An experimental investigation of surfactant flooding as a good candidate for enhancing oil recovery from fractured reservoirs using one-quarter five spot micromodels: The role of fracture geometrical properties, Chemical and Petroleum Engineering Department, Sharif University of Technology, Tehran, Iran.

Kneafsy, T.J. and Pruess, K. (1998). Laboratory experiments on heat driven two-phase flows in natural and artificial rock fractures. Water Resource Research, 34(12), pp: 3349 -3367.

Kolev, N.I. (2013). Multiphase flow dynamics 1 Fundamentals. Fourth Edition. Springer-Verlag Berlin Heidelberg. E-ISBN 978-3-642-20605-4

Konzak, J. S. (2001). Numerical simulation of single- and two -phase flow in a rough-walled fracture (Order No. NQ59529). Available from ProQuest Dissertations & Theses Global. (304742569).

Kopf-Sill A. R. and Homsy G. M. (1987), Bubble motion in a Hele-Shaw Cell. Physics of Fluids, vol. 31, no. 1, pp: 18-27.

Kulatilake, P.H.S.W. 2001. Fracture characterization and network modeling. Eurock Pre-symposium course. Helsinki University of Technology.

Lafitte, V., Lee, J.C., Ali, S.A., Sullivan, P.F. (2013). Fluids and methods including Nanocellulose. US Patent US 20130274149 A 1.

Lakatos, I., Lakatos, S, J and Toth, J., 1981. Factors influencing polyacrylamide adsorption in porous media and their effect on flow behavior. Plenum Press New York, N.Y., pp: 821-842.

Lenk, D.A., Penny, G.S., Westland, J.A., (1992). Drilling mud compositions. Patent W01992022621 A1.

Lenorman, R., Touboul, E. and Zarcone, C. (1988). Numerical models and experiments on immiscible displacements in porous media. Journal of Fluid Mechanics. Vol. 189, pp. 165-187.

Leonce, D. (2012). Synthesis and Properties of soap. University of Dar Es Salaam.Fluid Flow Simulation in Fractured Reservoirs Mon., Vol. 19, 1954, pp: 38-41.

Liombas, J., Mouza, A., and Paras, S. (2006). Effect of surfactant additives on co-current gas-liquid down flow. Chemical Engineering Science, pp: 4605 – 4616.

Liu, H.-H., Wei, M.-Y., & Rutqvist, J. (2013). Normal-stress dependence of fracture hydraulic properties including two-phase flow properties. Hydrogeology Journal, 21(2), pp:371–382.

Lockhart, R.W. and Martinelli, R.C. (1949). Proposed correction of data for isothermal two-phase two-component flow in pipes. Chemical Engineering Progress. Vol. 45. pp: 39 – 48.

Longino, B.L., Kueper, B.H. (1999). Nonwetting phase retention and mobilization in rock fractures. Water Resource Res., 35(7), pp: 2085-2093.

Louis, C. (1969). A study of groundwater flow in jointed rock and its influence on the stability of rock masses. Imperial College Rock Mechanics Research Report No. 10, 90 pp.

Mandhane, J.M., Gregory, G.A., Azizi, K.A. (1974). A flow patter map for gas liquid flow in horizontal pipes. Int. J. Multiphase flow, 1, pp: 537 – 553.

McLean, J.W. and Saffman, P.G., (1981). The effect of surface tension on the shape of fingers in a Hele-Shaw cell. Journal of Fluid Mechanics (1981), vol. 102, pp: 455 – 469.

McQuillan, K. and Whalley, P. (1985). Flow patterns in vertical two-phase flow. Int. J. Multiphase Flow. 11(2), pp: 161 - 175

Meloney, D., Doggett, K. (1997). Multiphase flow in fractures. SCA – 9730.

Mendoza, C.A., Sudicky, E.A. (1991). Hierarchical scaling of constitutive relationships controlling multi-phase flow in fractured geologic media. Third International Conference on Reservoir Characterization Requirements for Different Stages of Development. Tulsa, Okla: Department of Energy.

Merrill Jr LS. (1975). Two phase flow in fractures. Ph.D. dissertation, Denver, CO: Petroleum Engineering, University of Denver.

Mishima, K., Hibiki, and Nishihara, H. (1992). Some characteristics of gas liquid flow in narrow rectangular ducts. Int. J. Multiphase Flow 22, pp: 703 – 712.

Moore, T.F. and Slobod, R.L. (1955). Displacement of oil by water – effect of wettability, rate, and viscosity on recovery. Pre-print, Fall Meeting of the Petroleum Branch of AIME. Petroleum Branch, ADE Fidelity Union Building, Dallas, Texas. Paper number 502-G.

Mungan, N. (1971). Improved waterflooding through mobility control. The Canadian Journal of Chemical Engineering, Vol. 49, Issue 1, February 1971. pp: 32 - 37

Nelson, R.A., (2001). Geologic analysis of naturally fractured reservoirs. (Second Edition). Gulf Professional Publishings. pp: 3, 101 – 124

Neuman. S.P. Jacobson, E.A. (1984). Analysis of nonintrinsic spatial variability by residual kriging with application to regional groundwater levels. Int. J. Math. Geol., 16(5), pp:499-521.

Nicholl, M.J. and Detwiler, R.L. (2001). Simulation of flow and transport in a single fracture: Macroscopic effects of underestimating local head loss. Geophysical Res. Letters, 22(23), pp: 4355 – 4358.

Pan, X. (1999), Immiscible Tow Phase Flow in a Fracture, Ph.D. Thesis, University of Calgary, Calgary, Alberta, Canada.

Pan, X., Wong, R.C., Maini, B.B. (1996). Steady state two-phase in a smooth parallel fracture. 47th Annual Technical Meeting of the Petroleum Society in Calgary, Alberta, Canada, June 10 – 12, 1996. The Petroleum Society, Paper 96 -39.

Park, C. W.; Maruvada, S.R.K.; Yoon, Do-Young, (1994). The influence of surfactant on the bubble motion in Hele-Shaw cell, Phys. Fluids 6 (10), October, American Institute of Physics, 1994.

Park, C.W., Gorell, S. and Stanley, H.E. (1984). Two phase displacement in Hele Shaw cell: experiments on viscously driven instabilities. Journal of Fluid Mechanics. 314, pp: 141 - 144

Penney, R., Moosa, R., Shahin, G., Hadhrami, F., Kok, A., Engen, G., … Kharusi, B. (2005). Steam injection in fractured carbonate reservoirs: Starting a New Trend in EOR. In International Petroleum Technology Conference. pp. 21–23.

Persoff, P. and Pruess, K. (1995). Two-phase flow visualization and relative permeability measurement in natural rough-walled rock fractures. Water Resources Research, Vol. 31, No. 5, pp: 1175 – 1186, May 1995.

Pieters, D.A., and Graves, R.M. (1994). Fracture relative permeability: Linear or non-linear function of saturation. Presented at the 1994 SPE Internation Petroleum Conference and Exhibition, Soc. of Eng. Veracruz, Mexico.

Polonsky, S., Barnea, D. Shemer, L. (1998). Averaged and time-dependent characteristics of the motion of an elongated bubble in a vertical pipe. Int. J. Multiphase Flow, 25. pp: 795 – 812.

Polubarinova-Kochina, P. Ya. (1962). Theory of groundwater movement. Translated by J. M. R. DeWiest, Princeton, New Jersey: Princeton University Press, 613 pp.

Ponjavic, A., Dench, J., Morgan, N., Wong, J.S.S. (2015). In situ viscosity measurement of confined liquids. Royal Society of Chemistry, RSC Adv., 2015, 5, 99585.

Porter, M.R., (1991). Handbook of surfactants. Glasgow, Blackie. ISBN: 0216929024

Pruess K, Tsang YW. (1990). On two-phase relative permeability and capillary pressure of rough-walled rock fractures. Water Resource Res 1990; 26: pp: 1915–1926.

Putra, E., Alfred, D., Schechter, D. S. (2004). Modeling fluid flow through a single fracture using experimental, stochastic and simulation approaches. SPE/DOE Fourteenth Symposium on Improved Oil Recovery held in Tulsa, Oklahoma, USA., 17-21 April 2004.

Pyrak-Nolte, L.J., Nolte, D.D., Myer, L.R., Cook, N.G.W. (1990). Fluid flow through single fractures. Barton N, Stephansson O, editors. Rock joints. Rotterdam, Netherland: A.A. Balkema; p. 405–412.

Razmi, R., Sedghat, M.H., Janamiri, R. and Hatampour, A. (2012). Application of SDS/LABS in recovery improvement from fractured models. World Academy of Science, Engineering and Technology, Vol 6 2012-12-27.

Reis, J.C. (1990). Oil recovery mechanisms in fractured reservoirs during steam injection. SPE/DOE 20204, presented at SPE/DOE Enhanced Oil Recovery Symposium, 22 – 25 April, at Tulsa, Oklahoma, 1990.

Rincon-Torres, M.T.and Hall, L.J., (2013). Cellulose nanowhiskers in well services. US Patenet US 20130196883 A1.

Rodriguez, E., Roberts, M.R., Yu, H., Huh, C., and Bryant, S.L. (2013). Enhanced migration of surface treated nanoparticles in sedimentary rocks. SPE 124418. SPE Annual Technical Conference and Exhibition

Romm, E.S., (1966). Fluid Flow in Fractured Rocks; Publisher: Phillips Petroleum Company; 1st English edition (1972)

Rosen, M.J., Kunjappu, J.T. (2012). Surfactants and interfacial phenomena (4^{th} edition). Wiley, A John Wiley and Sons, Inc., Publication. P:1

Rossen, W.R., Kumar, A.T.A. (1994). Effect of fracture relative permeabilities on performance of naturally fractured reservoirs. The SPE Int. Petrol. Conf. & Exh. at Mexico, Velacruz, Mexico, Oct. 10-13, 1994. SPE-28700

Rossen. W.R., Kumar, A.T.A. (1992). Single- and two-phase flow in natural fractures. The 67th Annual Technical Conference SPE, Washington, D.C., Oct. 4-7, 1992. SPE-24195

Rozenblit, R., Gurevich, M., Lengel, Y., Hetsroni, G. (2006). Flow patterns and heat transfer I vertical upward air-water flow with surfactant. Int. J. of Multiphase Flow, pp: 889 – 901.

Russel, TW.F. and Charles, M.E. (1959). The effect of the less viscous liquid in the laminar flow of two immiscible liquids. Canadian J. of Chemical Engineering, 37. pp: 18-24.

Rutqvist, J., Wu, Y.-S., Tsang, C.-F., & Bodvarsson, G. (2002). A modeling approach for analysis of coupled multiphase fluid flow, heat transfer, and deformation in fractured porous rock. International Journal of Rock Mechanics and Mining Sciences, 39(4), pp:429–442.

Sadatomi, M., Sato, Y., Saruwartari, S. (1982). Two –phase flow in vertical noncircular channels. International Journal of Multiphase Flow 8, 641 – 655.

Saffman, P.G., Taylor, S.G. (1958). The penetration of a fluid into a medium or Hele-Shaw cell containing a more viscous liquid. Proceedings of the Royal Society of London, Series A, Mathematical and Physical Sciences, Vol 245, No. 1242 (Jun. 24, 1958), pp:312-329.

Salas, C., Nypelo, T., Rodriguez-Abreu, C., Carrillo, C., Rojas, O.J. (2014). Nanocellulose properties and applications in colloids and interfaces. Current Opinion in Colloid & Interface Science 19 (2014), pp:383-396.

Samanta, A., Ojha, K., Sarkar, A., Mandal, A. (2011) Surfactant and surfactant-polymer flooding for enhanced oil recovery. Advances in Petroleum Exploration and Development. Vol. 2, No. 1, 2011, pp 13 -18.

SayedAkram, N. I., Aramco, S., & Mamora, D. (2011). Simulation study on surfactant-polymer flood performance in fractured carbonate reservoir. In SPE Enhanced Oil Recovery Conference 2011 - “From Science to Success: More, Faster, Greener, Cheaper”, EORC 2011 (Vol. 2, pp. 1635–1646).

Scheidegger, A.E. (1974). The physics of flow through porous media. University of Toronto Press, ISBN 0802018491.

Schlumberger (2016). Carbonate reservoirs. Home Services & Products Technical Challenges Carbonate Reservoir, http://www.slb.com/services/technical_challenges/carbonates.aspx

Seethepalli, A., Adibhatla, B., & Mohanty, K. (2004). Physicochemical interactions during surfactant flooding of fractured carbonate reservoirs. SPE Journal, 9(4), pp: 17–21.

Shad, S., Gates, I. D. (2008a). Multiphase flow in fracture: Co-current and counter-current flow in a fracture. Journal of Canadian Technology, Vol.49, No.2. February 2010

Shad, S., Maini, B. B., Gates, I. D. (2009). Investigation and visualization of liquid-liquid flow in a vertically mounted Hele-Shaw cell: flow regimes, velocity and shape of droplets Measurement. Science and Technology, Volume 20, Issue 11, article ID. 114005, 9, pp. (2009).

Shad, S., Maini, B. B., Gates, I. D. (2010). Effect of gap and flow orientation on two-phase flow in an oil-wet gap: relative permeability curves and flow structures. International Journal of Multiphase Flow, Volume 57, December 2013, pp: 78–87.

Snow, D. T. (1965). A parallel plate model of fractured permeable Media. Ph.D. thesis, University of California, Berkeley, 331 pp.

Sotiriadis, A.A., Thrope, R.B., Cheung C. (2003). Slugs in vertically downward two-phase flow. Anglo Japanese Conference on Two Phase Flow, Guildford, Surrey, UK, April, p:10

Standnes, D.C., Austad, T. (2000). Wettability alteration in chalk: 2. Mechanism for wettability alteration from oil-wet to water-wet using surfactants. Journal of Petroleum Science and Engineering 28(3): pp: 123-143. Oct. 2000

Sumnu, M.D. (1995). A study of steam injection in fractured media. PhD Thesis, Stanford University, Stanford, California.

Szabo, M.T. (1975). Some aspects of polymer retention in porous media using a C14-tagged Hydrolyzed Polyacrylamide. SPE Journal (August 1975), pp: 323-337.

Tabeling, P., Zochi, G., Libchaber, A. (1986). Film draining and the Saffman-Taylor problem. Phy. Rev. A33, pp: 794 - 796

Tabor, J. J. (1969). Dynamic and static forces required to remove a discontinuous oil phase from porous media containing both oil and water. Soc. Pet. Eng. J. 9, pp: 3–12

Teare, M., Cruickshank, R., Miller, S., Ovrland, S., Marsh, R. (2014) organizers of Alberta's Energy Reserves 2013 provided and Supply/Demand Outlook 2014-2023, by Alberta Energy Regulator.

Terry, R.E. and Rogers, J.B. (2014). Applied petroleum reservoir engineering. Third Edition. Pearson Education Inc. pp: 1-7, pp:357-399

Troniewski, L. and Ulbrich, R. (1984). Two phase gas liquid flow in rectangular channels. Chem. Eng. Sci. 39(4): pp: 751-765

Wasan, D.T. and Nikolov, A.D. (2003). Spreading of nanofluids on solids. Letters to Nature, 423 (6936), pp. 156-159 (8 May 2003).

Wassmuth, F.R., Arnold, W., Green, K., Cameron, N. (2009). Polymer flood application to improve heavy oil recovery at East Bodo. Journal of Canadian Petroleum Technology, 48(2), pp: 55–61.

Westland, J.A., Penny G.S., Stephens, R.S. and Winslow, A.R. (1994). Method of supporting fractures in geological formations and hydraulic fluid composition for same. US Patent US 5350528 A.

Westland, J.A., Penny, G.S., Lenk D.A. (1994). Drilling mud compositions. US Patent US 5362713 A.

Wilkens, R., Thomas, D., and Glassmeyer, S. (2006). Surfactant use for slug flow pattern suppression and new flow pattern types in a horizontal pipe. Transactions of the ASME, pp: 164 – 169.

Wilmarth T. and Ishii M. (1993). Two phase flow regimes in narrow rectangular vertical and horizontal channels. Int. J. Heat Mass Transfer vol. 3. No. 12, pp: 1749 – 1758.

Wu, J., He, J., Torsaeter, O., Zhang, Z. (2012). Effect of nanoparticles on oil-water flow in a confined nanochannel: a molecular dynamics study. SPE 156995. SPE International Oilfield Nanotechnology Conference

Wu, Y., Shuler, P., Blanco, M., Tang, Y. and Goddard, W.A., (2005). A study of branched alcohol propoxylate sulfate surfactants for improved oil recovery, SPE paper 95404, SPE Annual Technical Conference and Exhibition, 9-12 October, Dallas, Texas, 2005.

Wu, Y., Shuler, P.J., (2000). A virtual node method for handling well bore boundary in modeling multiphase flow in porous and fractured media. Water Resource Research, Vol. 36, No. 3. pp: 807 – 814.

Wu, Y., Shuler, P.J., Tang, Y. and Goddard Ill, W.A. (2008). An experimental study of wetting behavior and surfactant EOR in carbonates with model components. SPE 99612. SPE Journal, (March), pp: 26–34

Xhanari, K., Syverud, K., Stenius, P. (2011). Emulsions stabilized by microfibrillated cellulose: The effect of Hydrophobization, concentration and O/W ratio. Journal of Dispersion Science and Technology, 32:3, pp: 447 – 452.

Ye, Z., Liu, H.H., Jiang, Q., Zhou, C. (2015). Two-phase flow properties of a horizontal fracture: The effect of aperture distribution. Advances in Water Resources 76 (2015), pp: 43 – 54.

Ying-jie, Y., Ji-rui, H., Feng-Ian, Z., Chun-sheng, Y. Feng-min, Z., (2013). Research on influence rules of pore structure on water and polymer flooding using etched glass micro-model. SL, vol. 10, no. 1, pp: 59-70, 2013.

Zhang, T., Davidson, D., Bryant, S., & Huh, C. (2010). Nanoparticle-stabilized emulsions for applications in enhanced oïl recovery. Proceedings of SPE Improved Oil Recovery Symposium. http://doi.org/10.2118/129885-MS

Zolotukhin, A.B., Ursin, J.R. (2000). Introduction to petroleum reservoir engineering. Hoyskoleforlaget, Norwegian Academic Press, 2000.

Appendix-A

AIP PUBLISHING LLC LICENSE TERMS AND CONDITIONS

Aug 04, 2016

This Agreement between Salim Raza ("You") and AIP Publishing LLC ("AIP Publishing LLC") consists of your license details and the terms and conditions provided by AIP Publishing LLC and Copyright Clearance Center.

License Number	3921750702652
License date	Aug 04, 2016
Licensed Content Publisher	AIP Publishing LLC
Licensed Content Publication	Physics of Fluids
Licensed Content Title	Two phase flow of liquids in a narrow gap: Phase interference and hysteresis
Licensed Content Author	Salim Raza, S. Hossein Hejazi, Ian D. Gates
Licensed Content Date	Jul 5, 2016
Licensed Content Volume Number	28
Licensed Content Issue Number	7
Type of Use	Thesis/Dissertation
Requestor type	Author (original article)
Format	Print and electronic
Portion	Excerpt (> 800 words)
Will you be translating?	No
Title of your thesis / dissertation	Phase Interference in Multiphase Flow in Thin Gaps
Expected completion date	Aug 2016
Estimated size (number of pages)	200

Terms and Conditions

AIP Publishing LLC -- Terms and Conditions: Permissions Uses

AIP Publishing hereby grants to you the non-exclusive right and license to use and/or distribute the Material according to the use specified in your order, on a one-time basis, for the specified term, with a maximum distribution equal to the number that you have ordered. Any links or other content accompanying the Material are not the subject of this license.

1. You agree to include the following copyright and permission notice with the reproduction of the Material: "Reprinted from [FULL CITATION], with the permission of AIP Publishing." For an article, the credit line and permission notice must be printed on the first page of the article or book chapter. For photographs, covers, or tables, the notice may appear with the Material, in a footnote, or in the reference list.
2. If you have licensed reuse of a figure, photograph, cover, or table, it is your responsibility to ensure that the material is original to AIP Publishing and does not contain the copyright of another entity, and that the copyright notice of the figure, photograph, cover, or table does not indicate that it was reprinted by AIP Publishing, with permission, from another source. Under no circumstances does AIP Publishing purport or intend to grant permission to reuse material to which it does not hold appropriate rights.
   You may not alter or modify the Material in any manner. You may translate the Material into another language only if you have licensed translation rights. You may not use the Material for promotional purposes.
3. The foregoing license shall not take effect unless and until AIP Publishing or its agent, Copyright Clearance Center, receives the Payment in accordance with Copyright
   Clearance Center Billing and Payment Terms and Conditions, which are incorporated herein by reference.
4. AIP Publishing or Copyright Clearance Center may, within two business days of granting this license, revoke the license for any reason whatsoever, with a full refund payable to you. Should you violate the terms of this license at any time, AIP Publishing, or Copyright Clearance Center may revoke the license with no refund to you. Notice of such revocation will be made using the contact information provided by you. Failure to receive such notice will not nullify the revocation.
5. AIP Publishing makes no representations or warranties with respect to the Material. You agree to indemnify and hold harmless AIP Publishing, and their officers, directors, employees or agents from and against any and all claims arising out of your use of the Material other than as specifically authorized herein.
6. The permission granted herein is personal to you and is not transferable or assignable without the prior written permission of AIP Publishing. This license may not be amended except in a writing signed by the party to be charged.
7. If purchase orders, acknowledgments or check endorsements are issued on any forms containing terms and conditions which are inconsistent with these provisions, such inconsistent terms and conditions shall be of no force and effect. This document, including the CCC Billing and Payment Terms and Conditions, shall be the entire agreement between the parties relating to the subject matter hereof.

This Agreement shall be governed by and construed in accordance with the laws of the State of New York. Both parties hereby submit to the jurisdiction of the courts of New York County for purposes of resolving any disputes that may arise hereunder.

Questions? customercare@copyright.com or +1-855-239-3415 (toll free in the US) or **+1-978-646-2777.**